CONTROL OF MICROSTRIP ANTENNA FAR FIELD PHASE WITH ITS PARAMETERS IN PHASED ARRAY APPLICATIONS

By:

MOJGAN DANESHMAND

A Thesis
Submitted to the Faculty of Graduate Studies
in Partial Fulfilment of the Requirements
for the Degree of

Master of Science

Department of Electrical and Computer Engineering
The University of Manitoba
Winnipeg, Manitoba, Canada.

THE UNIVERSITY OF MANITOBA

FACULTY OF GRADUATE STUDIES

*****

COPYRIGHT PERMISSION PAGE

Control of Microstrip Antenna Far Field Phase With Its Parameters in Phased Array Applications

BY

Mojgan Daneshmand

A Thesis/Practicum submitted to the Faculty of Graduate Studies of The University of Manitoba in partial fulfillment of the requirements of the degree of

MASTER OF SCIENCE

ABSTRACT

In this thesis, a novel technique for generating required inter-element phase shifts in microstrip phased arrays antennas without the use of phase shifter is introduced. It is based on reconfigurable patches and MEMS technology where the array takes advantage of the antenna elements' inherent phase shift obtained due to the frequency shift and slightly different element sizes.

This theory is examined on circular single and staked microstrip antennas. Various analytical solutions such as transmission line and cavity model analysis are considered to determine the phase shift. Then, the numerical analysis is utilized to confirm the results. The variation of single antenna cavity dimension (i.e. patch radius, height, and probe location) leads to achieve about 70 degrees phase shift. For stacked antennas, one parameter (i.e. lower patch radius, upper patch radius, substrate thickness, separation between the patches, and probe location) is not sufficient and both upper and lower patch parameters are required to shift the frequency from one patch to the other, leading up to 180 degrees phase shift.

After observing single and stacked microstrip antennas phase properties, a linear-four element array configuration is utilized and the antennas behaviour in phased arrays are discussed. It is deduced that the proposed method leads to a scan angle of 14 degrees which can be increased by the use of a single digit phase shifter.

ACKNOWLEDGMENTS

I wish to express my sincere appreciation and gratitude to my advisor Professor Lot Shafai for his knowledge, insight, enthusiasm, valuable guidance, and continuous encouragement and support throughout this research. Indeed, my gratitude to him can not be expressed in a few words.

I would like also to thank Dr. G. Bridges, and Dr.M. Chaturvedi for serving on my committee and for their constructive criticisms and suggestions in the preparation of the final report.

Thanks are owed to Ms. S.Girardin for extending help whenever it was needed and also to Mount-first Ng and Guy Jonatschick for their excellent cooperation.

Financial support during this study was provided by the Natural Science and Engineering Research Council of Canada (NSERC) through a grant to Dr. Shafai. Their contribution is greatly appreciated.

Extended thanks to my MOM and DAD for their support, patient, and sacrifice during my education life and also to my brother and sister for their valuable encouragement. Last, but not the least, my deep appreciation and indebtedness to my best friend, my husband, for his valuable guidance, support, and generous love. This thesis is dedicated to them.

TABLE OF CONTENTS

LIST OF FIGURES

LIST OF TABLES

Chapter 1

Introduction

1.1.Preface

The concept of microstrip antennas was proposed by Deshamps in 1953 [1], and developed extensively since early 1970. The interest in microstrip antennas is because of their several desirable characteristics. They have low profile configuration which makes them convenient to place on a vehicle body or a package lid instead of requiring an extra mount or structure. Light weight is another advantage. They can also be low cost to manufacture as machining of complicated parts is not required. The antenna is highly integrated, as antenna circuit board can include the radiating elements and feeding network. This is due to the fact that, the antenna can be placed on the same substrate as the other ciruitry, to further increase the level of integration.

Due to microstrip antennas advantages, they have become a subject of interest in not only as single elements but also in array geometries. They have been used in terrestrial communication links and satellites. They are also employed on imaging systems,[2]. In addition, they have found important applications in phased arrays geometries such as in radar antennas and telephone and satellite communications.

Several microstrip antenna configurations have been used in phased array applications such as different geometrical shapes or various number of layers, [3]. However, they need phase shifters to generate the required inter-element phase shift. This restricts phased

array applications in extremely high frequencies (EHF) and millimetre waves due to high losses of the phase shifters. In spite of much investigation that has been done on microstrip antenna elements, their phase properties for phased array applications have not been studied.

This study is an attempt to use single layer and stacked circular microstrip antennas in a phased array configuration and take advantage of the antenna's inherent phase shift. Numerical analysis based on the moment method and analytical techniques based on circuit model of the antennas are utilized.

1.2.Background

Circular single and stacked patch microstrip antennas have been studied extensively in phased array geometries, [3]. Several numerical and analytical techniques have been used to analyze different characteristics of the antennas. But none of them has been concentrated on phase properties of the microstrip antennas in terms of their various antenna parameters.

Three analytical techniques have been developed to study this type of antennas and they are: the cavity model, the transmission line model, [4], and the modal expansion model. The cavity model and transmission line model are used in this study. In the cavity model, the antenna is considered as a cavity with a perfect electric conductor on top and bottom and perfect magnetic conductor at the side walls. This provides the antenna electric field inside the cavity, mode sequence, and the magnetic radiating currents around the

cavity. However, in the transmission line model, the antenna patches are approximated by transmission lines and the apertures are substituted by their equivalent admittance. This technique provides the antenna characteristics such as the input impedance and resonance frequency.

Numerical techniques are also developed which are based on the method of moment and finite element, etc. Method of moment solution is based on Maxwell's equation and surface segmentation. It divides the patch surface into small segments and solves the Greens' function for all the segments in matrix form which can be realized by computer. In this thesis, all *MOM* solutions are obtained using Ansoft-Ensemble 6 which is an electromagnetic simulation software package that computes s-parameters and full wave fields for the microstrip and planar microwave structures including microstrip antennas, [5].

In this study, transmission line model, cavity model, and method of moment are used to study the far field characteristics of single and stacked patch microstrip antennas in terms of their dimensions. It is assumed that the dimensions can be varied slightly. This assumption is based on the use of microelectromechanical systems (MEMS) and micromachining techniques. MEMS contain extremely small mechanical elements often integrated with electronic processing circuitry. Micromachining is the name referring to techniques used to fabricate such structures and their moving parts by employing microelectronic fabrication techniques or their slightly modified counterparts, [6].

1.3.Objective of the Thesis

The purpose of this research is to introduce a novel technique for generating required inter-element phase shifts in microstrip phased array antennas without the use of phase shifter. In this method, the array takes advantage of the antenna elements' inherent phase shift obtained due to slightly different element sizes. Various analytical solutions such as transmission line and cavity model analysis are considered to determine the phase shift. Then, the numerical analysis is utilized to confirm the results and discuss the performance of the technique in array configuration.

Some of the expressions that are used in this thesis are as follow:

- **Far Field Phase**: This expression stands for the phase of the radiated electric field at the far field and $\theta=0$ without considering the effect of the distance, r. This is illustrated by writing the radiated electric field at the far field in the following form:

$$E_{Co-Pol} = E(\theta, \phi)\frac{e^{-jkr}}{r} \tag{1-1}$$

where the far field phase will be that given by $E(\theta, \phi)$

- **Inherent Phase Shift:** This term defines the phase shift which is due to the antenna structure and there is no external reason for that. It can be modified by varying the antenna parameters.
- **Transfer Function of the Antenna**: This is a function that represents the antenna role in transferring the phase shift from the input to the far

field. It is obtained from the antenna circuit model and will be discussed in details in the up coming chapters.

1.4. Structure of the Thesis

Applications and importance of the microstrip antennas are stressed in this chapter. As mentioned in the previous section, this antenna can be a good candidate to use in phased array configurations. This suggests development of various analytical tools and physical models to analyse the phase properties of the microstrip antenna. A review of phased array antenna theory and phase shifter's drawbacks are addressed in chapter 2. This is not meant to be an exhaustive review on them as the area is too wide to be covered in a single chapter. Nevertheless, it is hoped to provide sufficient background on the basic issues used in this thesis and the problems are faced in design of phased array antennas. In addition, a concept to overcome these difficulties and generating the inherent phase shift from the antenna elements, based on the cavity model, is established.

In chapter 3, this concept is utilized on circular microstrip antennas and the effect of antenna dimensions variations at the far field phase is obtained. The results from the cavity model are compared to those of the MOM and good agreement is shown. Some extra parameters such as stub and short pin are added to the antenna geometry and their performance is investigated. Using the proposed technique and reconfigurable patches, an array configuration is designed and its radiation pattern and bandwidth are studied.

To modify single patch performance, the circular stacked microstrip antenna is

investigated in chapter 4. Effect of the antenna parameters variation such as lower and upper patch radii, substrate thickness, distance between two patches, and probe location at the far field phase is investigated. The results obtained by transmission line analysis is compared to that of the MOM. Due to the antenna's dual resonance frequencies, a wider bandwidth and thus larger phase shift is achievable in contrast with the single patch. This inherent phase shift of the antenna gives the capability to design a reconfigurable phased array. Performance of the array such as radiation pattern and bandwidth of the antenna is also studied.

Chapter 2

Phased Array Antenna Theory

2.1.Introduction

With a phased array the main lobe of the radiation pattern can be moved or scanned by electronic phase shift between the antenna elements, conventionally, using phase shifters. This beam motion is more rapid and flexible than a mechanical motion. In many cases the overall array has a more smaller size than an equivalent single antenna requiring mechanical movement,[7].

A radar or communication designer sees the array antenna as a component with measurable input and output and a set of specifications. However, an array designer sees the details of the array and the physical and electrical limitations to epitomize the design. In this chapter, The general principles of the phase array antenna and some conventional phase shifters are discussed in details. Then, to overcome the difficulties associated with the phase shifters, a theory established to use the inherent phase of the antenna elements.

2.2. General Principle of Phased Array Antenna

Array theory is shared by all array systems and the analysis of that is the first step toward designing an optimize phased array antenna. Linear antenna arrays can be a good starting to array theory because of the good insights they lend into beam forming. And,

planar phased array antenna which is more general case is the next step to understand this concept better.

2.2.1. Linear Array

The linear array, shown in figure 2.1. consists of N elements with the distance between consecutive elements equal to s. Neglecting the mutual coupling, the resulting far-field pattern of the array, E, is the product of the far field pattern corresponding to one element, $f(\theta,\phi)$, and the array geometric factor, (AF), which includes the sum of contributions of the N antenna elements,[8]:

$$E = f(\theta, \phi) \times (AF) \tag{2-1}$$

If we assume the same illumination for all the antenna elements, the sum of all voltage contributions in the far field pattern, or the AF is given by:

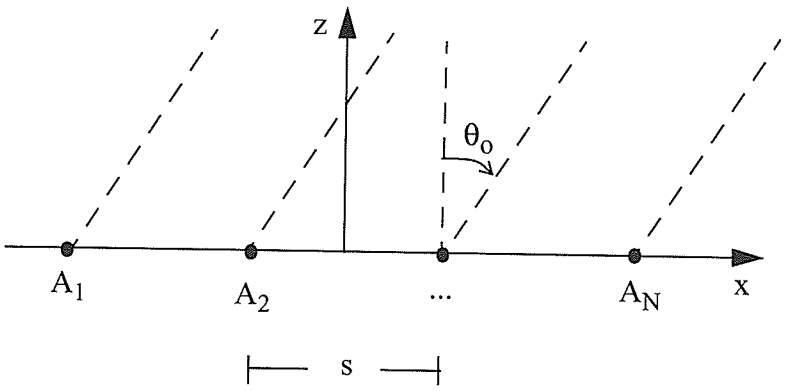

Figure 2.1: A linear phased array antenna of equidistant antenna elements

$$AF = 1 + \exp(j\psi) + \exp(j2\psi) + \exp(j3\psi) + \ldots + \exp(j(N-1)\psi)$$
$$= \sum_{1}^{n=N} \exp(j(n-1)\psi) \tag{2-2}$$

where:

$$\psi = ks\sin\theta + \beta \tag{2-3}$$

and β is the excitation phase between elements and $k=2\pi/\lambda$. For steering the array beam to a direction θ_0, by inserting a phase shift β between adjacent antenna elements, the following condition should be satisfied:

$$\psi = ks\sin\theta_o + \beta|_{\theta=\theta_o} = 0 \tag{2-4}$$

or

$$\beta|_{\theta=\theta_o} = -ks\sin\theta_o \tag{2-5}$$

Thus, by changing β, the peak of the radiation pattern can be directed toward any direction to form a scanning array. If a N-element linear phased array antenna of omnidirectional antenna elements has an East-West orientation, the resulting main beam and grating lobes will extend from North to South.

Another issue in phased array antenna is the resulting grating lobe which consumes a great amount of power. If a linear array is scanned to θ_0, the equation for the resulting array geometric factor is:

$$AF = \frac{\sin Ns\pi[(\sin\theta - \sin\theta_o)/\lambda]}{N\sin[s\pi(\sin\theta - \sin\theta_o)/\lambda]} \tag{2-6}$$

Grating lobes occur whenever the denominator of equation (2-6) vanishes. Therefore, we have:

$$\frac{s\pi(\sin\theta - \sin\theta_o)}{\lambda} = \mp\pi, \mp 2\pi, \mp 3\pi, \ldots \tag{2-7}$$

If the angle of first grating lobe is θg, we can conclude:

$$\sin\theta_g = \sin\theta_o \mp \frac{\lambda}{s} \tag{2-8}$$

or the condition for no grating lobe:

$$\left|\sin\theta_o\right| - \frac{\lambda}{s} < -1 \tag{2-9}$$

If the array is to be scanned to ± 90, $sin\theta_0 = 1$ and $s < \lambda/2$. Thus, the condition that the spacing between antenna elements is shorter than λ/2, is enough for not having grating lobe in broadside. On the other hand, mutual coupling which alters each elements radiation pattern increases by decreasing *s*. Therefore, λ/2 is a superior distance for antenna elements.

2.2.2. Planar Array

To extend the array theory for planar arrays, consider the rectangular array shown in Figure 2.2 with spacings between elements of s_x and s_y along the *x*-direction and *y*-direction. The usual spherical coordinates is used with separate excitations along the rows and columns. Having *M* by *N* antenna elements along the *x*- and *y*-directions, *AF* becomes:

$$AF|_x = \sum_{m=1}^{M} I_m \exp j(m-1)(ks_x \sin\theta\cos\phi + \beta_x) \tag{2-10}$$

and

$$AF|_y = \sum_{n=1}^{N} I_n \exp j(n-1)(ks_y \sin\theta\sin\phi + \beta_y) \tag{2-11}$$

while β_x and β_y are the phase shift between antenna elements along x- and y-directions.

The total array factor is:

$$AF|_{array} = AF|_x AF|_y \tag{2-12}$$

When all the amplitude excitations are equal we can write:

$$AF|_{array} = \frac{1}{M}\frac{\sin(M\psi_x/2)}{\sin(\psi_x/2)}\frac{1}{N}\frac{\sin(N\psi_y/2)}{\sin(\psi_y/2)} \tag{2-13}$$

where

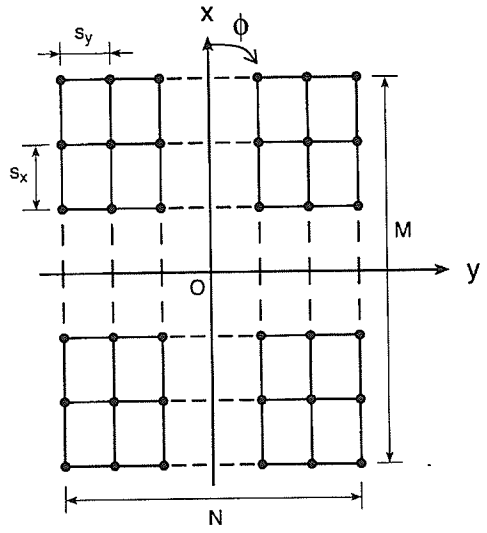

Figure 2.2: A plane view of rectangular array of $M \times N$ elements,[8]

$$\psi_x = ks_x \sin\theta\cos\phi + \beta_x$$
$$\psi_y = ks_y \sin\theta\sin\phi + \beta_y \qquad (2\text{-}14)$$

and the condition for beam scanning at $\theta=\theta_0$ and $\phi=\phi_0$ can be derived:

$$ks_x \sin\theta_o \cos\phi_o + \beta_x = 0$$
$$ks_y \sin\theta_o \sin\phi_o + \beta_y = 0 \qquad (2\text{-}15)$$

Therefore:

$$\tan\phi_o = \frac{\beta_y s_x}{\beta_x s_y}$$
$$\sin\theta_o = \frac{\beta_x^2}{(ks_x)^2} + \frac{\beta_y^2}{(ks_y)^2} < 1 \qquad (2\text{-}16)$$

This condition is valid for beam forming when the excitations of the array columns and rows are separable. The grating lobes condition along x- and y-axes are the same as the equations derived when linear phased arrays were considered. Nevertheless, The grating lobes in any other planes are not easily derived,[8].

Therefore, for beam steering in phased arrays, normally, the elements are placed in the distance of half a wavelength and excited with different inter-element phase shifts that satisfy the equation (2-16). As it will be discussed in the next section, this phase shift can be achieved using RF phase shifters in the form of a phase delay. Or, inherent phase of the antenna can be used to introduce phase shift between the elements, which will be discussed in details in section 2.4.

2.3. Phase Shifter

A phase shifter is a control device found in many microwave communication and radar systems. It's main application is implementing inter-element phase shift between the antenna elements in phase array antennas. Consequently, they also introduce insertion loss to the system. The magnitude of the loss depends on the type of phase shifter and their operating frequency. It can be neglected at lower frequencies, but becomes excessively high at the EHF or millimetre wave frequencies, requiring new solutions.

There are currently two types of electronic phase shifters suitable for practical phased arrays: the ferrite phase shifters and semiconductor-diode phase shifters [9]. Ferrite phase shifters can handle large RF power into several kilowatts. However, They require large applied energy for activation. They are not usually monolithic but to do so they have been recently investigated using novel ferroelectric materials, such as Barium Strontium Titanates. However, they are somewhat lossy, and loss increases rapidly for frequencies above 20 GHz. In addition, they require very large bias voltage, above 250V, to demonstrate reasonable phase shifts, [10]. They are also very sensitive to the ambient temprature. Performance characteristics of possible realization dual mode reciprocal ferrite phase shifter is given in Table 1, [11]. It can be realized that for phased array antennas with large number of elements, they are too bulky. Due to this fact and their high fabrication cost, they have been restricted to military applications.

Semiconductor device based phase shifters have been more flexible in design and

Table .1: Possible utilization of 3-5 bit ferrite phase shifters, [11].

Frequency (GHz)	3	10	35
Bandwidth (%)	6	6	5
Insertion loss peak value (dB)	0.9	0.9	1.4
Power peak (W)	1000	300	100
Temperature range (operating) ($°C$)	0-50	-40-+70	-40-+85
Switching energy (μJ)	800	200	50
Length (mm)	140	42	38

application due to their small size and small bias voltage. But, they are lossy and can only handle small amount of power. Most of them is based on the PIN junctions whose loss level increases with frequency. According to [9], total diode insertion loss can be linearly approximated by $\frac{f}{f_c}$ where f_c is the cut off frequency of the PIN junctions. As a result, the loss increases with operating frequency. For instance, some of the x-band phase shifters, shown in table 2, have about 6dB loss (4037MICRONETICS) which increases to 10dB or more in some other cases (4043MICRONETICS) when larger phase shifts or wider bandwidth is required, [12]. Moreover, their performance becomes weaker as the frequency increases. Although, they have been recently improved by implementing MEMs and MMIC technologies but they are still poor at millimetre wave frequencies.

Table .2: Electrical characteristics of two types of MICRONETICS phase shifters, [12]

Part	Type	Frequency (GHz)	Loss (dB)	Phase shift (degree)	RF power (dBm)
4037	variable	12-18	6.5	180	10
4033	5 Bit	6-18	10	360	10

Semiconductor phase shifters can be realized with either analogue or digital control. Single -stage reflection-type phase shifter is a simple example of analogue phase shifter, which is shown in Figure(2.3). It is composed of one directional coupler and two terminating impedances at its ports which are easy for fabrication using MMIC technology. However, it has either a narrow bandwidth, with a good phase error performance at all phase states or a wide bandwidth, with a poor phase error performance at most phase states. A novel method for implementing a true wide band analogue phase shifter with a low phase error performance is cascaded-match reflection-type phase shifter which is shown in figure (2.4). But it suffers from complexity of design and big volume and high insertion loss level especially to be applied in large scale phase array antenna with high number of elements,[13].

Another approach to improve performance of the phase shifters is to use digital phase shifters such as digital reflection type phase shifters in one or more states, Figure (2.5). Here, the terminations consist of a switchable load impedance for reflection. Compared to the analogue phase shifters they show better performance. However, they need special foundry process to realize high quality switches with many power lines. In addi-

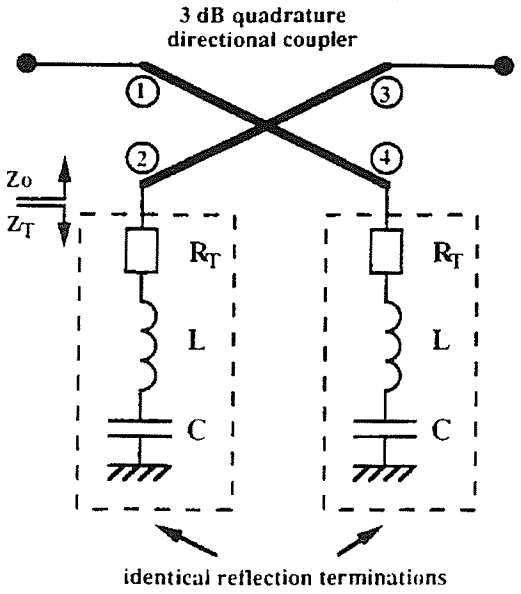

Figure 2.3: Basic topology of a single-stage reflection-type phase shifter,[13].

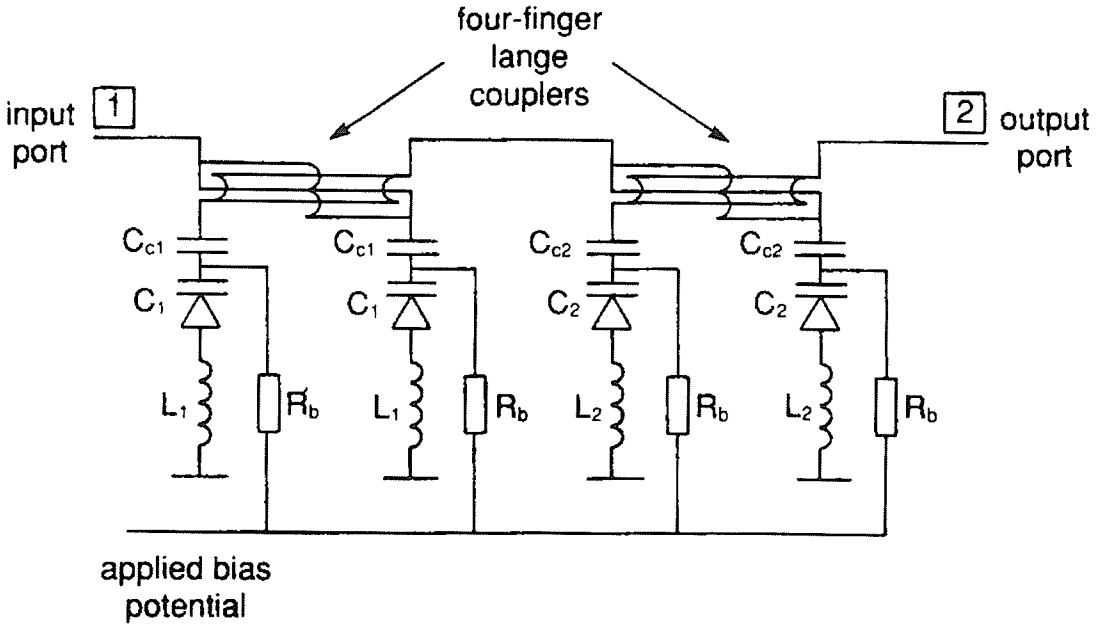

Figure 2.4: Topology of the cascaded-match reflection-type phase shifter,[13].

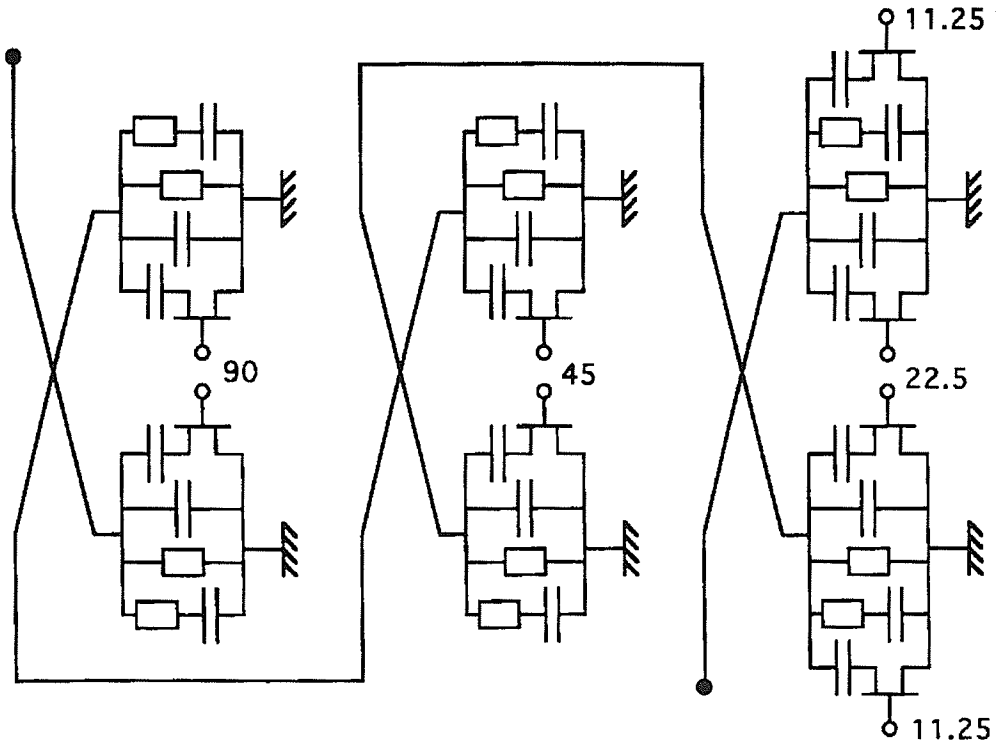

Figure 2.5: Digital reflection-type phase shifters with switchable load impedance,[13].

tion, they suffer from quantization error that appears in radiation pattern of applying phased array antennas, [13].

In this section, the characteristics of different phase shifters have been defined. The main types of phase shifters such as Ferrite based and Semiconductor based phase shifters have been reviewed and their relative advantages and drawbacks were discussed. In overall view, they are lossy at high frequencies and bulky components in large number of applications and add to the complexity of the design. Therefore, next remarkable step can be removing the entire phase shifters from the phased array antennas using MEMs technology and taking advantage of inherent phase of microstrip antenna. This will be discussed in the next section.

2.4. Proposed Theory.

For beam-forming network of an adaptive phased-array antennas, the required phase shifts are applied using phase shifters. Since, they are often made up of many elements, it is advantageous to reduce the size, weight and cost of the electronics supporting of each element. Size and weight constraints are increasingly challenging for airborne and space flight systems, especially when high performances are expected. To simplify the array one possibility is to use the antenna parameters as variables to modify its impedance characteristics, and thus the insertion phase. This possibility is becoming realistic, recently, by the use of MEMS technology,[14].

Over the past two decades, a great deal of research has been devoted to develop accurate models for microstrip antennas such as transmission line or cavity model. One of the main reasons is to predict the quantities such as the input impedance, loss effects, patterns and gain. They have advantages in terms of computational simplicity and in providing a physical insight that is usually missing in more numerical solutions. Based on the cavity model analysis of microstrip antenna [15,16], a theory is established to use the inherent phase properties of microstrip patch antennas instead of using phase shifters in the phased arrays.

2.4.1. General Circuit Model

The cavity model may be used to represent the equivalent network of each mode in various microstrip antenna configurations, [18]. Abboud et al. [17] and Edimo et al. [25] have developed circuit models for single and stacked patch microstrip antennas, shown in Fig-

ure 2.6. In the circuit model analysis, usually the stored energy models by inductance and capacitance and the lost or radiated energy is shown by a resistor. Various feeds can be replaced by different circuit elements. For instance, the probe feed effect is shown by a series Inductance, in Figure 2.6. Edge feed, aperture coupled and proximity coupled feed

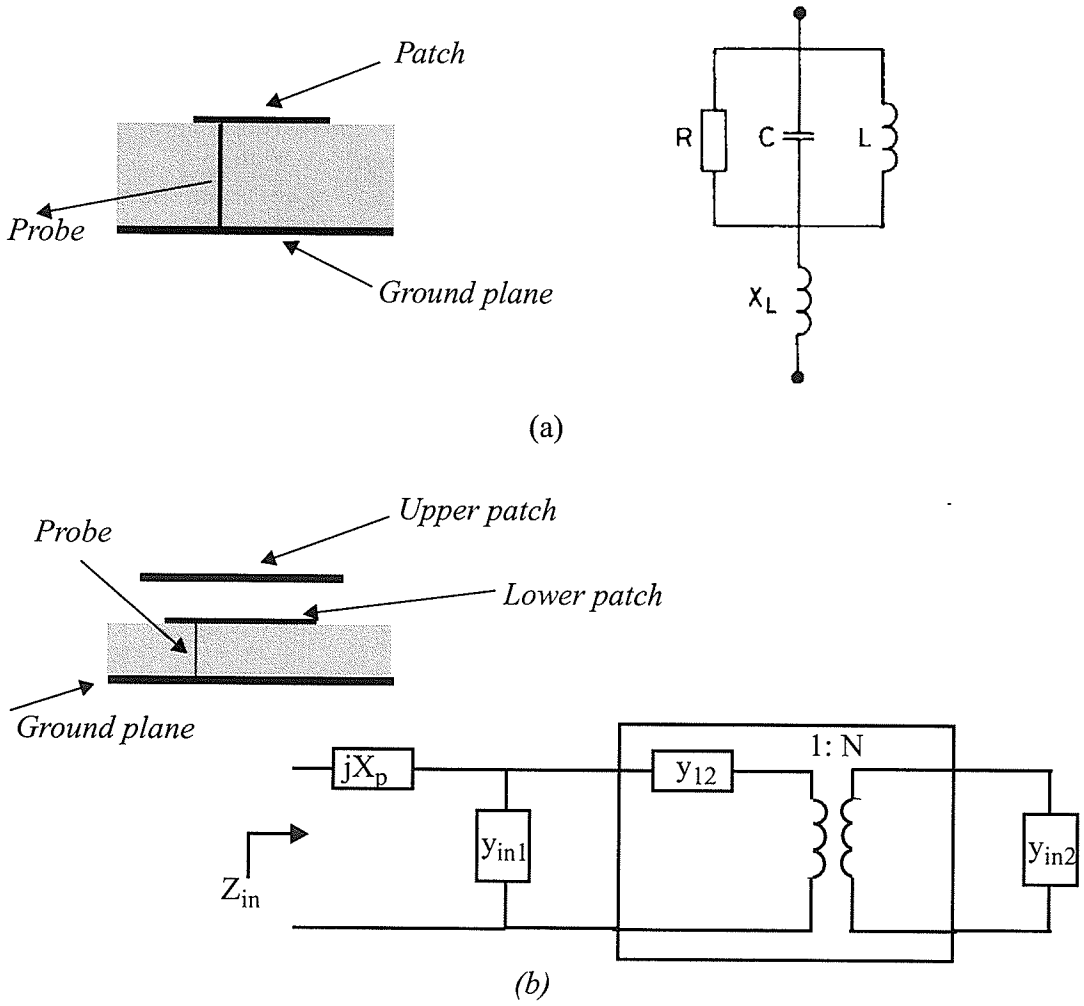

Figure 2.6: (a) Cavity model of single microstrip patch,[17],(b) Cavity model of stacked rectangular microstrip antenna while y_{in1} and y_{in2} are RLC circuit model due to the first and the second patch, respectively, and ground plane and y_{12} is mutual impedance between the patches,[25].

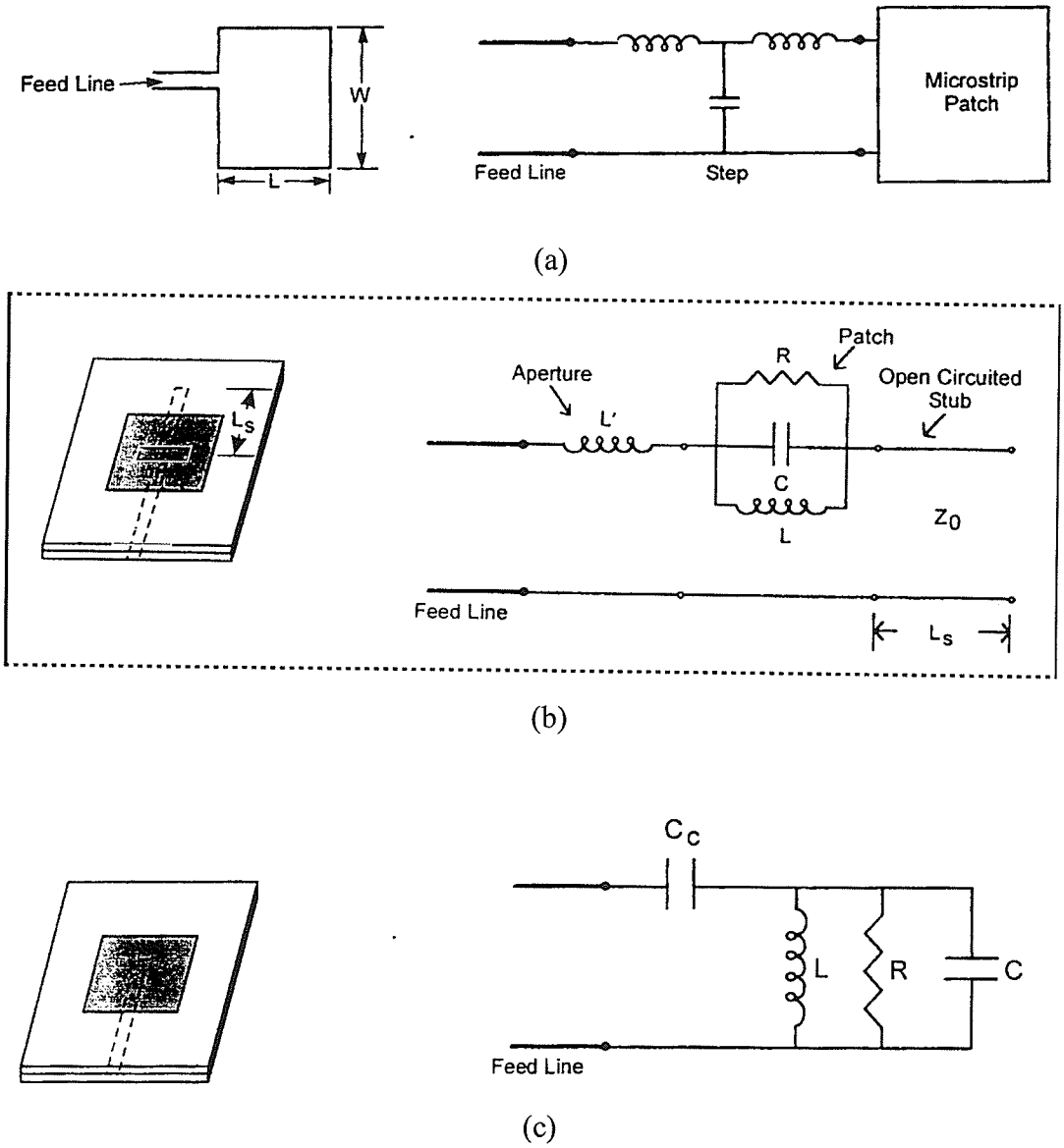

Figure 2.7: Circuit model of different feeding microstrip antennas, (a) Microstrip feed at the radiating edge, (b) aperture coupled microstrip feed and (c) Proximity coupled microstrip feed, [27]

systems are demonstrated in Figure 2.7. Aperture coupling shows more inductive characteristics while proximity coupled feed is capacitive.

If all the components except the resistor due to the radiation is represented by a black box, a general model for microstrip antenna can be found. Figure 2.8 shows the model of resonator antenna in the radiation mode. In this figure, R stands for the radiation loss, R_s is the transmission line impedance, Z_{in} is the input impedance of the antenna, the black box indicates the effect of the cavity which is made by the antenna and ground plane and V_s is the input voltage source with a constant phase.

We know that the electric field at the far field can be represented in terms of vector potential:

$$E = -j\omega A \tag{2-17}$$

which indicates that the electric field, E, has 90 degrees phase shift compared to the vector potential, A, and thus the radiation source current,[19]. On the other hand, according to the model, the current on the radiation resistor can be considered as the radiation source current in the actual antenna. Considering the fact that the resistor does not add any phase change to the current, the far field phase can be expressed in terms of the resistor voltage, V_{out}:

$$Far\ \ Field\ \ Phase = \angle V_{out} + 90° \tag{2-18}$$

With a simple voltage division we have:

$$V_{out} = T \times \frac{1}{1 + \frac{R_s}{Z_{in}}} \times V_s \tag{2-19}$$

where T=V_{out}/V_{in}, and it can be named the transfer function of an antenna. It shows the

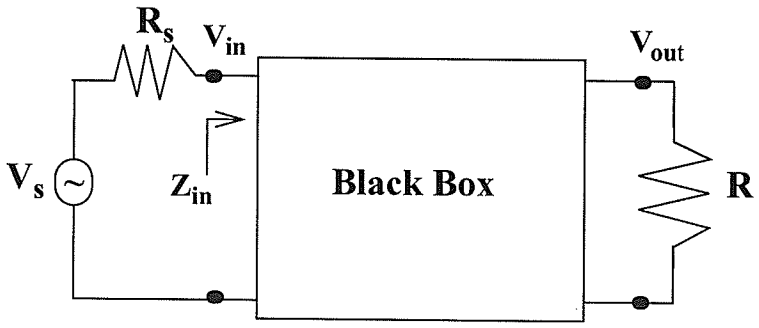

Figure 2.8: General Model of an antenna.

effect of the black box and strongly depends on the antenna configuration and its feed system. This equation shows that for a well matched antenna, the input impedance phase is not able to affect the output phase considerably and the most important parameter is the transfer function.

2.4.2. Transfer Function

The transfer function of a system can be represented by different diagrams such as Bode diagrams. In Bode diagram the amplitude and phase are shown separately, therefore, it is suitable for our discussion. It is customary to show the angle in degrees against the common logarithm of the input frequency. We will see that the total amount of phase variation changes by the order of function.

There are three different kinds of factors that may occur in a transfer function such as Poles at the origin ($j\omega$), Poles on the real axis$(1+j\omega\tau)$, and complex conjugate poles$(1+(2\xi/\omega n)j\omega+(j\omega/\omega n)^2)$. The phase angle for these four factors can be determined

and then, utilize any general form of the antenna transfer function.

Phase curve of a single Pole at the origin is a horizontal line and doesn't add any phase shift. A first-order system with real pole on the axis has the following transfer function:

$$T = \frac{1}{1 + j\omega\tau} \tag{2-20}$$

while τ is a constant. The phase angle for this system is given by:

$$\phi(\omega) = -tan^{-1}\omega\tau \tag{2-21}$$

when

$$\phi(\omega) \rightarrow 0°, \omega \ll 1/\tau$$
$$\phi(\omega) = 45°, \omega = 1/\tau$$
$$\phi(\omega) \rightarrow -90°, \omega \gg 1/\tau$$

It's plot is shown in Figure 2.9. It can be seen that as the frequency increases, ϕ starts at $0°$ and approaches $-90°$ and the total phase shift is 90 degrees.

A second-order system with conjugate poles, which usually represents a resonator, has the following transfer function:

$$T = \frac{1}{1 + (j\omega)\frac{2\xi}{\omega n} + (j\omega)^2\frac{1}{\omega n^2}} \tag{2-22}$$

where, ξ is the damping ratio and ωn is the system constant. The phase angle is:

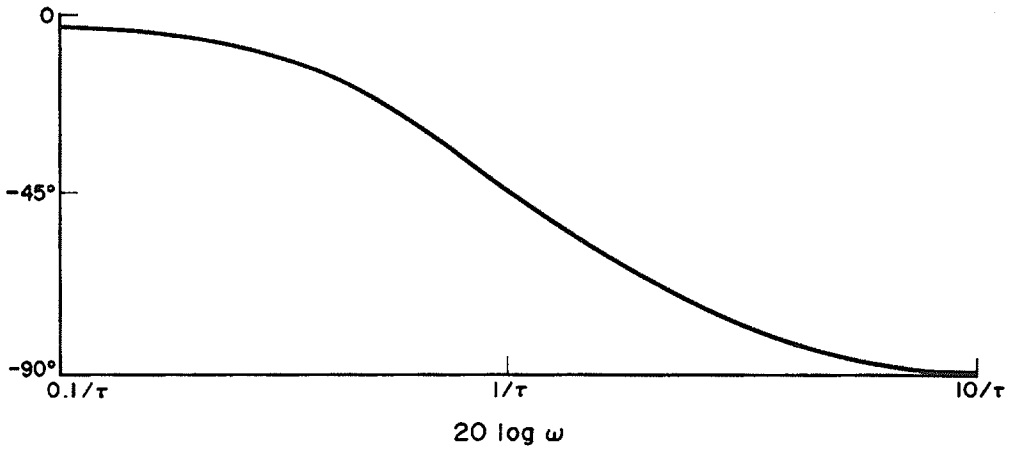

Figure 2.9: Phase plot of first order system,[20].

$$\phi(\omega) = -tan^{-1}\frac{2\zeta(\omega/\omega n)}{1-(\omega/\omega n)^2} \tag{2-23}$$

when

$$\phi(\omega) \to 0°,\ \omega/\omega n \ll 1$$
$$\phi(\omega) \to -180°,\ \omega/\omega n \gg 1$$

Figure2.10 shows the phase plot of the system against frequency. It can be seen that for all second order systems regardless of ξ, the phase angle starts at $0°$ for low frequencies and decreases to $-180°$ as a limit at high frequencies and the total amount of phase shift, $180°$, is always constant.

To find phase curve of any other transfer function, typically the curves for each factor are obtained separately and then added together graphically to obtain the curves for

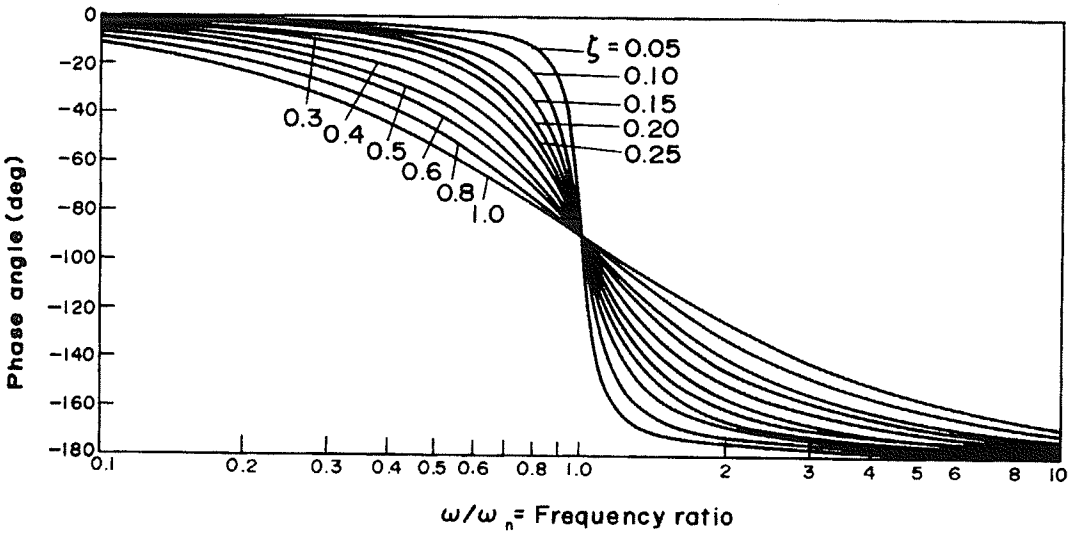

Figure 2.10: Phase plot of a simple second order system,[20].

the complete transfer function. Therefore, by increasing the number of poles the amount of total achievable phase shift increases. However, adding any zero to the function will add positive phase and can cancel the effect of poles. More details can be found in references [20,21].

2.4.3. Frequency Shift

In section 2.4.1. and 2.4.2. The effect of transfer function and its phase shift on the antenna far field phase in terms of frequency were studied. However, many communication systems such as radar and phase array antennas require phase shift in a fixed frequency band. The proposed technique is to keep the operating frequency constant and move the resonance frequency and thus the phase curve on the frequency axis to be able to obtain a desired phase shift.

In a real system, the input impedance matching of the antenna is the most significant problem that affects the radiation behaviour of the antenna. Conventional antennas radiate efficiently only over their frequency bandwidth and this limits the applicable range of the phase curve to a small band pass range. To overcome this difficulty, a wide band antenna is necessary.

In this thesis, due to many advantages of microstrip antenna, it's phase properties are investigated. Stacked configuration is used not only to extend the bandwidth but also to increase the total phase shift. Their dimensions are modified such that their input impedance match remains in the acceptable range of $S_{11} < -10dB$.

2.5.Summary

In this chapter, a basic review of the phased array antennas was provided. Conventional phase shifters and the difficulties associated with them such as complexity and high loss level were studied. Then, a concept were proposed to replace the phase shifters with the inherent phase shift of the antenna.

In both linear and planar phased array antennas, the inter-element phase shift causes the beam to sweep in space. The maximum scan range depends not only on the amount of phase shift between the elements, but also on their separation distance.

To date, ferrite and semiconductor phase shifters have been two main devices that have been used to generate inter-element phase shifts. Ferrite phase shifters require high control voltages and occupy large volumes. However, semiconductor phase shifters, either

analogue or digital, need small control voltages and are easy to fabricate. But, in large number of applications they are still bulky and introduce large insertion losses.

A novel method was introduced to take advantage of inherent phase shift of the antenna. A general model for an antenna was presented while its radiation loss was represented by a resistor. Considering the phase shift between the current and the far field pattern, the resistor voltage phase can be assumed as far field phase. In addition, the transfer function of an antenna witch is the most effective parameter defining the resistor phase shift, was explained. To use the phase shift of the transfer function, tuning the antenna resonance frequency by modifying its parameters, while keeping S_{11}<-10dB, was proposed.

Chapter 3

Circular Microstrip Patch Antenna Phase Properties

3.1. Introduction

Circular microstrip patch antenna is one of the most popular configurations which has attracted much of attention not only as a single element, [22], but also in phase arrays,[23]. In some applications the circular geometry offers certain advantages over other configurations. For instance, by variation of its dimensions, the order of the modes does not change. The modes supported by the circular patch antenna can be found by treating the patch, ground plane and the material between the two as circular cavity. As the substrate thickness is considered much smaller than the wavelength, the antenna has just one degree of freedom, the patch radius. Therefore, changing the relative dimensions of the patch does not change the order of its modes, but changes their magnitude, [19].

The analysis techniques can be separated into two categories of approximate methods based on simplifying assumption, and exact full-wave solutions. Examples of the former include the transmission line model and the cavity model. These models generally treat the element as a transmission line or cavity resonator, thus simplifying the analysis considerably. Full wave analysis that includes method of moment is more accurate but it doesn't offer any physical view for better understanding of the problem. In this chapter, both techniques are investigated.

It has been shown that the circular disk microstrip antennas can be modified to pro-

duce a range of impedances, radiation patterns, and frequencies of operation,[16]. However, the phase properties of this antenna has not been investigated adequately. In this chapter, the phase shift and input characteristics of a single layer circular microstrip antenna in terms of its different parameters as well as matching stub and short pin are discussed. Then, an array configuration is selected and shown that by using this technique its beam can be scanned.

3.2. Cavity Model Analysis

3.2.1. Circular Patch Microstrip Antenna Cavity model

Figure 3.1 shows a simple configuration of probe fed circular microstrip antenna. a is the radius of the antenna, ρ is the probe location from the centre of the patch, t is the dielectric thickness, and ε_r is the dielectric relative permittivity. We know that a microstrip antenna can be considered as a cavity, with perfect electric conductor on top and bottom, and a perfect magnetic conductor on the side walls. In general the cavity can be modelled by an RLC circuit, while the stored energy inside the cavity determines its equivalent inductance and capacitance and the energy dissipated or radiated by the antenna determines its equivalent resistance.

Figure 3.2 shows the utilized circuit for the circular microstrip antenna,[16]. This is a parallel *RLC* circuit which resonates at the same resonance frequency as the microstrip patch, with the same input characteristics. R stands for three parallel resistors which are due to the imperfect dielectric substrate R_d, finite conductivity R_c, and radiation loss R_r:

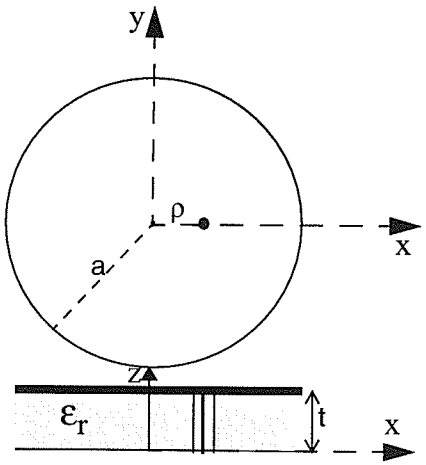

Figure 3.1: Geometry of circular patch microstrip antenna

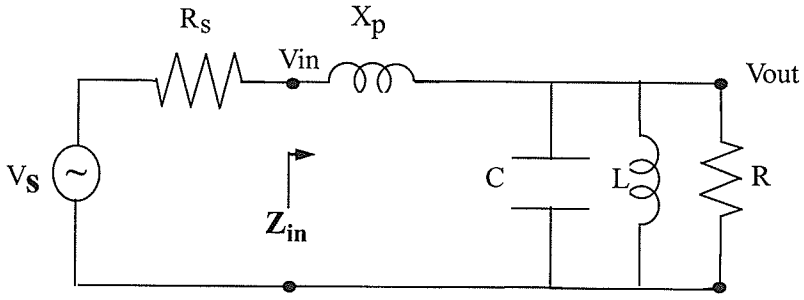

Figure 3.2: Cavity model of a circular microstrip antenna

$$R_t = R_r \| R_d \| R_c \tag{3-1}$$

Radiation resistance can be found from the following equation,[16]

$$Rr = \frac{V^2}{2p_r} = \frac{480}{(a_e k_o)^2 I_o} \times \frac{J_1^2(k\rho)}{J_1^2(ka)} \tag{3-2}$$

where $V = tE_o J_1(ka)$ and

$$I_0 = \int_o^{\frac{\pi}{2}} [\{J_2(k_o a\sin\theta) - J_0(k_o a\sin\theta)\}^2 + \cos^2\theta\{J_2(k_o a\sin\theta) + J_0(k_o a\sin\theta)\}^2]\sin\theta d\theta \quad (3\text{-}3)$$

and

$$R_c = \frac{V^2}{2P_c} = \frac{t^2 J_1^2(k\rho_o)(\mu\omega)^2}{6.609\times 10^{-7}\sqrt{f}} \quad (3\text{-}4)$$

$$R_d = \frac{V^2}{2P_d} = 0.2103\times 10^{-5}\frac{tf}{\tan\delta} \quad (3\text{-}5)$$

While R_r and P_r are indicating the radiation resistance and power, R_c and P_c are expressing the conduction resistance and power of copper and R_d and P_d stand for the dielectric resistance and power, respectively. a_e is the effective radius, and ρ_o is the probe position from the centre. J is the bessel function, k_o is the free space wave number, f is the operation frequency, μ is the permeability and $tan\delta$ indicates the dielectric loss tangent. The resonance frequency f_r, Quality factor Q, inductor L, and capacitor C, can be obtained from the following equations, [16]:

$$f_r = \frac{1.8412c}{2\pi a_e\sqrt{\varepsilon_r}} \quad (3\text{-}6)$$

$$Q_t = \left[\frac{1}{t(\pi f\mu\sigma)^{1/2}} + \tan\delta + \frac{t\mu f(k_o a)^2 I_o}{240\{(ka^2) - n^2\}}\right]^{-1} \quad (3\text{-}7)$$

$$L = \frac{R}{2\pi f_r Q_t} \quad (3\text{-}8)$$

$$C = \frac{Q_t}{2\pi R f_r} \tag{3-9}$$

where c is the velocity of light in a vacuum. A series inductor models the feed inductance X_p that is usually observed in a probe-fed microstrip antenna, shown in Figure 3.2. it can be written as shown in [25]:

$$Xp = \frac{120\pi ft}{c} Ln\left(\frac{c}{\pi f d_p \gamma_e \sqrt{\varepsilon_r}}\right) \tag{3-10}$$

where d_p is the probe diameter and γ_e=0.57721 [26] is Euler constant.

3.2.2. Transfer Function

Using Figure 3.2, one can observe that the transfer function of a probe fed circular microstrip antenna, $T=V_{out}/V_{in}$, is a second-order function with complex conjugate poles that can be written in the form of equation 2-22:

$$T = \frac{K}{1 + (j\omega)\frac{2\xi}{\omega n} + (j\omega)^2 \frac{1}{\omega n^2}} \tag{3-11}$$

where

$$\omega n = \sqrt{\frac{1}{C}\left(\frac{L_p + L}{LL_p}\right)} \tag{3-12}$$

$$\xi = \frac{1}{2R}\sqrt{\frac{1}{C}\left(\frac{LL_p}{L + L_p}\right)} \tag{3-13}$$

$$K = \frac{1}{(1 + L_p/L)} \tag{3-14}$$

Here, ωn is the resonance frequency and ξ is the damping ratio.

As an alternative approach, to prove the idea, a moment method solution is used to determine the transfer function phase of a circular microstrip antenna, (Figure 3.3a). It is computed using ENSEMBLE 6 when a= 5.112mm, t=1.6mm, and ρ=1.85mm. The results obtained from the software is modified using equation 2-19 where $\angle V_s = 0°$, R_s=50, $\angle V_{out} = FFP - 90°$ and Z_{in} is the input impedance of the antenna. This figure may be compared by Figure 2.10 with resonance frequency of 10GHz and $\omega n = 2\pi \times 10GHz$ where ξ=0.035 (obtained from equation 3-13 using antenna dimensions). It shows that, as expected, the phase of the transfer function of a circular microstrip antenna moves similar to that of second order function.

Figure 3.3b shows the return loss of the circular microstrip antenna obtained from ENSEMBLE. 6 Corresponding to Figure 3.3a, for a range of frequency with S_{11}<-10dB, 60 degrees of phase shift can be obtained. Therefore, one can expect to achieve the same phase shift behaviour by shifting the resonance frequency while operating frequency is constant, i.e. $\omega = 2\pi \times 10GHz$.

As a result, the transfer function is studied versus ωn as a variable instead of ω. Equation 3-11 is a function of three parameters, K, ξ, and ωn. Among these three parameters, K is constant and does not affect the output phase and ξ in the range of interest does not vary considerably, (Appendix I, Figures I.1, I.2, and I.3) and the only important parameter is ωn.

Figures 3.4a and b demonstrate the transfer function and S_{11} versus resonance frequency at 10GHz. This plot is achieved by using cavity model analysis written in Matlab code. In this study, the antenna dimensions for best impedance matching at 10GHz is used,

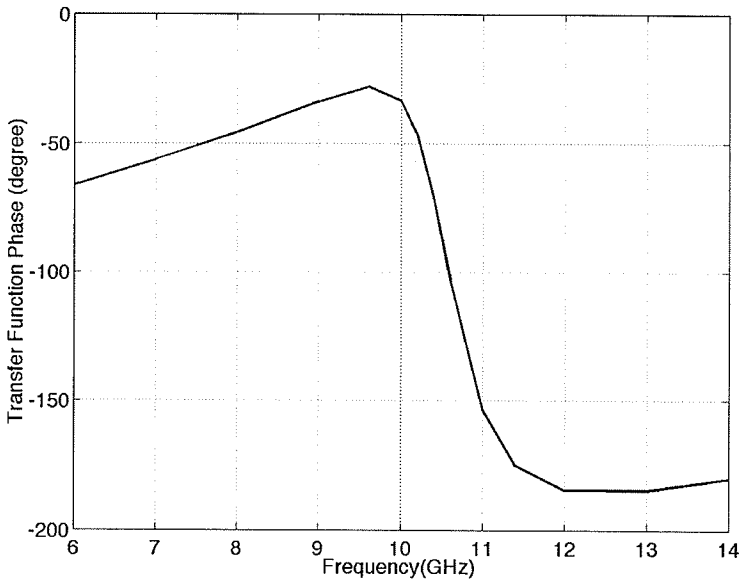

(a)

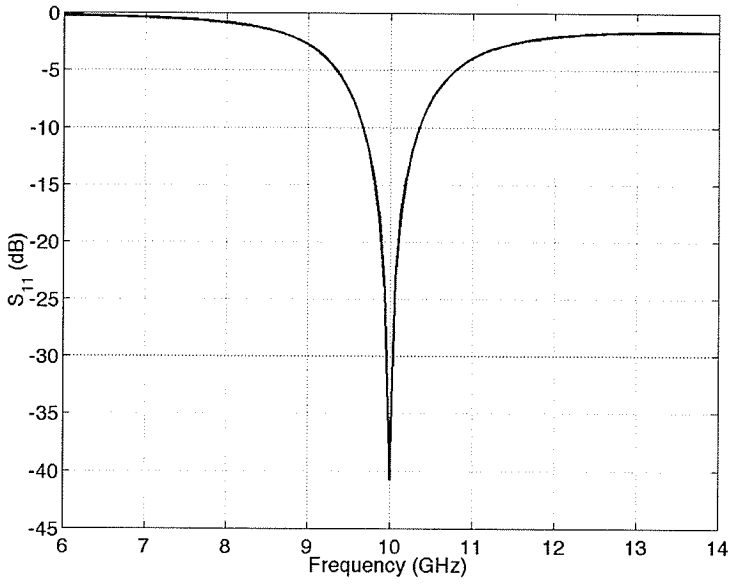

(b)

Figure 3.3: (a) Transfer function phase and (b) S_{11} for circular microstrip antenna achieved by MOM implemented by Ansoft-Ensemble 6, for a= 5.112mm, *t*=1.6mm, ρ=1.85mm and ε_r=2.5.

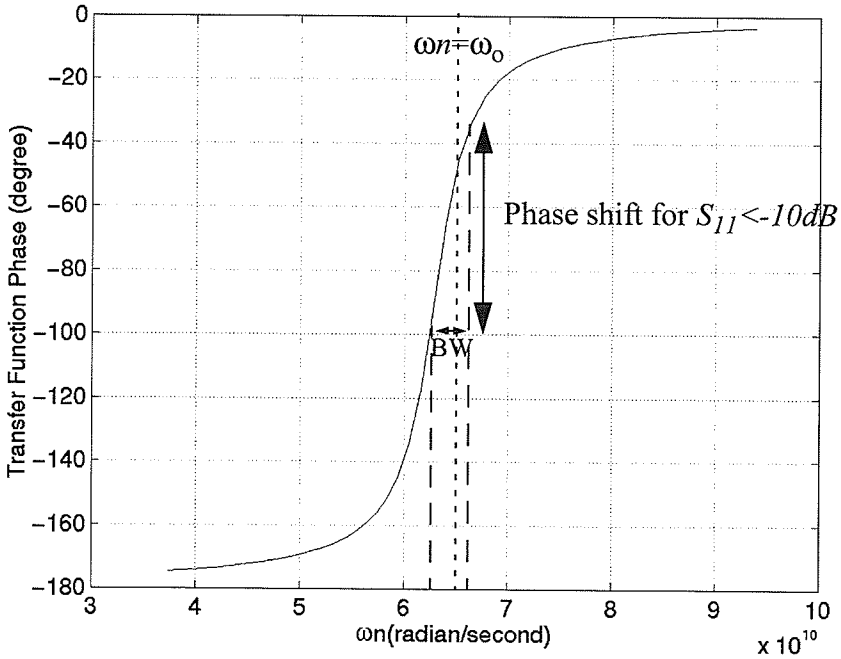

(a)

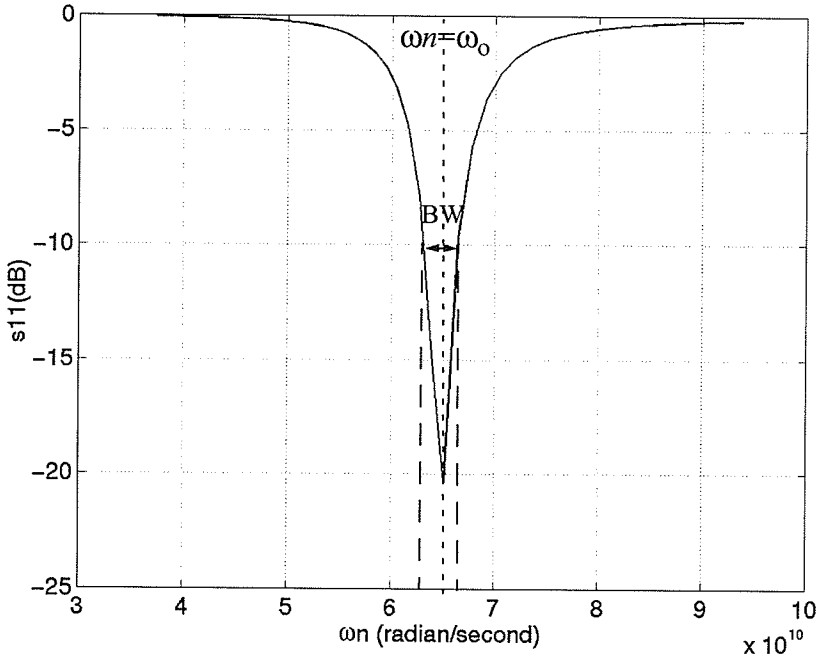

(b)

Figure 3.4: (a) Transfer function phase and (b) S_{11} versus resonance frequency ωn *where* a= 5.112mm, t=1.6mm, ρ=1.85mm, and ε_r=2.5 obtained by cavity model analysis.

a=5.112mm, t=1.6mm, ρ=1.85mm, and εr=2.5 where $\omega = 2\pi \times 10 GHz$, then, ωn is varied. Note that this cavity model gives slightly different resonance frequency of 10 GHz for the patch as compared with Figure 3-3b, determined by ENSEMBLE. In spite of the antenna narrow bandwidth, due to the sharp slope of the phase curve at the match point, up to 70 degrees (-100° to -30°) can be achieved with the desired input characteristics.

Looking back to Figure 2.7 and the probe-fed patch transfer function, due to the similarity of the circuit model and transfer function order, the same total amount of phase shift can be expected from the aperture coupled feed system without stub and proximity coupled feed. However, the edge feeding may show slightly different behavior.

3.3.Antenna Parameters

In the previous section, the transfer function in frequency domain was discussed and was found that by modifying the resonance frequency, a phase shift at given frequency, can be obtained. ωn may be changed by varying the antenna parameters, i.e. the cavity dimensions or probe location. In addition, in the frequency band of interest, the dependency of ωn on the radius of the patch, substrate thickness and probe position is approximately linear, (Appendix I, Figures I.4, I.5, and I.6). Therefore, one can expect similar range of phase shifts by varying any of these three parameters.

Figures 3.5, 3.6, and 3.7 show the effect of the patch radii, substrate thickness, and probe location variations on the far field phase, respectively. To plot these graphs, first, the

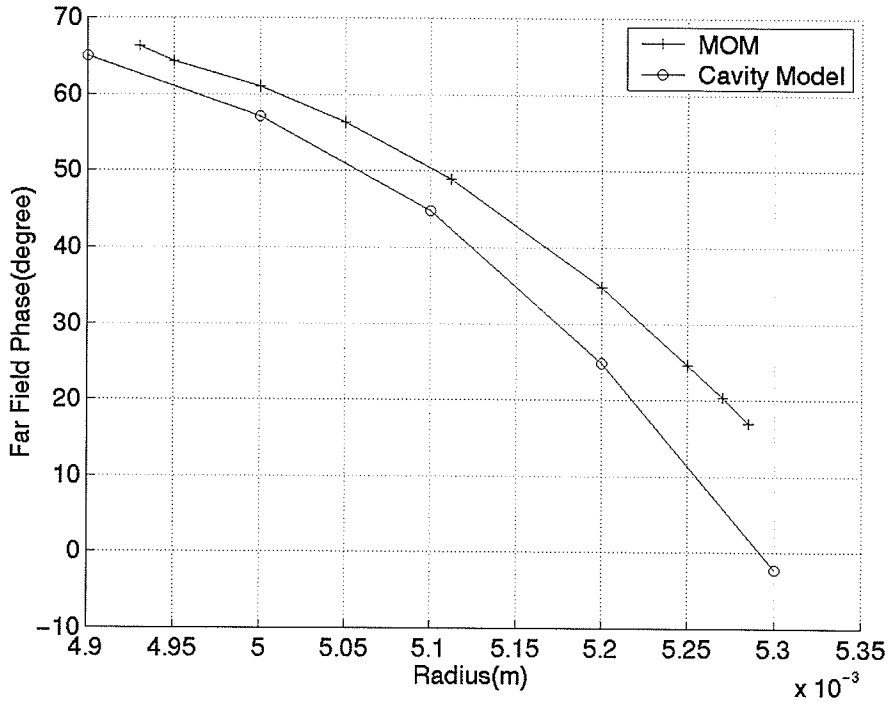

Figure 3.5: Far field phase of circular microstrip antenna versus radius when ε_r=2.5, t=1.6mm and ρ=1.85mm

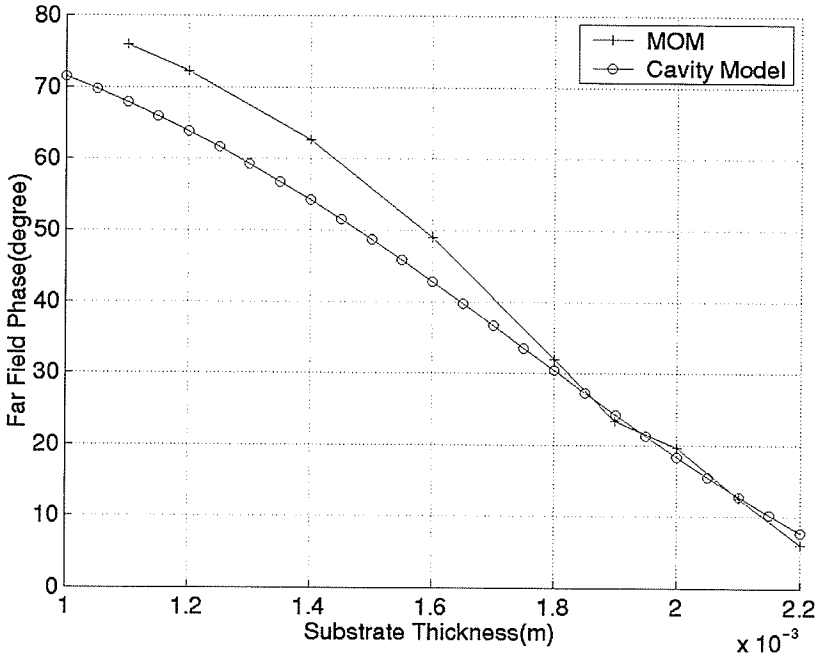

Figure 3.6: Far field phase of circular microstrip antenna versus substrate thickness when ε_r=2.5, a= 5.112mm and ρ=1.85mm

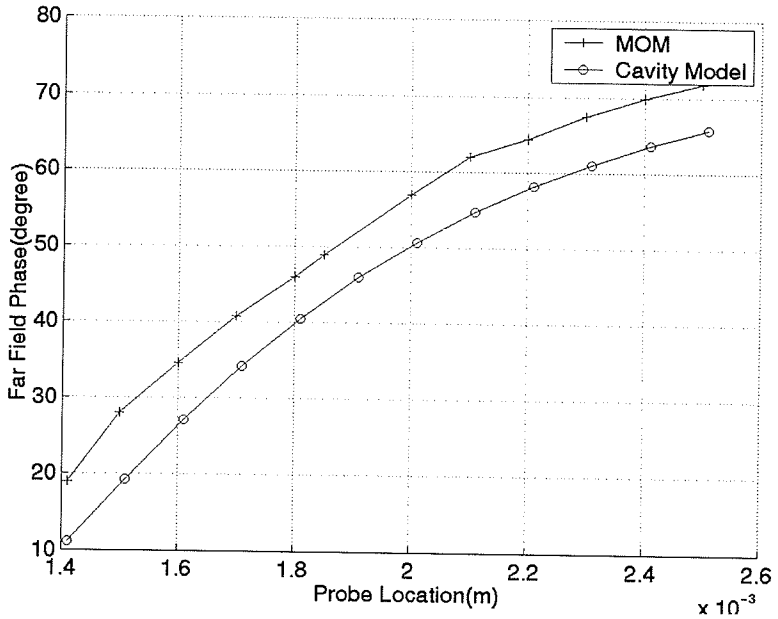

Figure 3.7: Far field phase of circular microstrip antenna versus probe location when ε_r*=2.5, a=5.112mm and t=1.6mm.*

antenna is matched at 10 GHz with 7% bandwidth (a= 5.112mm, t=1.6mm, ρ=1.85mm, and εr=2.5), then these three parameters are varied and the results at 10 GHz are sampled. It should be mentioned that for a thicker substrate, the surface wave excitation will increase and for a thinner substrate the bandwidth will reduce, and as a result, a smaller phase shift range will be achievable. In these figures, S_{11} is maintained at better than -10dB and further variation of the antenna parameters leads to serious input impedance mismatch.

Although the effect of each one of these parameters at the far field phase is almost similar, they change the input characteristics of the antenna differently. For the radius and probe location variations, antennas impedance location on the smith chart moves almost on an open loop. However, for the substrate thickness variation, the trend is a closer loop. The details are available in Appendix II.

3.4. Adding Shorting Pin and Stub

Shorting pins and matching stub can be used to modify the resonant frequency of the patch, or the input impedance. Their effects on the phase shift range are, therefore, investigated as well.

3.4.1. Shorting Pin

Lan and Sengupta [28] have described a technique for controlling the operating frequency of a rectangular and circular microstrip antennas using shorting posts at appropriate location within the antenna's boundary. Therefore, it will be interesting to use the shorting pin to shift the patch resonant frequency and achieve a phase shift.

In order to obtain the radiation fields of different resonance frequencies in the same polarization plane, shorting posts must be placed in the plane containing the probe and the patch axis. It has been shown that the existence of shorting posts produce pure inductive impedance in their equivalent model,[29]. Thus, by changing the number and position of the posts, the resonance frequency can be tuned over a wide range.

Figure 3.8 shows the circular microstrip antenna with one shorting pin located at the negative x end, in the opposite side of the feed probe location. The antenna is matched at 10 GHz by setting a= 5.55mm, t=1.6mm, ρ=2.1mm, ρ_s=–2.4mm and ε_r=2.5. Figure 3.9 shows the result of moving the shorting pin along the x-axis. It can be seen that although the shorting pin has good frequency shift ability, its performance at the far field is not as good as those of the antenna parameters.

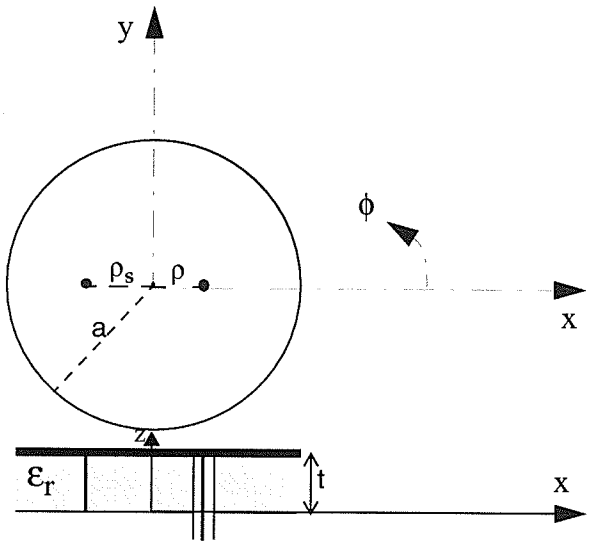

Figure 3.8: Antenna configuration with one shorting pin along the x axis.

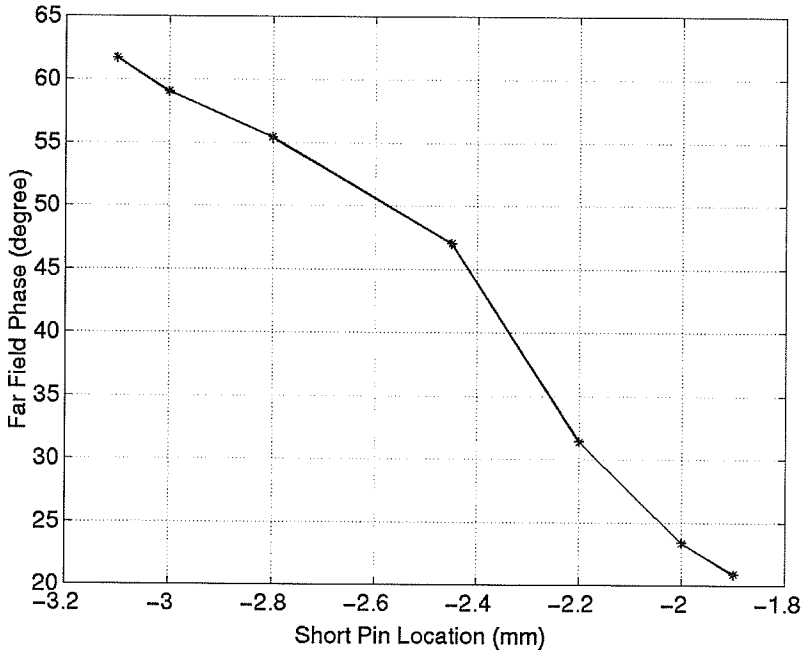

Figure 3.9: Effect of short pin location variation on the far field phase of a circular microstrip antenna while the short pin located along the x axis. The antenna dimensions are: a= 5.55mm, *t*=1.6mm and ρ=2.1mm.

3.4.2. Single Stub Matching

For matching a load to a transmission line, stub is applied frequently; more details in stub design can be found in reference [30]. A stub at the input of an antenna can be used not only to increase the bandwidth which in a sense utilizes more phase variation of Figure 3.3a, but also to add extra phase shift to the input of the antenna. In this section the effect of an open circuit single stub at the far field phase is investigated

An antenna is designed with a single stub to match a 50Ω line at 10GHz. The patch resonance is at a slightly higher frequency. Then, the patch radius and stub length are varied to shift the resonance frequency down to provide the maximum phase shift range.

Figure 3.10 shows the antenna configuration with a variable stub length (*SL*) and fix stub position (*SP*). To avoid coupling between stub and the patch, the feed system is located under the ground plane. A via is used to make the electrical connection between the line and the patch. The radius of the hole on the ground plane is equal to 0.4 mm while

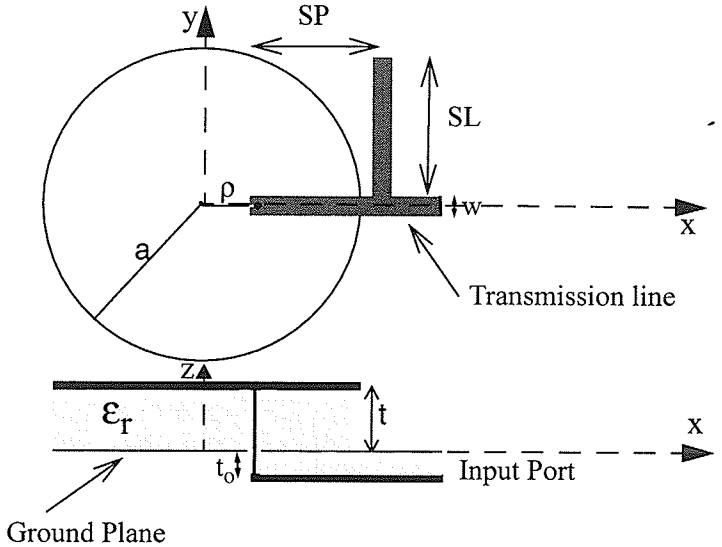

Figure 3.10: Circular microstrip antenna configuration with open circuit stub

the via radius is 0.33mm. It is worth mentioning that Ensemble assumes a line current source in the middle of the via with a zero radius. The transmission line characteristics impedance is 50 ohm, with a line width w=0.684mm, substrate thickness t_o=0.24mm and εr=2.5. The stub is positioned at SP=3.358mm away from the via and has the same width as transmission line, while its length is variable. The antenna parameters which are used at 10GHZ are εr=2.5, t=1.6mm, and ρ=1.65mm.

Figure 3.11 shows the far field phase variation of circular microstrip antenna, while its radius and the stub length are changing. Near to the patch resonance frequency,

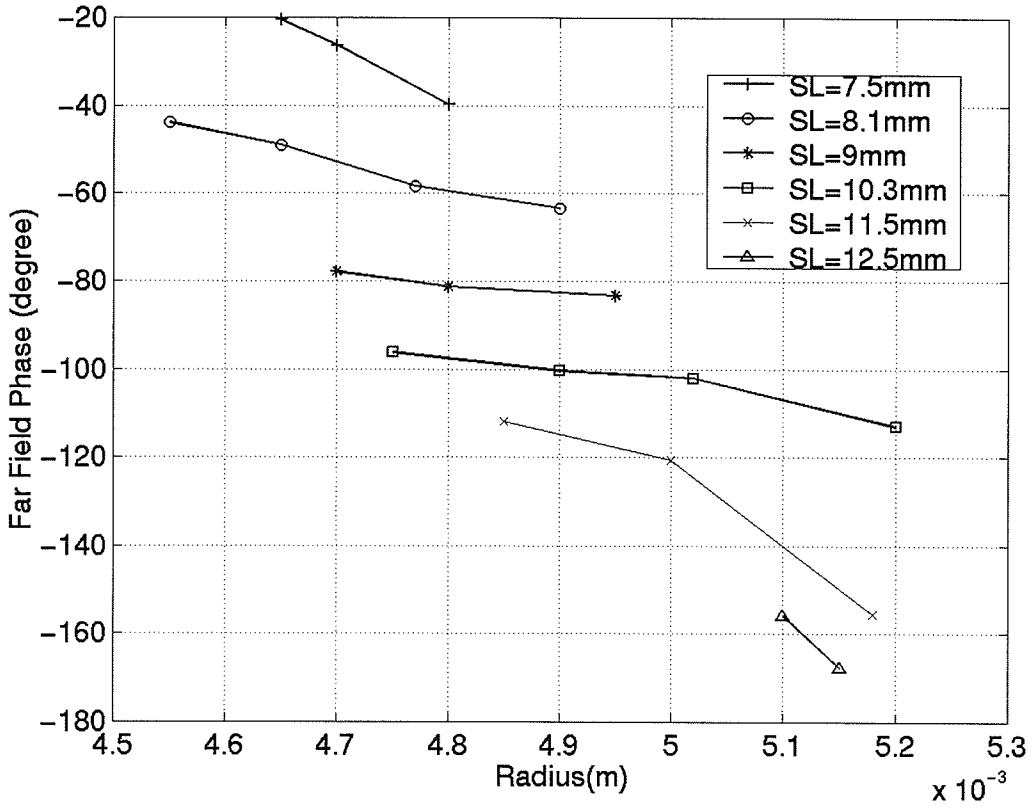

Figure 3.11: Far field phase shift of the circular microstrip antenna versus stub length, SL, and patch radius variation

when the length of the stub is around λ/2, the patch radius effect on the far field phase is more dominant than the stub length. However, away from the patch resonance while the antenna is matched by the stub, its length shows more effect. It should be mentioned that if the stub is used to match the antenna far away from the antenna resonance, due to the lower antenna directivity, it will face gain reduction problem.

3.5. Microstrip Array Design Using Proposed Technique

Having studied the phase properties of circular microstrip antenna, it seems logical to investigate its performance in a phased array configuration. For this reason, a four element linear phased array antenna is discussed. Two examples are considered. In the first one, the elements are fed separately, using synchronized independent sources. It is numerically investigated. In the second example, using transmission line power spliter, a feed system is designed, which provides more realistic beam scanning. Then, their performance is discussed.

3.5.1. Circular Microstrip Array with Ideal Synchronized Feeds

A four element array with an inter-element sapcing of λ/2 is selected. Equation 2-5 gives the required phase shift.

Figure 3.12 shows the array configuration with four elements and probe feeds. The operating frequency is 10 GHz and thus the inter-element spacing, s_x, is 15mm. From equation 2-5, to have about 4.8 degrees scan angle, the inter-element phase difference, β=15 degrees is required. Figures 3.5, 3.6, and 3.7 can be used to find the corresponding

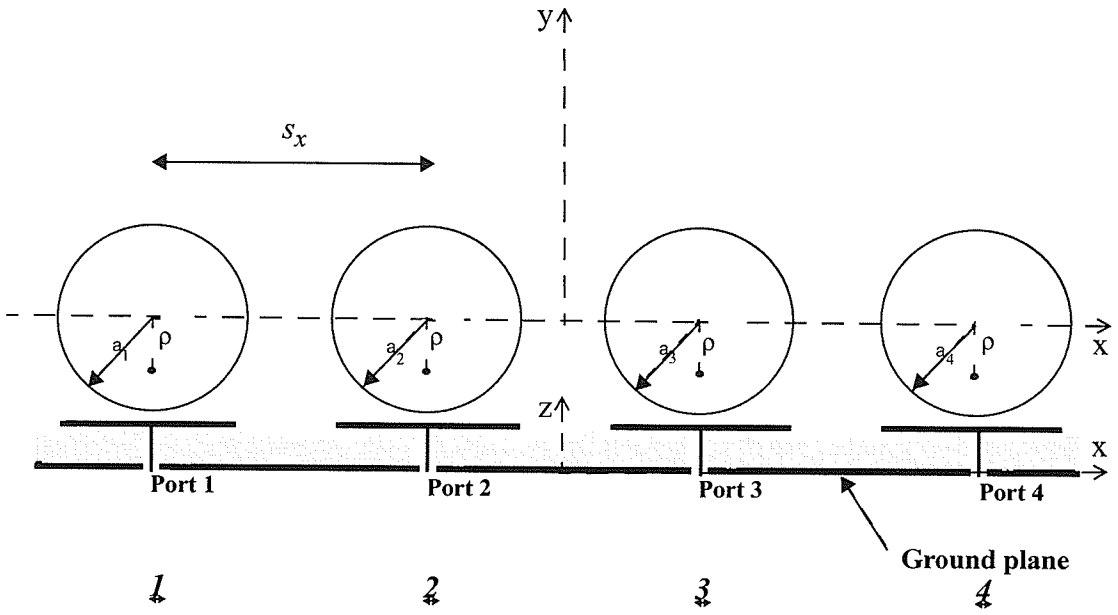

Figure 3.12: Four elements circular microstrip array configuration

Table .3: Details of the design parameters for Figure3.12 with t=1.6mm,ρ=1.85mm, and εr=2.5 to achieve 4.8degrees scan angle.

Antenna element	Radius (mm)	Individual element's far field phase (degree)	Ideal phase	S_{11} at 10GHz as an individual element (dB)	S_{11} at 10GHz in the array (dB)	Resonance Frequency of each element (GHz)
1	4.945	65.2	65	-10.7	-10.03	10.3
2	5.103	50.1	50	-36.96	-29.63	10
3	5.1985	35.07	35	-15.59	-13.63	9.82
4	5.271	20.09	20	-10.65	-9.3	9.7

dimensions of each circular patches to obtain the desired phase shift. In this design, different radii are used to achieve the phase shifts. According to Figure 3.5, by increasing the circular microstrip antenna radius, its far field phase reduces. In other words, the far field pattern due to the larger radius has a phase delay compared to the smaller ones. Consequently, for a 4.7 degrees clockwise beam scan angle, the radii must be a_1=*4.945mm,* a_2=*5.103,* a_2=*5.1985,* and a_4=*5.271,* Table3. Figure 3.13 shows its gain pattern, compared to a uniform four-element linear array. The dimensions for uniform array are: t=1.6mm, ρ=1.85mm, εr=2.5 and $a_1=a_2=a_3=a_4$=5.112mm with β=0 degree. It can be seen that the beam is scanned almost 5 degrees, which is in good agreement with the theory.

Figure 3.14 shows radiation patterns obtained using the MOM when the inter-element phase shift is 15 degrees. One of the curves is obtained by using the conventional

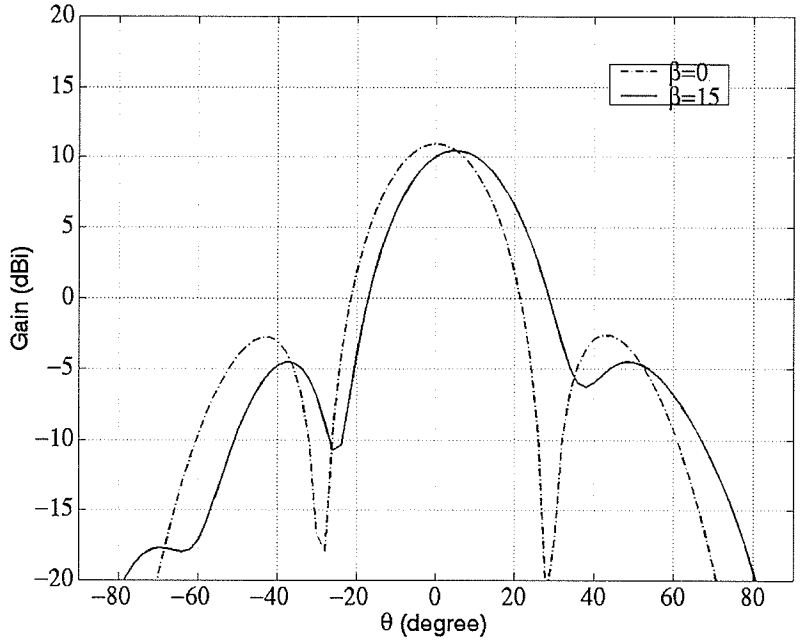

Figure 3.13: Radiation pattern of a linear four elements circular microstrip array for β=*0 with* $a_1=a_2=a_3=a_4$=*5.112mm and* β=*15 with* a_1=*4.945mm,* a_2=*5.103,* a_2=*5.1985,* and a_4=*5.271; the other parameters are t=1.6mm,* ρ=*1.85 and* εr=*2.5.*

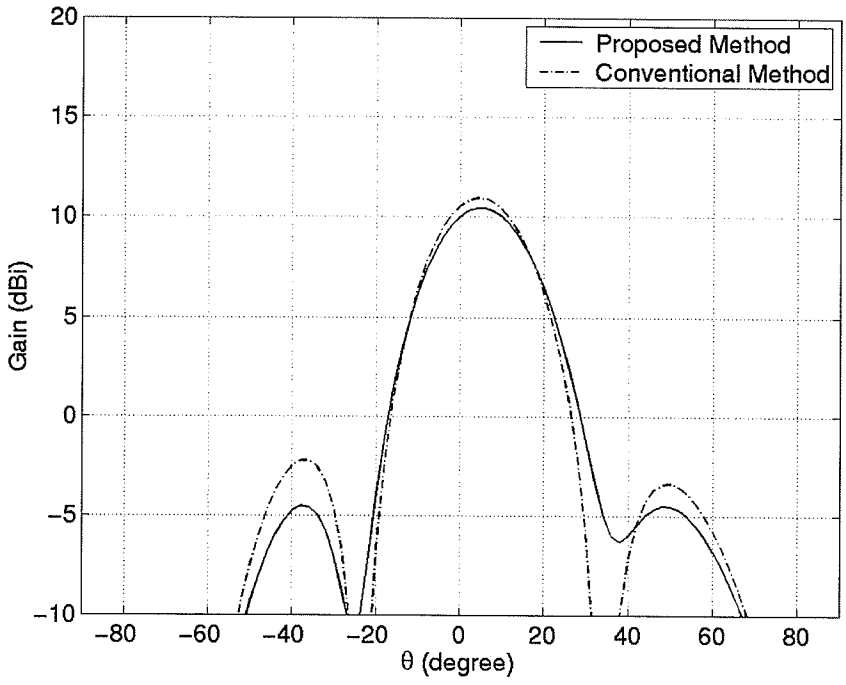

Figure 3.14: Radiation pattern of circular microstrip phased array when the inter-element phase shift is 15 degrees, utilized by the conventional method with uniform patches, $a_1=a_2=a_3=a_4=5.112mm$, and proposed method with $a_1=4.945mm$, $a_2=5.103mm$, $a_2=5.1985mm$, and *$a_4=5.271mm$; the other parameters are $t=1.6mm$, $\rho=1.85mm$ and $\varepsilon r=2.5$.*

method and implementing external phase shifts at the input of the elements. In this case, all patches are of the same size, $a_1=a_2=a_3=a_4=5.112mm$, $t=1.6mm$, and $\rho=1.85mm$, while the input phase decreases with 15 degrees step from left to right in Figure 3.12. To achieve the same pattern using the new method, the phase delay can be utilized by enlarging the patch radius. Thus, a_4, the largest patch introduces 45 degrees phase delay, compared to a_1, the smallest patch. Design details are represented in Table3. Results show good agreement in scanning angle.

Another issue in phased array antenna is its gain. By increasing the scan angle, the gain reduces slightly. According to Figure 3.14, the proposed method, gives about 0.5dB less gain as compared to the ideal phase shifting at the input port of the elements.

3.5.2. Circular Microstrip Phased Array with Feed System

In practice, symmetric excitation can be obtained by microstrip line power dividers. Wilkinson power divider is a common example to achieve equiphase-equiamplitude outputs. Its geometry is a hybrid junction with internally connected resistors to provide isolation between the output ports, [31]. In this section, a linear array of circular patches

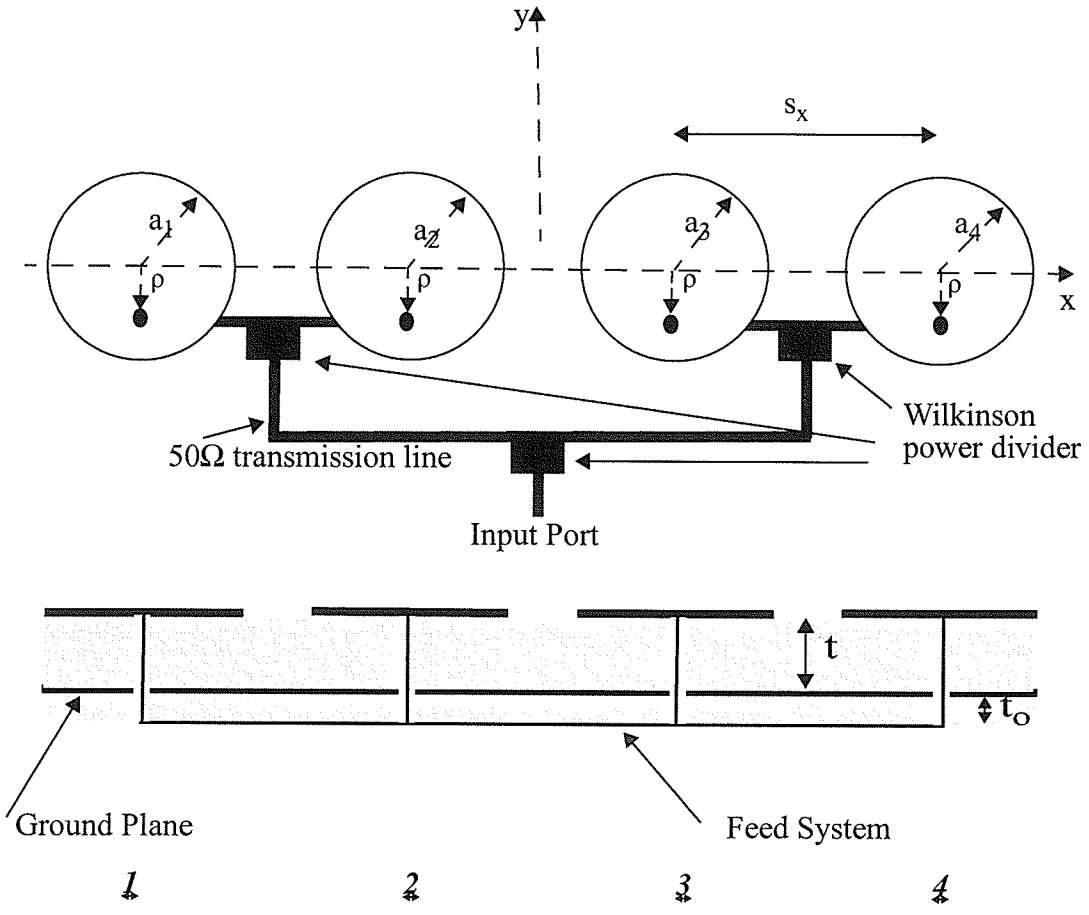

Figure 3.15: Circular microstrip linear array configuration with feed system

with its feed system constructed by Wilkinson power divider is investigated.

Figure 3.15 shows the array configuration with the feed system positioned below the ground plane to avoid coupling with the radiating elements. Three Wilkinson power dividers, connected by 50 ohm transmission lines, are used to split the power equally between the four antenna elements.

Figure 3.16 shows the results for the array presented in Figure 3.15. The required

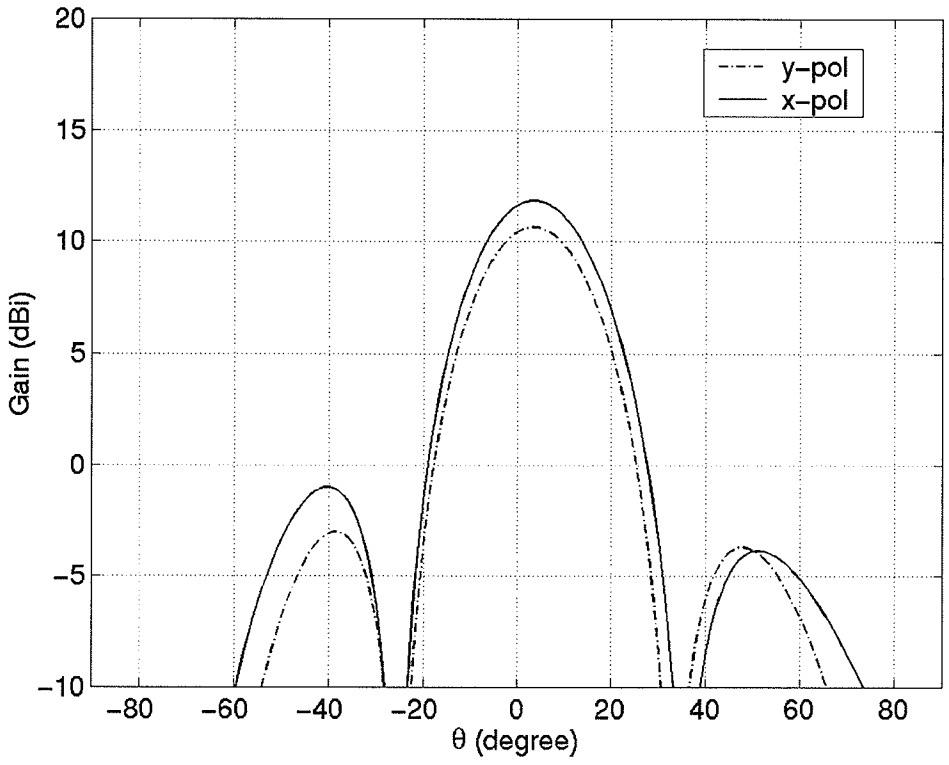

Figure 3.16: scanned beam of circular microstrip phased array for β*=15degrees, utilized by proposed method for both x- and y-polarized configurations,* a_1*=4.945mm,* a_2*=5.103,* a_2*=5.1985,* and a_4*=5.271; the other parameters are t=1.6mm,* ρ*=1.85 and* εr*=2.5.*

phase shift is generated by various radii for both *x*- and *y*-polarized elements. It shows a slightly better impedance matching performance, and higher gain for the *(x*-polarized array, S_{11}=-11.59dB for *x*-polarized while S_{11}=-9.5dB for *y*-polarized). The design dimensions are the same as Table3.

3.5.3. Bandwidth

As a single microstrip antenna, an issue of concern is the element impedance bandwidth (EIBW). This issue becomes more significant in the proposed technique for signal bandwidth (SBW) which can be defined as the range of frequency that the antenna element is matched for all the required phase shifts. In other words, SBW is a part of EIBW which is always matched for all the frequency shifts and depends only on the maximum amount of generated phase shift.

Figure 3.17 shows the S_{11} curves for three different patch sizes where substrate thickness is 1.6mm, the probe is located at 1.85mm from the centre of the patch and ε_r=2.5. The solid curve shows the return loss for a=5.112mm when the antenna is at its best match for 10GHz. It can be seen that its EIBW is about 7.5%. Shifting the frequency by varying the radius of the patch from 5 mm to 5.271mm (dashed curves in Figure 3.17) gives up to 45 degrees phase shift (Figure 3.5). SBW which is also shown in the figure for this phase shift is about 2%. One notices that to have a larger SBW, less frequency shift and so less phase shift can be used. To use all the 60 degrees phase shift, obtained in Figure 3.5, SBW is limited to a single frequency while to have the largest bandwidth SBW=EIBW, no inherent phase can be generated. Finally, It should be mentioned that SBW is an element bandwidth and does not depend on the array size.

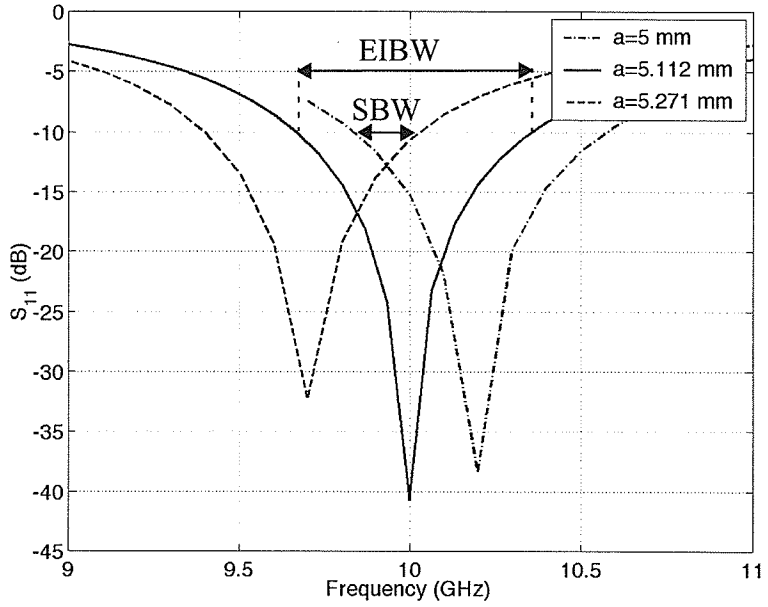

Figure 3.17: Return loss for three different patch sizes where t=1.6mm, Probe location=1.85mm from the centre of the patch and εr=2.5.

Using this 2% signal bandwidth and 45 degrees total phase shift at 10 GHz, four element phased array is designed where t=1.6mm, ρ=1.85, and εr=2.5, as shown in Figure 3.15. Different patch sizes are used to generate 15 degrees inter-element phase shift; a_1=5mm, a_2=5.103mm, a_3=5.1985mm, and a_4=5.271mm. Figure 3.18 shows the array return loss for each patch, including mutual coupling. Figure 3.19 shows each element's far field phase in terms of frequency while each element's return loss is less than -10dB. It does not include the effect of mutual coupling. β_1,β_2, and β_3 show the inter element phase shift of the patches. Figure 3.20 compares this phase shifts for SBW to a conventional phase shifter which is composed of a transmission line and generates 15 degrees phase shift at 10GHz.

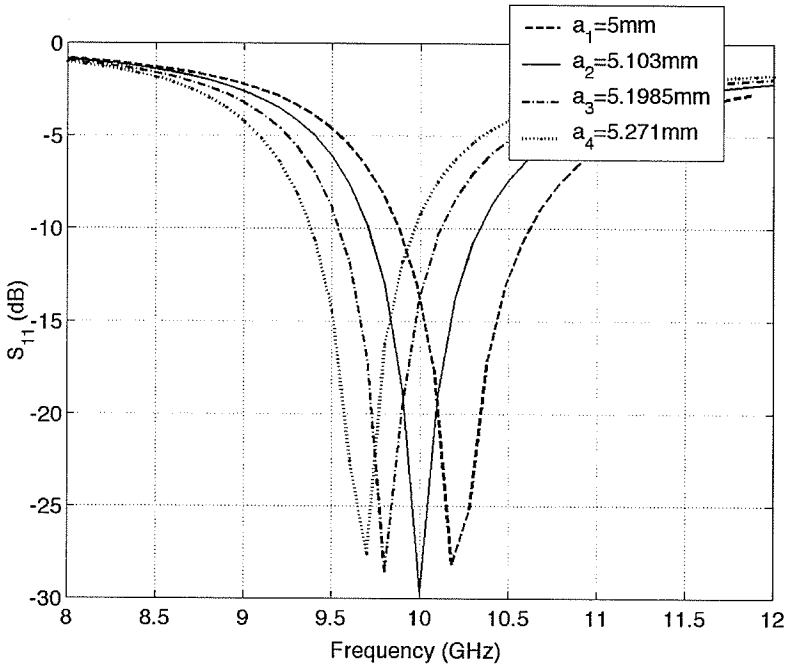

*Figure 3.18: Return loss for each patch in a four element circular microstrip array in terms of frequency (*t=1.6mm, ρ=1.85, and εr=2.5)

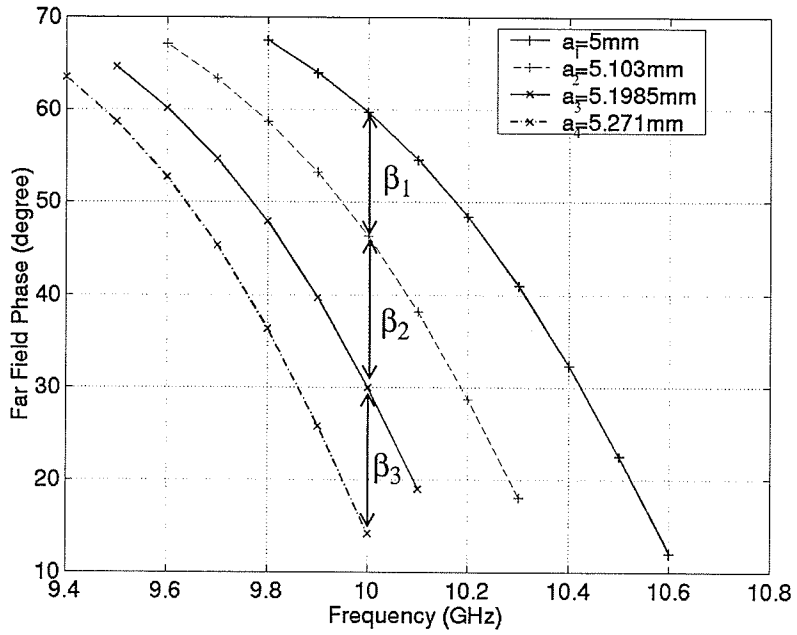

*Figure 3.19: Far field phase variation of each patch in a four element circular microstrip array in terms of frequency where S_{11}<-10dB (*t=1.6mm, ρ=1.85, and εr=2.5).

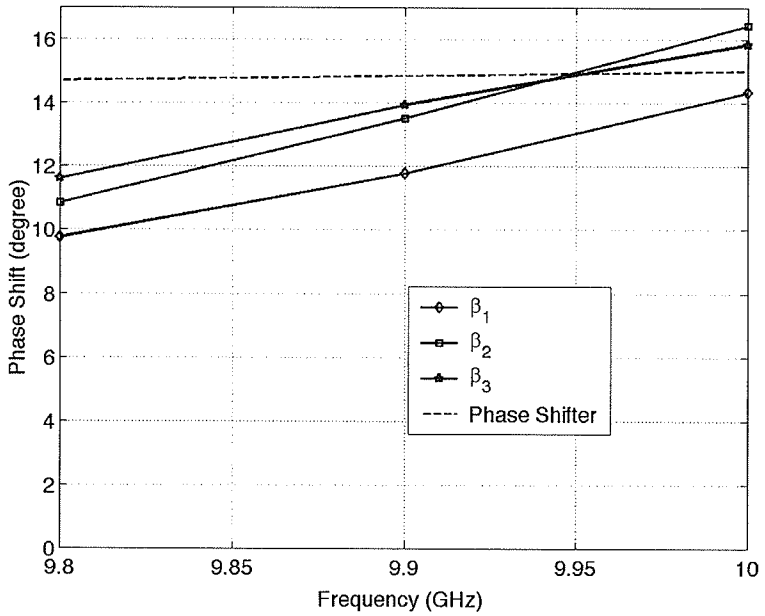

Figure 3.20: Comparison between the inter-element phase shift generated by proposed method (Figure 3.19) and conventional transmission line phase shifter.

Moreover, its array impedance bandwidth (AIBW) can be introduced as the range of frequency that total array S_{11} including all the elements is less than -10dB. Return loss for the same design is shown in Figure 3.21 with array impedance bandwidth of 6.1%. It is worth mentioning that over the SBW all the elements are always matched but for AIBW some of the them may not be. But the overall return loss is less than -10dB.

However, the scan angle and gain are not constant for the entire range of AIBW. Figure 3.22 shows the scan angle of the array over its AIBW with variation from 2.6° to 3°. The array gain in terms of frequency is illustrated in Figure 3.23 which varies between 10.54 dBi to 10.91dBi.

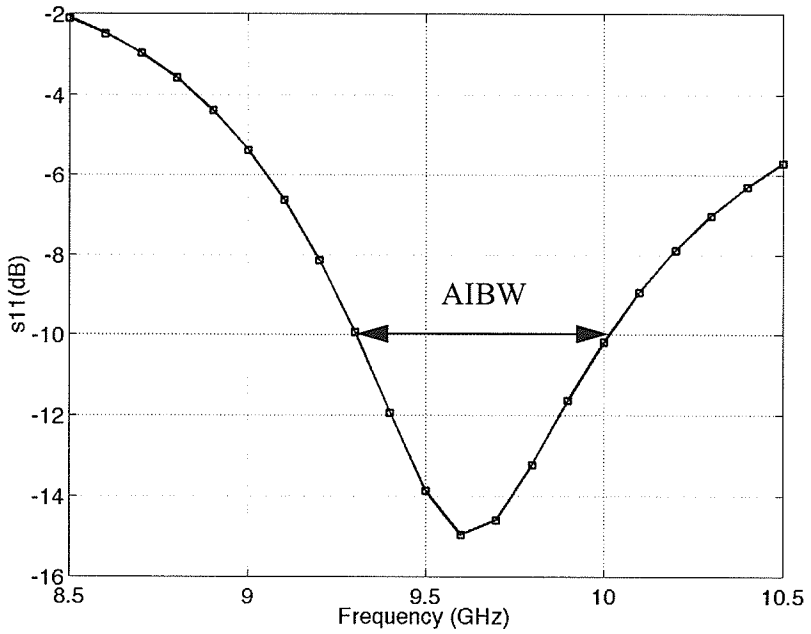

Figure 3.21: Return loss for four element circular microstrip linear phased array designed by the proposed technique where substrate thickness=1.6, probe location=1.85, er=2.5, a_1=5mm, a_2=5.103mm, a_3=5.1985mm, and a_4=5.271mm

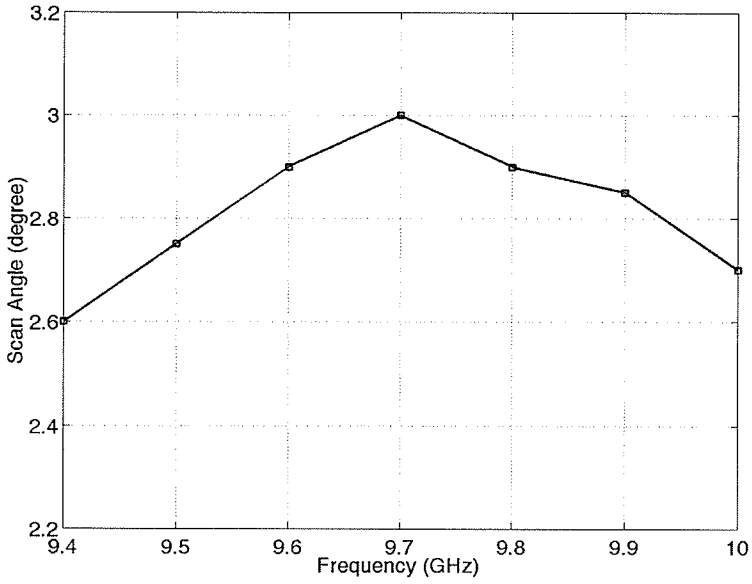

Figure 3.22: Scan angle for the frequency range of array impedance bandwidth, shown in Figure 3.21.

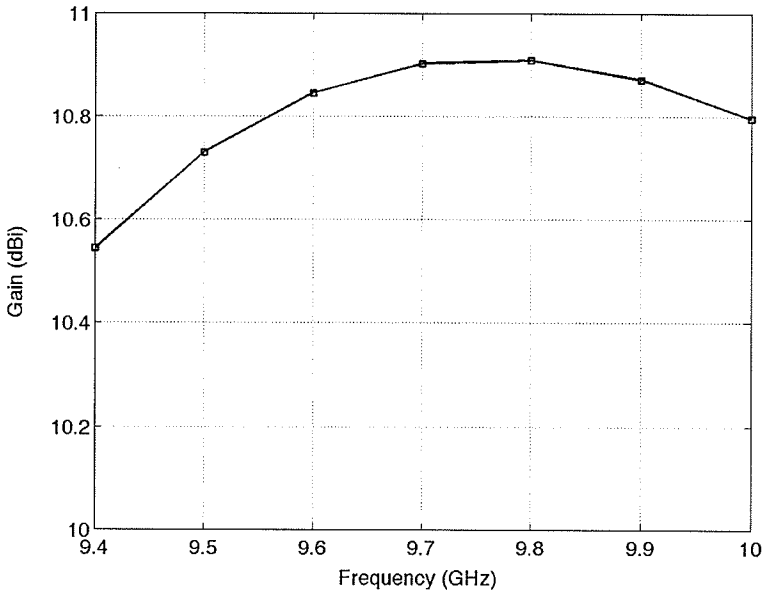

Figure 3.23: Array gain in terms of frequency over AIBW, shown in Figure3.21.

3.6. Summary

In this chapter, the theory presented in Chapter 2 was applied to circular microstrip patch antennas to generate its possible inherent phase shift for beam scanning.

The cavity model analysis was utilized and the transfer function expression of a single patch microstrip antenna was derived. Only up to 70 degrees out of 180 degrees of the inherent phase shift of the transfer function could be used due to the antenna input matching problems. Different techniques were suggested to change the phase at a fixed frequency, such as the antenna parameters variation or adding extra shorting pins and varying their location. To enhance the bandwidth of the antenna and utilize more phase shifts, an open circuit stub was also added to the input port and up to 150 degrees phase shift was

achieved.

The results obtained from reconfigurable disc were applied to a four-element linear phased array and a good agreement between this technique and conventional phase shifting at the antenna input was achieved. Both x- and y-polarized antennas were examined.To achieve larger scan angles, more phase shifts are required, which can be obtained by the help of digital phase shifters or extra transmission lines at the input with different insertion phases.

It should be mentioned that phased array designs using the proposed technique and variable heights needs more investigation. This is due to the fact that, the infinite substrate of the higher patches may load other elements unless they are truncated. And this can affect the far field phase shift of individual patches in array configuration.

Utilization of the technique on a single microstrip patch suffers from narrow bandwidth and insufficient phase shift of the antenna. To overcome these problems, an antenna configuration with more poles at the transfer function and wider bandwidth is required. Stacked microstrip antennas which have two patches and two resonance frequencies can be a good example to be investigated. This issue will be discussed in details at the next chapter.

Chapter 4

Stacked Circular Microstrip Antenna Phase Properties

4.1.Introduction

As indicated in the previous chapter, narrow bandwidth of microstrip patch antennas limits their useful bandwidth and the range of phase shift over the band using the proposed method. Therefore, it becomes important to develop broadband antennas so as to enhance the range of phase shift due to the microstrip antenna.

In the last decade, much progress has been made to broaden the bandwidth of microstrip antennas by adding a parasitic patch on top. Liu et al. [32] and Waterhouse [33] have investigated planar stacked patches to make broadband microstrip antennas. Waterhouse utilized a probe-fed stacked patch configuration, and obtained a bandwidth approaching 25%.

In this chapter, the proposed theory is applied to stacked circular microstrip antennas to obtain a better performance and larger far field phase shift. Its transfer function is studied and the far field phase achieved from ANSOFT-ENSEMBLE 6 is confirmed by the transmission line model analysis. The effect of different parameters such as the antenna dimensions, stub, and shorting pin are examined and an array configuration is studied.

4.2. Transfer Function of Stacked Circular Microstrip Antenna

As it is shown in Figure 4.1, a stacked circular patch microstrip antenna is composed of two slightly different sized circular discs. Through a proper choice of the two disc diameters and their spacings, two resonances can be found and adjusted to the desired values. Each resonance is due to one patch and can be expected to have almost the same performance as a single patch, [34]. When these two resonances are separated widely, the antenna becomes dual band. Bringing these two resonances close together a wide band antenna can be achieved.

Due to the fact that each complex conjugate pole in the transfer function indicates one resonance, increasing the number of poles can be expected from the stacked antenna configuration. Figure 4.2 shows the transfer function of stacked circular patches while the antenna resonates at 10GHz and 14GHz. This case corresponds to a dual band antenna and bringing those two resonances closer, a wide band antenna can be achieved. These results are obtained using a MOM solution by ANSOFT-ENSEBLE 6 and help of equation 2-19. In this design the dimensions are: lower patch radius a_1=5mm, upper patch radius a_2=6mm, substrate thickness t=0.8, spacing between two elements h=0.8mm, and the probe location, ρ=2.12mm from the centre of the patch. Substrate permittivity between the ground plane and the lower patch is εr_1= 2.5 and the material between the two patches is air εr_2=1.

It can be easily seen that there are two 180 degrees steps at the transfer function phase each one indicating one of the resonances. As a result, it is expected to obtain more

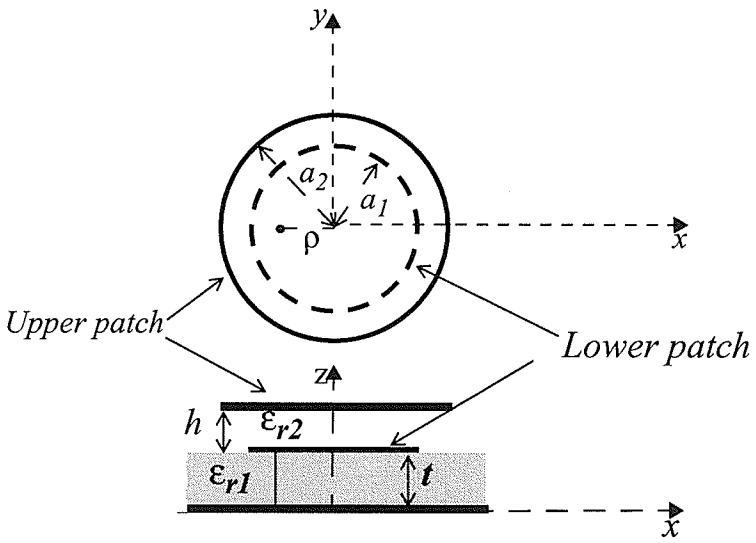

Figure 4.1: Stacked circular microstrip configuration

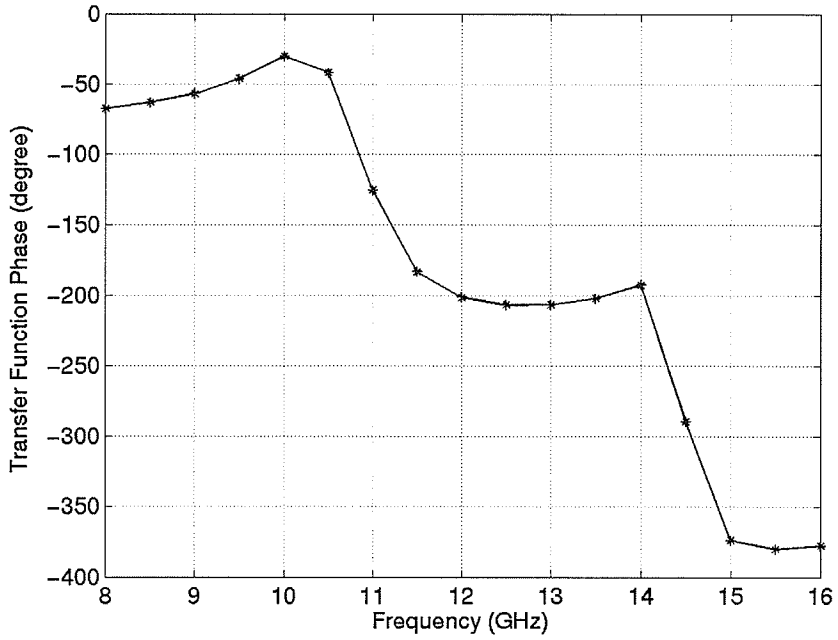

Figure 4.2: Dual band stacked circular microstrip antenna transfer function. The parameters shown in Figure 4.1 are as the following: a_1=5mm, a_2=6mm, t=0.8, h=0.8mm, and ρ=2.12mm

phase shifts than from one single patch, not only due to a larger total phase variation of the transfer function but also because of its extended bandwidth

4.3. Transmission Line Model

As an alternative choice to investigate the far field phase of the antenna, the transmission line model analysis of the stacked circular microstrip antenna is performed. The purpose of this section is to provide an analytical model of the electromagnetic-coupled stacked circular microstrip antenna fed by a coaxial probe, and compare it with the numerical results.

The proposed network model shown in Figure 4.3 is born from physical considerations via different analysis and from results developed by different authors, [25, 35]. It uses the transmission line method and reaction theorem and leads to the model for input impedance and far field phase in terms of frequency and antenna parameters, while the thickness of the substrate is assumed very small, $t \ \& \ h \ll \lambda$. The equivalent network consists of two parallel single patch circuit models operating at the fundamental TM_{11} mode and separated by a two port network, which represents the electromagnetic coupling between the two patches. The effect of mutual admittance is considered at the lower patch model.

A series inductor models the feed inductance X_p that is usually observed in probe-fed microstrip antennas. It is shown in equation 3-10, where t is the substrate thickness between the lower patch and the ground plane.

y_{in1} and y_{in2} in Figure 4.3, stand for the input impedance of the lower patch and upper patch with the ground plane, respectively. Bhattacharyya has represented a transmission line model for an annular ring microstrip antenna, [37], and has utilized the same model also for a circular patch [38]. The same model by some modifications is used for a stacked circular microstrip antenna in this section, as shown in Figure 4.4.

To obtain the model for either of discs and the ground plane, the antenna patches can be divided in two part, the outer part, $\rho<r<a_1$, and the inner part, $r<\rho$. The outer part can be considered to be a radial transmission line terminated by load admittance on its periphery, due to circular cylindrical radiating aperture of radius a_1, and the inner part is assumed to be a transmission line terminated at a very small loop at the centre of the patch ($r \rightarrow 0$), which does not affect the electric field distribution inside the antenna cavity. g, g_p, q, and q_p elements in the figure show the g parameters of the assumed transmission lines. y_1 is the admittance due to the first patch and ground plane and y_2 stands for the effect of the second patch and ground plane. In this figure, y_{s1} and y_{s2} are the wall admittances on the microstrip apertures due to the lower patch and upper patch, and y_{12} shows

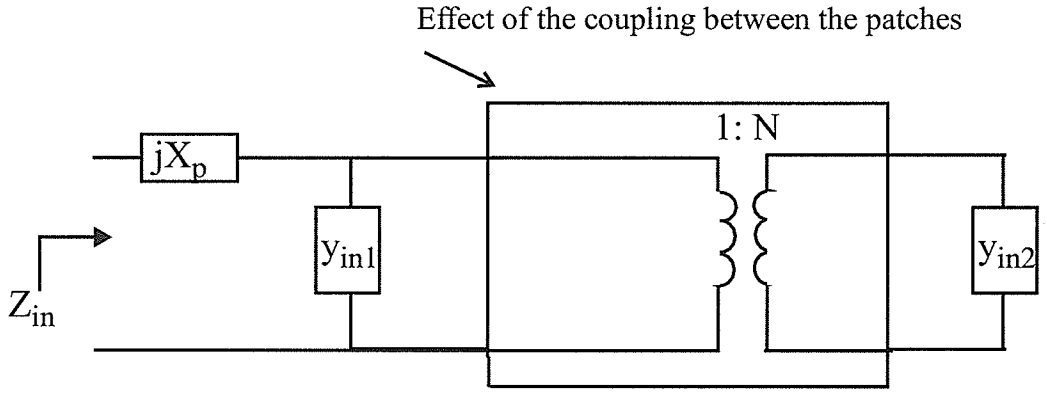

Figure 4.3: Equivalent network for circular stacked microstrip antenna.

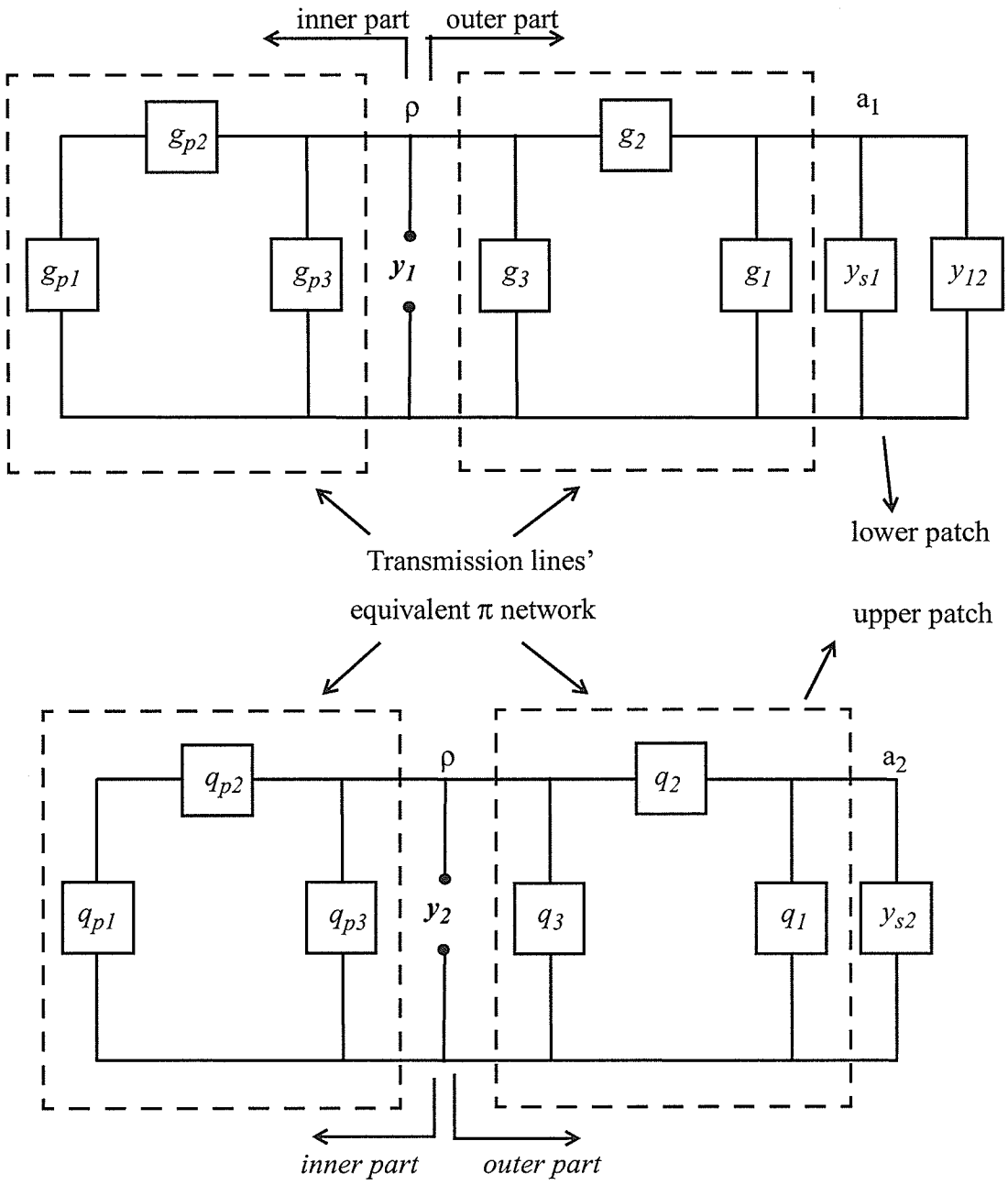

Figure 4.4: Equivalent circuit to obtain the first patch y_1 and second patch y_2 admittance in circular stacked microstrip antenna.

the mutual admittance between these two apertures

4.3.1. Transmission Line g Parameters

The assumed transmission lines between the antenna aperture and the probe location can be exchanged by their equivalent π network. g parameters of this network can be obtained from the admittance matrix, [37]:

$$\begin{bmatrix} I_{a1} \\ I_{\rho} \end{bmatrix} = \begin{bmatrix} Y_{11} & Y_{12} \\ Y_{21} & Y_{22} \end{bmatrix} \begin{bmatrix} V_{a1} \\ V_{\rho} \end{bmatrix} \tag{4-1}$$

with $I_{a1}=a_1 H\phi(a_1)$, $I_{\rho}=-\rho H\phi(\rho)$, $V_{a1}=E_z(a_1)$, and $V_{\rho}=E_z(\rho)$. The matrix element Y_{11} can be found from the following boundary condition:

$$Y_{11} = \left.\frac{I_{a1}}{V_{a1}}\right|_{V_{\rho}=0} \tag{4-2}$$

For the dominant mode, it can be found that:

$$Y_{11} = \frac{-jka_1}{\omega\mu}\frac{(J'_1(ka_1)Y_1(k\rho)-Y'_1(ka_1)J_1(k\rho))}{J_1(ka_1)Y_1(k\rho)-Y_1(ka_1)J_1(k\rho)} = \frac{-jka_1}{\omega\mu}\frac{\Delta_1(a_1,\rho)}{\Delta(a_1,\rho)} \tag{4-3}$$

where

$$\Delta_1(a_1,\rho) = J'_1(ka_1)Y_1(k\rho)-Y'_1(ka_1)J_1(k\rho) \tag{4-4}$$

and

$$\Delta(a_1,\rho) = J_1(ka_1)Y_1(k\rho)-Y_1(ka_1)J_1(k\rho) \tag{4-5}$$

similarly,

$$Y_{12} = \frac{2j}{\omega\mu\pi\Delta(\rho, a_1)} \tag{4-6}$$

where $\Delta(\rho,a_1)$ is defined in the same manner as $\Delta(a_1,\rho)$. It has been shown that $Y_{12}=Y_{21}$, [37]. The expression for Y_{22} is given by

$$Y_{22} = \frac{jk\rho}{\omega\mu}\frac{\Delta_1(\rho, a_1)}{\Delta(\rho, a_1)} \tag{4-7}$$

The elements of the *Y*-matrix which is obtained above, are used to determine the *g*-parameters of the π-network of Figure 4.4. The relationships are as follows:

$$g_2 = -Y_{12} \tag{4-8}$$

$$g_1 = Y_{11} + Y_{12} \tag{4-9}$$

$$g_3 = Y_{22} + Y_{12} \tag{4-10}$$

The expressions for g_{p1}, g_{p2}, and g_{p3} are obtained by replacing a_1 by ρ and ρ by a very small value, $\rho \to 0$.

Similar equations can be used to obtain the corresponding *g* parameters of the upper disc and the ground plane, named as *q* elements in Figure 4.4, while a_2 is replaced by a_1. ρ remains the same indicating that the second patch has fictitious probe located at the same co-ordinates. Physically, this means that the internal field distributions in the second cavity is very similar to that of the first one. The second cavity is partially filled with the dielectric and in order to account this inhomoginity, equivalent complex permittivity should be used in the above equations,[25]:

$$\varepsilon'_r = \frac{(t+h)\varepsilon_r}{h\varepsilon_r + t}$$

4.3.2. Self Admittance

The self admittance y_s is the wall admittance of the apertures on the disk peripheries, without considering the effect of mutual coupling. It can be decomposed into self-conductance g_s and self-susceptance b_s.

The expression for self conductance of the TM_{11} mode for the lower patch is given by, [37]:

$$g_{s1} = \frac{t}{2\eta_o}[(k_o a_1)^2 I_1 + I_2] \tag{4-11}$$

where

$$\eta_o = \sqrt{\frac{\mu_o}{\varepsilon_o}}$$

$$I_1 = \int_o^{\pi} [J'_1(k_o a_1 \sin\theta)]^2 \sin\theta d\theta$$

$$I_2 = \int_o^{\pi} \frac{cos^2\theta}{\sin\theta} J_1^2(k_o a_1 \sin\theta) d\theta$$

For the upper patch self admittance g_{s2}, a_1 and t in equation 4-11 should be substituted by a_2 and $(h+t)$, respectively.

The expression for wall susceptance b_s for the TM_{11} mode has been derived from the magnetic wall model [37]. The effective radius for a circular microstrip disc is used here to model the fringing effect. For the lower patch, it is given by

$$a_{1e} = a_1\left(1 + \frac{2tx}{\pi a_1 \varepsilon_r}\right)^{\frac{1}{2}} \tag{4-12}$$

where

$$x = \ln\left(\frac{a_1}{2t}\right) + 1.41\varepsilon_r + 1.77 + \frac{t}{a_1}(0.268\varepsilon_r + 1.65) \tag{4-13}$$

Consequently, the wall susceptance can be found from the following expression:

$$b_{s1} = -\frac{ka_1}{\omega\mu}[J'_1(ka_1)Y'_1(ka_{1e}) - Y'_1(ka_1)J'_1(ka_{1e})]/\Delta(a_{1e}, a_1) \tag{4-14}$$

For the upper patch susceptance b_{s2}, a_1, t, and ε_r in Equations 4-12 to 4-14, should be exchanged by a_2, $t+h$, and ε'_r.

4.3.3. Mutual Coupling

Effect of mutual coupling between two patches in the stacked microstrip antenna is shown by the coefficient N in Figure 4.3, and Y_{12} in Figure 4.4. N^2 shows the transformer power ratio from the second cavity to the first cavity [25], which is given by:

$$N^2 = \frac{t+h}{t} \tag{4-15}$$

The mutual admittance between the two apertures made by the upper patch and the ground plane, and the lower patch and the ground plane, can be found using the reaction concept [36]. Because t and h are much smaller than a wavelength, the magnetic current distributions of the apertures can be assumed as two circular radiating current sources separated by a distance h. Bhattacharyya has performed an analysis for mutual coupling

between two concentric, coplanar, circular radiating current sources for n=1 modes [39]. His solution which is based on the near field integration is modified to apply for two concentric circular current sources with a distance h in between:

$$y_{12} = \frac{ja_1a_2(t+h)}{2\pi^2\mu\omega}\int_0^{2\pi}\cos\phi\left[\int_0^{2\pi}\cos\alpha\left(\frac{e^{-jkr}}{r^3}\right)\times\{2\cos(\phi-\alpha)(1+jkr)\right.$$
$$+\frac{(a_1\cos(\phi-\alpha)-a_2)(a_1-a_2\cos(\phi-\alpha))}{r^2}\times(k^2r^2-3jkr-3) \qquad (4\text{-}16)$$
$$\left.+\cos(\phi-\alpha)\frac{h^2(k^2r^2-3jkr-3)}{r^2}\right\}d\alpha]d\phi$$

where a_1, a_2, t, and h are shown in Figure 4.1 and

$$r = [h^2+a_1^2+a_2^2-2a_1a_2\cos(\phi-\alpha)]^{1/2} \qquad (4\text{-}17)$$

It can be seen from the above that reciprocity holds, i.e. Y_{12}=Y_{21}. Thus, mutual admittance can be considered in parallel with the self admittance in the lower patch.

Now that y_s, y_{12} and g parameters in Figure 4.4 are found, y_1 and y_2 can be calculated. The calculated results show the impedance seen by the feed current, corresponding to the dominant mode and they are proportional to the height of the patches [37]. The impedance seen by the total feed probe current can be found as:

$$Z_{in1} = \frac{1}{y_{in1}} = -\frac{tE_z(\rho)}{I_o} = \frac{t}{\pi}\frac{E_z(\rho)}{I_1} = \frac{t}{\pi}\frac{1}{y_1} \qquad (4\text{-}18)$$

Here, I_1 is the feed current corresponding to the TM_{11} mode and I_o is the total probe current. similarly:

$$Z_{in2} = \frac{1}{y_{in2}} = \frac{t+h}{\pi}\frac{1}{y_2} \tag{4-19}$$

This model is programmed by Matlab for stacked circular microstrip antenna with dimensions as: a_1=5mm, a_2=6mm, t=0.8, h=0.8mm, εr_1=2.5, εr_2=1 and ρ=2.12mm from the centre. The results are compared to MOM that obtained by ANSOFT-ENSEMBLE 6. They are illustrated in Figure 4.5, and show good agreement. However, as the height of cavities increase the accuracy of the model decreases. It is due to the fact that in the procedure the cavity heights have been considered much smaller than a wavelength.

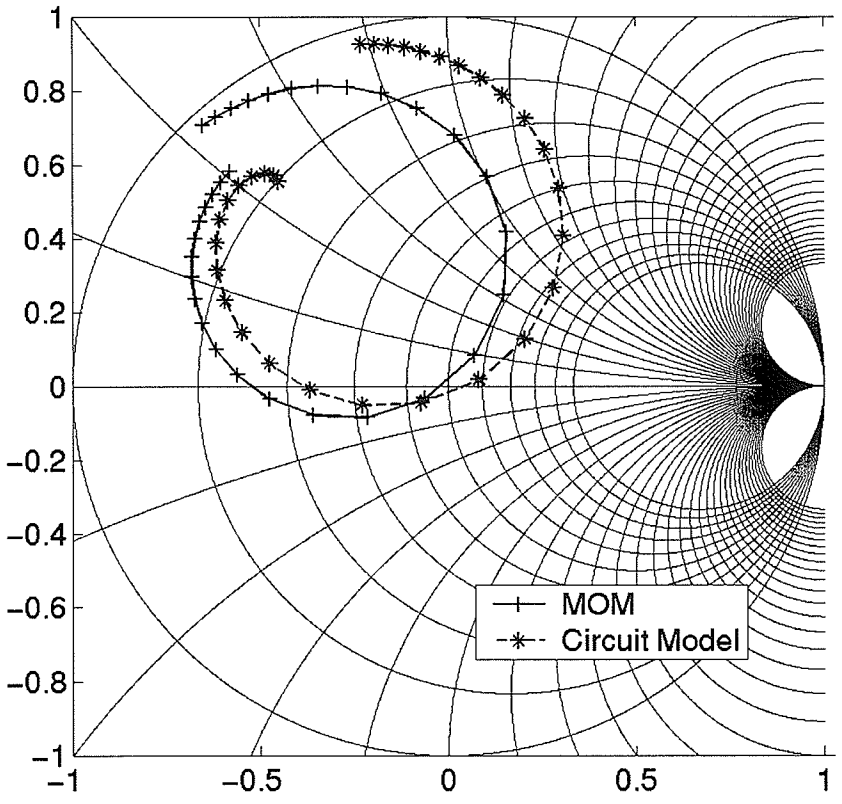

Figure 4.5: Input impedance of an x-band stacked circular patch antenna with a_1=5mm, a_2=6mm, t=0.8, h=0.8mm, εr_1=2.5, εr_2=1 and ρ=2.12mm

4.4.Effect of the Antenna Parameters on Far Field Phase

As it was discussed in previous chapters, the frequency shift leads to phase shift at the antenna far field. One technique to perform this, is to vary the antenna parameters. This is done in this section, and the effect of stacked circular microstrip antenna parameters on the far field phase variation in both dual band and wide band cases are investigated.

4.4.1. Dual band Stacked Antenna

There has been considerable interest in the development of dual-frequency microstrip antennas, because they are useful when the antenna is required to operate in two distinct frequencies. Figure 4.6 shows the return loss for dual band stack antenna while the first resonance is about 10GHz *and* a_1=5mm, a_2=6mm, t=0.8, h=0.8mm, and ρ=2.12mm. In this section, the far field phase variation of stacked microstrip antenna at its first band is investigated. It is performed by the MOM using ENSEMBLE 6 and transmission line model analysis. The second resonance frequency band is also expected to show similar performance but it has not been considered in this study.

In the transmission line model analysis, it is assumed that the radiation comes from the real part of the wall admittance of the second patch. In other words, the voltage phase on g_{s2}, considering the phase shift between the current and far field, indicates the far field phase of the actual antenna. Therefore, it is investigated with respect to the antenna parameters and the results are shown in Figures 4.7, 4.8, 4.9, 4.10, and 4.11. The initial dimensions are the same as Figure 4.6 with 4.5% bandwidth. Then, parameter is varied and the

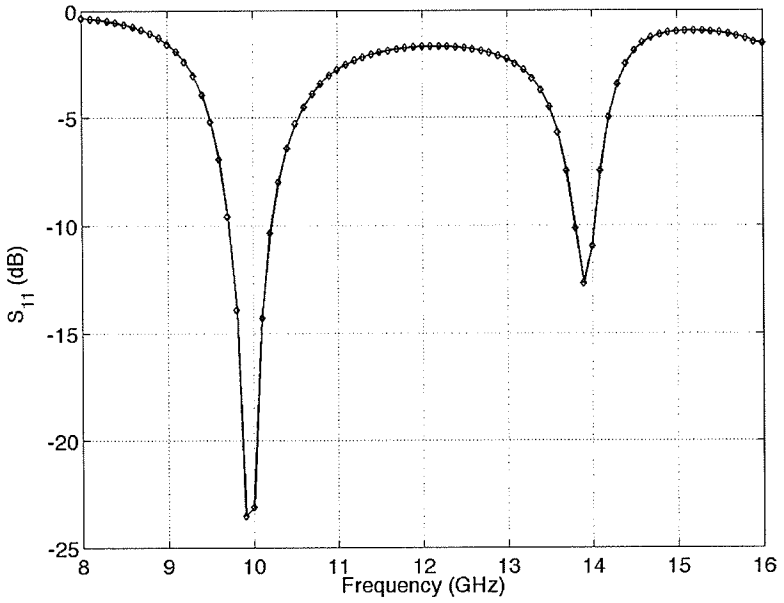

Figure 4.6: Return loss for dual band stacked microstrip antenna where a_1=5mm, a_2=6mm, t=0.8, h=0.8mm, and ρ=2.12mm.

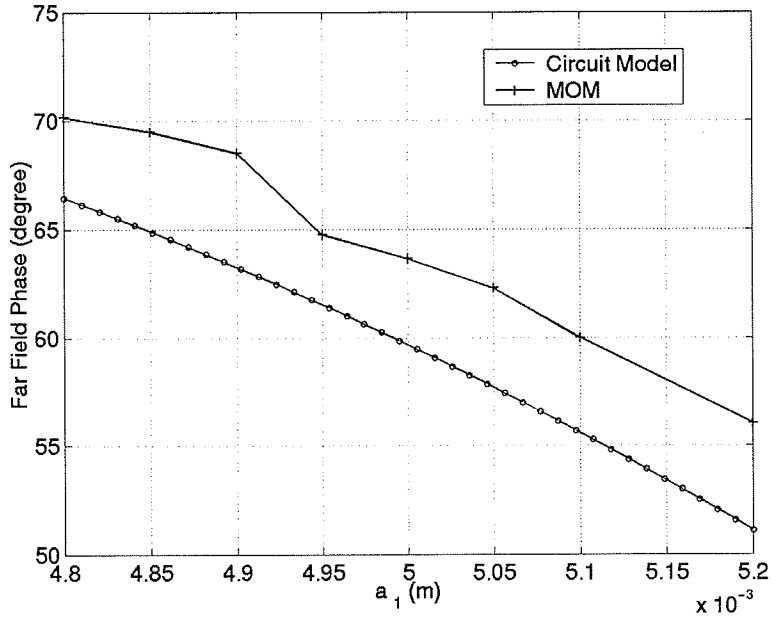

Figure 4.7: Effect of the lower patch radius variation at the far field phase for narrow band circular stacked microstrip antenna when a_2=6mm, t=0.8, h=0.8mm, and ρ=2.12mm

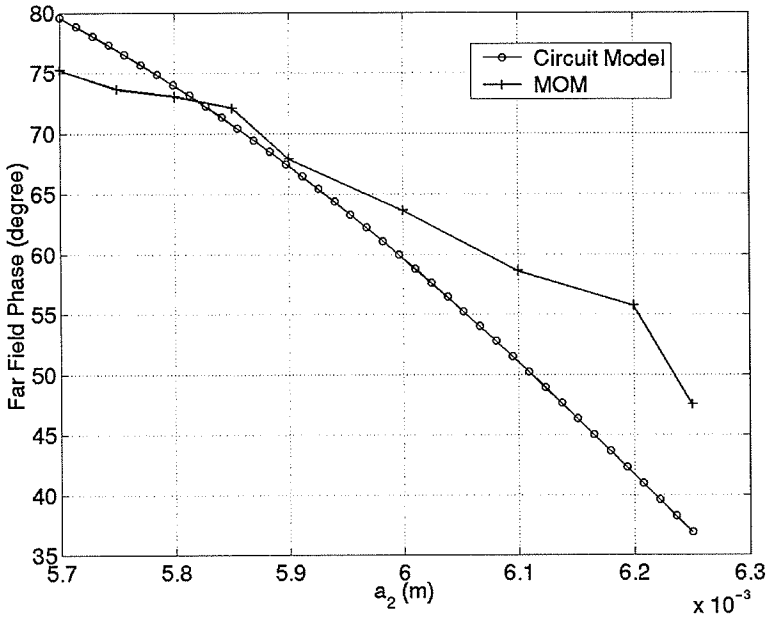

Figure 4.8: Effect of the upper patch radius variation at the far field phase for narrow band circular stacked microstrip antenna when a_1=5mm, t=0.8, h=0.8mm, and ρ=2.12mm.

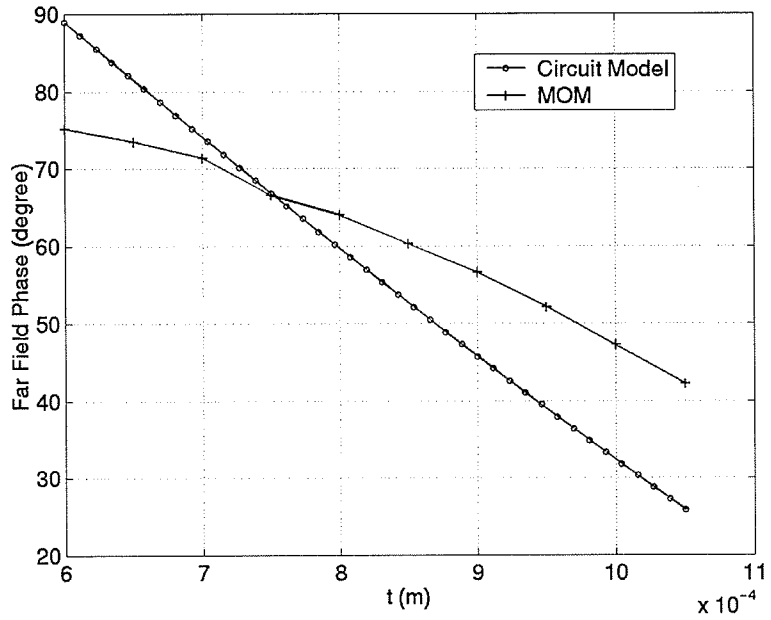

Figure 4.9: Effect of the substrate thickness variation at the far field phase of the stacked circular microstrip antenna when a_1=5mm, a_2=6mm, h=0.8mm, and ρ=2.12mm

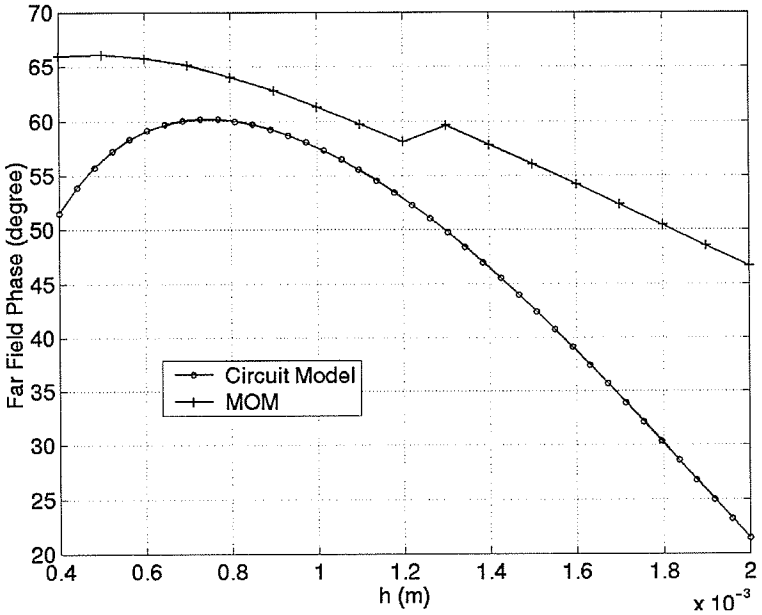

Figure 4.10: Effect of the separation variation between two patches at the far field phase of narrowband stacked circular microstrip antenna when a_1=5mm, a_2=6mm, t=0.8, and ρ=2.12mm

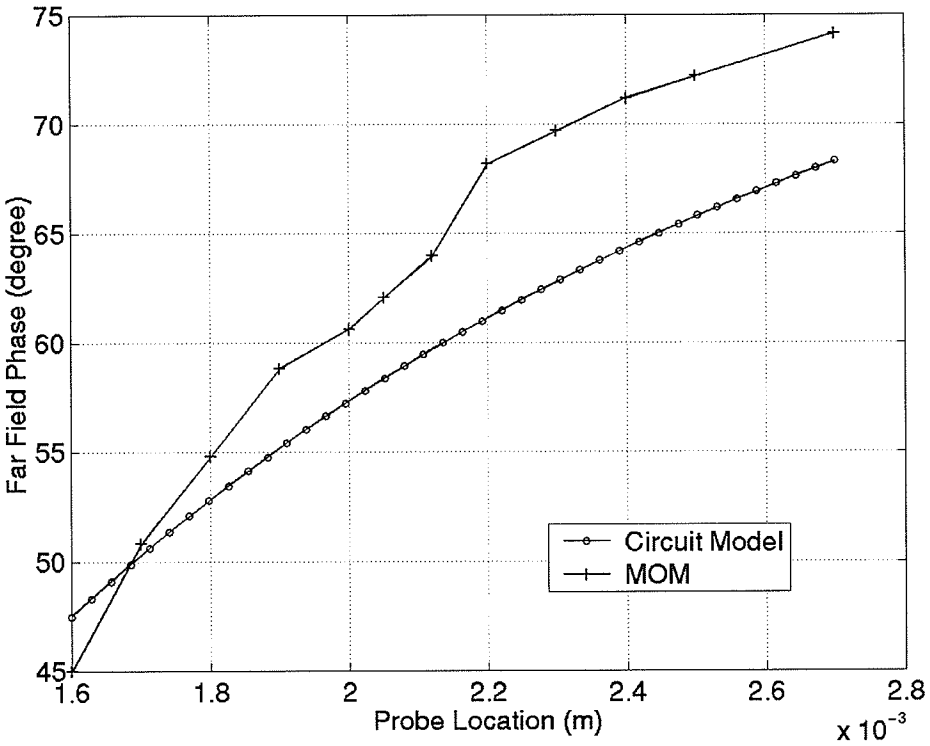

Figure 4.11: Effect of the probe location variation at the far field phase of narrow band stacked circular microstrip antenna when a_1=5mm, a_2=6mm, t=0.8, *and* h=0.8mm.

results are sampled at 10GHz. The method of moment is also used to confirm the results. It should be mentioned that for all the results the input impedance is in an accaptable range of S_{11}<-10dB and further variation in parameters leads to a significant mismatch problem.

By looking at the results, it is evident that although the total phase shift of the antenna is more than that of a single patch (Figures 4.2 and 3.3*a*), due to the narrower bandwidth of this design (4.5% in stacked patches as compared to 7% for a single one) only up to 35 degrees phase shift can be achieved. However, changing the design to obtain a wider bandwidth leads for achieving more phase shift.

It should be mentioned that when the upper patch becomes smaller than the lower one, its radius variation doesn't change the resonance frequency while it changes the input matching. Thus, no phase shift can be achieved by its variation.

4.4.2. Wide Band Stacked Antenna

Different stacked circular patch antennas with bandwidth larger than 25% were designed and used to investigate their phase properties. There are five parameters that can affect the far field phase. They are:

1. lower patch radius a_1
2. upper patch radius a_2
3. substrate thickness t
4. separation between the patches h
5. probe location ρ.

Several simulations were run to study the effect of these parameters on the stacked circular microstrip antenna far field phase. In summary, it can be deduced that the variation of the lower patch radius provides up to 50 degrees phase shift at the far field, while it resonates at 10GHz. The upper patch radius performs better results at the first resonance (up to 70 degrees). The distance variation between the second and first patches has the least effect on the far field phase and the most on the input characteristics. Therefore, by its variation the antenna easily becomes mismatch, but the far field phase does not change much (up to 20 degrees). Substrate thickness acts differently in various designs, in the best case up to 75 degrees can be achieved. Probe location variation also affects the far field and about 50 degrees phase shift can be obtained.

In stacked configuration, to have wide bandwidth, as shown in Figure 4.12, the

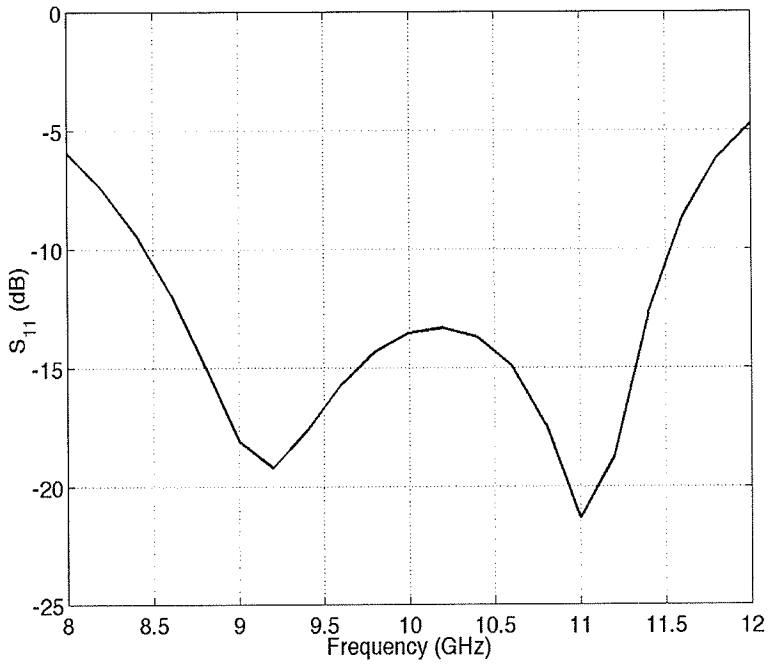

Figure 4.12: Return loss for wide band stacked circular microstrip antenna when t=2mm, h=3mm, a_1=5.75mm, a_2=6.2mm, ε_{r1}=2.5, ε_{r2}=1, and ρ=4mm for the configuration shown in Figure 4.1.

upper radius should be slightly larger than the lower one. Thus, when only one of themvaries the antenna may not any more operate in a wide frequency band. As a result, the available phase shift is limited to up to about 75 degrees. To overcome to this problem and using the entire bandwidth, more than one parameter variations are required. It means that to obtain a good phase shift at a fixed frequency, resonance needs to be transferred from one patch to the other. This can only be done by controlling both disc radii. Figure 4.13 shows the far field phase variation in terms of both radii, while the other parameters are:

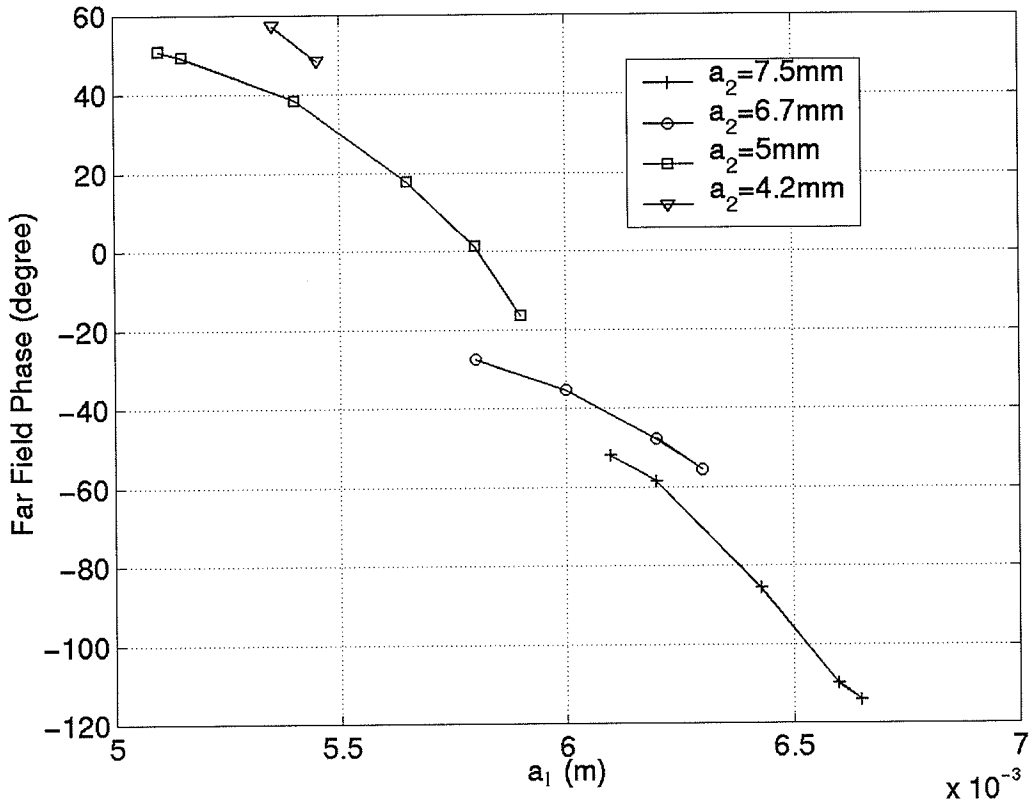

Figure 4.13: Far field phase shift of circular stacked antenna in terms of lower patch radius, a_1, and upper patch radius, a_2 when t=2mm, h=3mm, and ρ=4mm.

$t=2mm$, $h=3mm$, and $\rho=4mm$ (from the centre of the patch). Dielectric constant between the first patch and ground plane is 2.5 and the second patch located on a foam with $\varepsilon_r=1$. The second resonance frequency of the antenna is matched at 10GHz with 31% bandwidth. Then, the first patch radius is varied to achieve the phase shift, and at the same time the second patch radius is changed to help the antenna match as the frequency shifts. It can be seen that up to 180 degrees phase shift is obtained.

As a result, by adding a single digit phase shifter to the antenna, or two transmission lines with 180 degrees phase difference, one complete phase loop of 360 degrees can be achieved and used in phased array antennas.

4.5. Adding Shorting Pin and Stub

In this section, other alternatives for shifting the resonance frequency and obtaining wider band antennas which are shorting pins and stubs, are studied.

4.5.1. Shorting Pin

Shorting pins have been used to achieve not only frequency shifts, [28], but also to increase the stacked microstrip antenna bandwidth, [40]. Figure 4.14 shows a stacked microstrip configuration with a short circuited pin in the feed probe plane, passing through both patches. The pin gives an extra degree of freedom in the design of antenna and it allows to control the input impedance and far field phase. The shorting pin can be illustrated by an extra inductor in the circuit model which changes the resonance frequency by its variation.

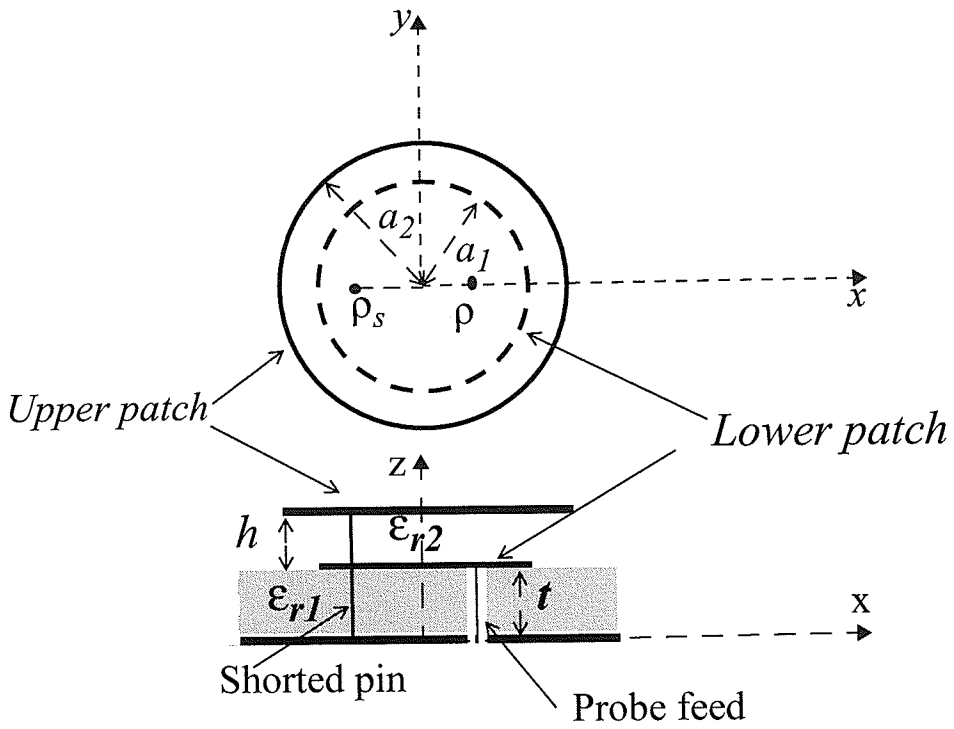

Figure 4.14: Shorted stacked circular microstrip antenna configuration.

Figure 4.15 shows the results for a shorted stacked circular microstrip antenna far field phase variation in terms of the shorting pin location. The antenna first was matched at 10GHz, then the shorting pin location was varied. The antenna dimensions at the match point are: a_2=*6.35mm*, a_1=*5mm*, *t=1.6mm*, *h=1mm*, ε_{r1}=*2.5*, ε_{r2}=*1*, ρ=*3.7mm*, and the shorting pin location ρ_s=-2.5 *mm*. It can be seen that, only up to 40 degrees can be achieved and further variations cause the antenna mismatch. However, more investigations on multi-pins are required.

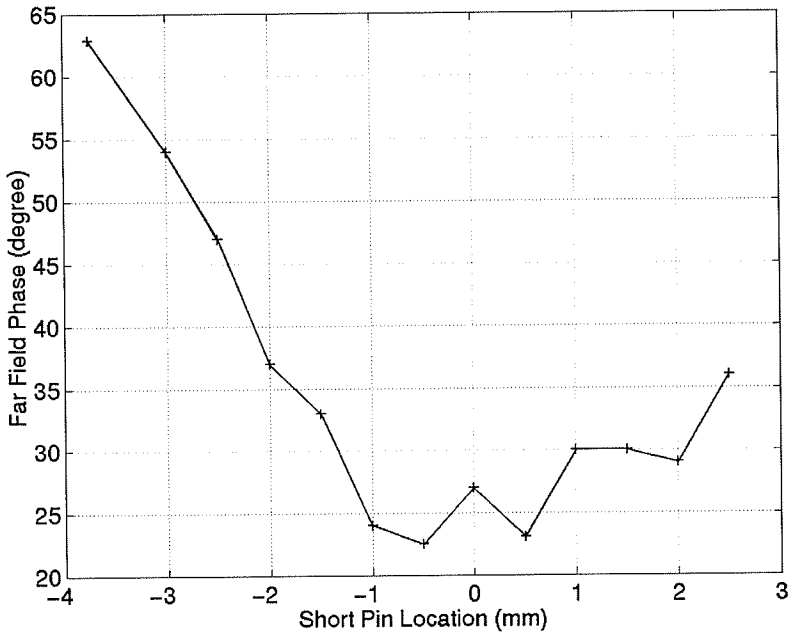

Figure 4.15: Effect of the short pin location variation of the far field phase for Figure 4.14, when t=1.6mm, h=1mm, a_1=5mm, a_2=6.35mm, ε_{r1}=2.5, ε_{r2}=1, and ρ*=3.7mm.*

4.5.2. Single Stub

There are two different kinds of stubs, the frequency control and impedance matching stubs which are shown in Figure 4.16 and 4.17. The effect of variation of each of them at the far field phase are investigated.

Figure 4.18 shows the far field phase in terms of the matching Stub Length "*SL*" variation at 10 GHz, while a_1=*5.5mm,* a_2=*6.1mm,* t_o=*0.24mm, t=2mm, h=3mm,* ε_{r1}=*2.5,* ε_{r2}=*1,* Stub Position "*SP*"=1.85mm from the feed probe, stub width=0.684mm, and the ρ=4mm. The obtained phase shift is about 65 degrees. A similar process for the frequency control stub is performed and shown in Figure 4.19. The initial dimensions are the same as

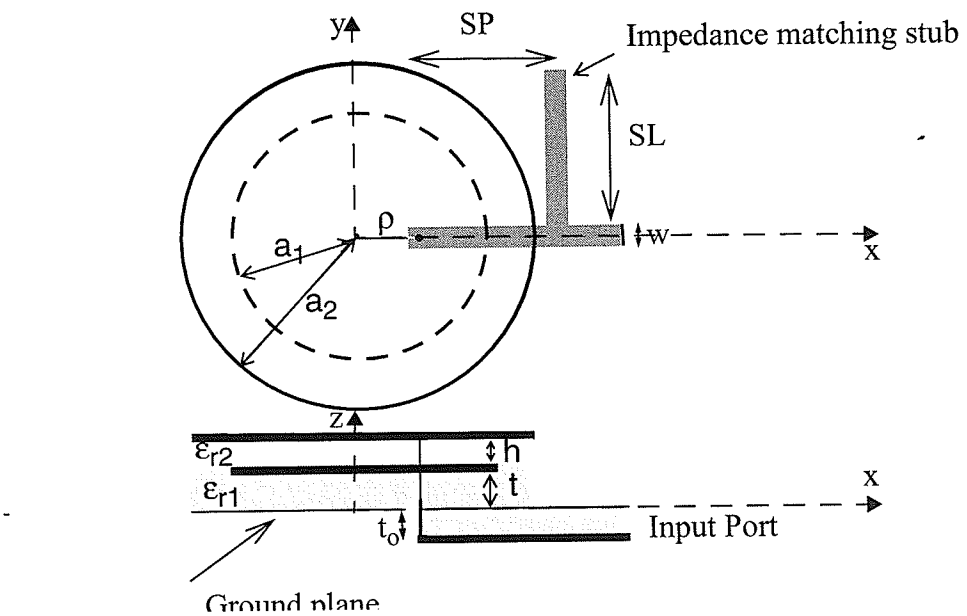

Figure 4.16: Stacked circular microstrip antenna configuration with open circuit impedance matching stub.

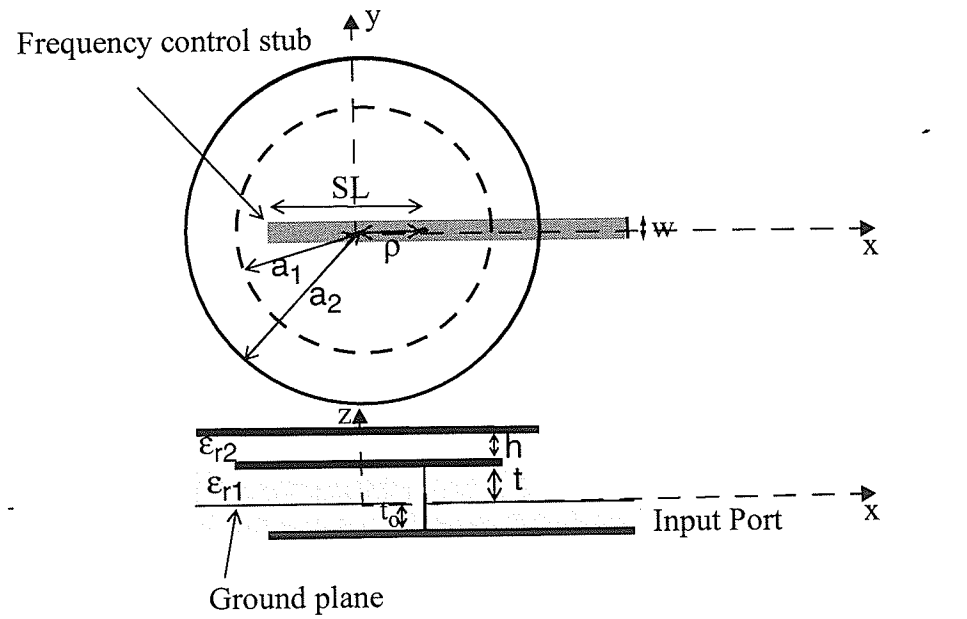

Figure 4.17: Stacked circular microstrip antenna configuration with frequency control stub

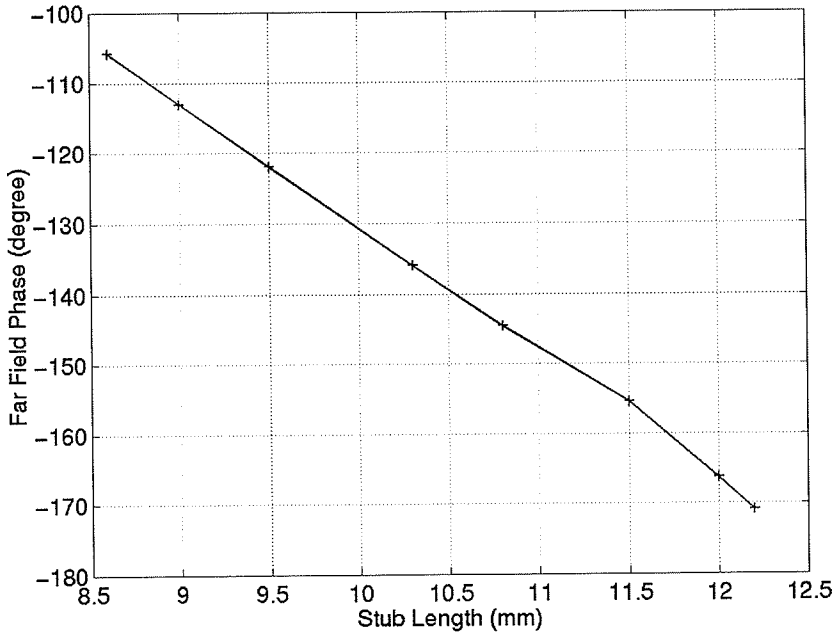

Figure 4.18: Effect of the open circuit matching stub length variation at the far field phase, where a_1*=5.5mm,* a_2*=6.1mm,* t_o*=0.24mm, t=2mm, h=3mm,* ε_{r1}*=2.5,* ε_{r2}*=1, stub width=0.684mm, and the* ρ*=4mm*

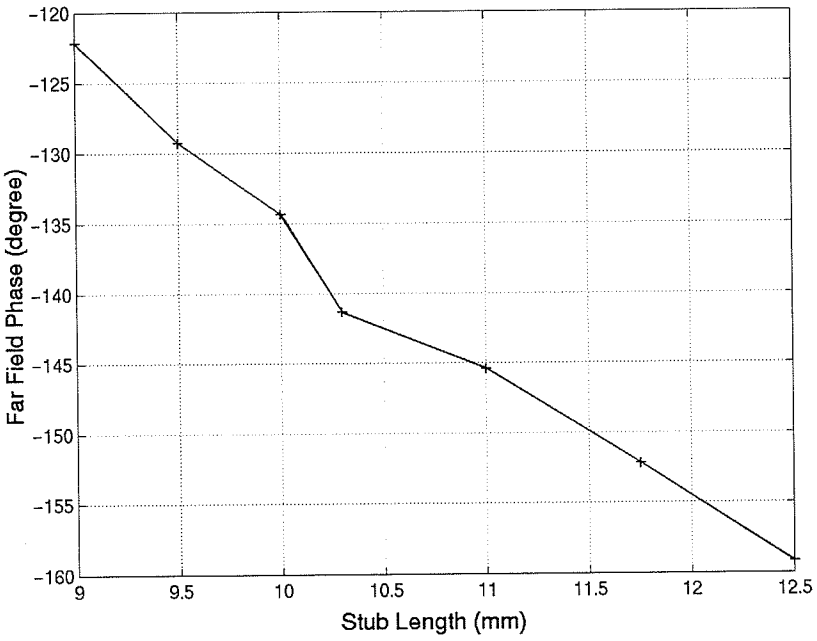

Figure 4.19: Effect of the open circuit frequency control stub length variation at the far field phase where a_1*=5.7mm,* a_2*=6.1mm,* t_o*=0.24mm, t=2mm, h=3mm,*ε_{r1}*=2.5,* ε_{r2}*=1, stub width=0.684mm, and the* ρ*=4mm.*

the matching stub, except the lower patch radius which is 5.7mm. The generated phase shift is about 35 degrees, which is less than that of the matching stub. It should be mentioned that in either case, only stub length variation can not shift the frequency bandwidth adequately and to take advantage of the stub bandwidth enhancement more than one parameter variation is required.

In section 3.4.2. a single stub was applied to match the single patch antenna at a slightly different frequency from the patch resonance, to obtain a wider bandwidth. The same method is also applied here, on dual patch microstrip antenna, to achieve more phase shifts. In this technique, using different parameters variation, the resonance at 10GHz is transferred from the lower patch to the upper patch and then to the lower frequencies which are matched by the stub; so a wider range of phase shifts can be expected.

Figure 4.16 shows a stacked circular microstrip antenna configuration with a single open circuit stub located under the ground plane. Antenna design is performed to achieve a broad bandwidth, about 39.1%. The initial dimensions are: a_1=*5.5mm*, a_2=*6.1mm*, *h=3mm*, *t=2mm*, t_o=*0.264mm*, ρ=*4mm*, ε_{r1}=*2.5*, ε_{r2}=*1*, *SL=10.3mm*, and *SP=1.85mm* from the feed point. The width of the stub is assumed to be the same as the microstrip line width, *w=0.684mm*, specified by the line impedance of *50* ohm, with the substrate dielectric constant of ε_r=2.5.

To extract the maximum phase shift, three of the antenna parameters, i.e. a_1, a_2 and *SL* are varied and the results are evaluated at 10GHz. Figure 4.20 shows that, up to 270 degrees phase shift can be achieved when S_{11}<*-10dB*. It is observed that, when the antenna lower patch is resonating, the most effective parameter at the far field phase is a_1,

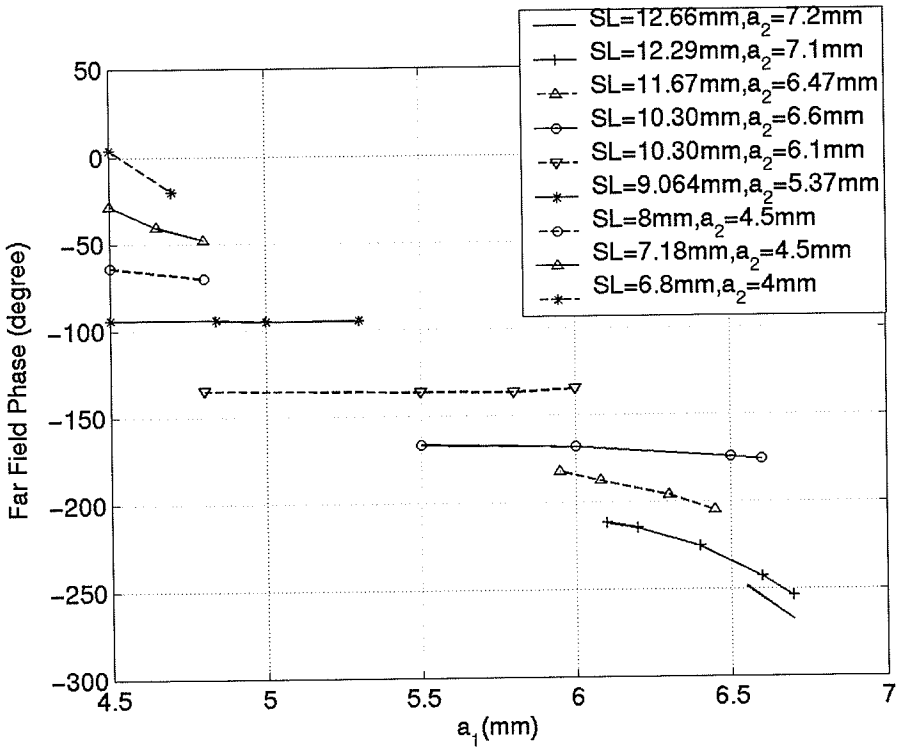

Figure 4.20: Far field phase variation of the stacked circular microstrip antenna shown in Figure 4.16 for various lower patch radius a_1, upper patch radius a_2, and stub length SL. The applied dimensions are: h=3mm, t=2mm, t_o=0.264mm, ρ=4mm, stub position SP=1.85mm, and stub width w=0.684mm.

and when the upper patch is resonating a_2 will be the most efficient one. Matching the antenna by the stub, *SL* variation shows superior performance. It should be noted that, the antenna gain does not remain constant for all the results. In the best case, the gain is about *8dBi*,when the upper patch is resonating, and at the worst case it drops to *6 dBi*.

For the stub design case it should be mentioned that, in contrast with the single patch case, in the stacked circular microstrip the upper modes are close to the dominant mode. It is, therefore, safer to extend the antenna bandwidth from the lower frequencies.

4.6. Stacked Microstrip Array

Having observed the stacked circular microstrip antenna phase properties, it is time to examine its behaviour in phased arrays. Therefore, a linear-four element array configuration is utilized and studied in two different cases. In the first example, the ideal synchronized feeds are considered and investigated numerically. Then, a feed system using three Wilkinson dividers is used and a more realistic situation is studied.

4.6.1. Stacked Circular Microstrip Array with Ideal Synchronized Feeds

In section 3.5.1. a single patch array was utilized and its performance was explored. The same procedure is performed here for a liner array of stacked circular patches.

Figure 4.21 shows the array configuration with four elements. The inter-element spacing, s_x, is considered to be equal to $\lambda/2$ which is 15mm at 10GHz. To obtain the inter-element phase shift, equation 2-5 can be used. For instance, for 14.5 degrees scan angle, a phase shift of β=45 degrees is required. Various radii can be used to introduce the desired phase difference to the array. According to Figure 4.13, enlarging the patches means introducing phase delays to the antenna (Table 4). Therefore, an antenna with a lower patch radius, $a_{L4}=6.512mm$, and upper patch radius, $a_{u4}=7.5mm$ has 135 degrees phase delay compared to the smaller one with $a_{L1}=5.3mm$ and $a_{u1}=5.285mm$.

Figure 4.22 shows the radiation pattern of the phased array configuration of Figure 4.21 for β=0 and 45degrees using the proposed method. For β=0 degree a uniform array

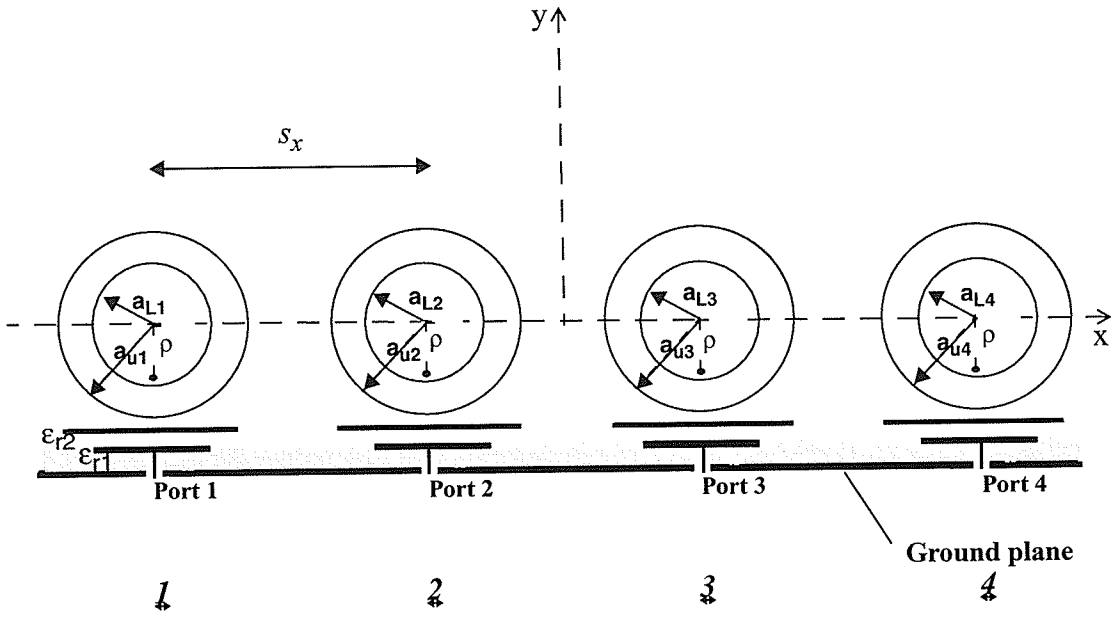

Figure 4.21: Circular stacked microstrip antenna linear phased array configuration

Table .4: Elements specifications for array configuration in Figure 4.21, t=2mm, h=3mm, ρ=4mm, and s_x=15mm for 45 degrees inter-element phase shift at 10 GHz.

Antenna Element	Upper Patch Radius, a_u (mm)	Lower Patch Radius, a_L *(mm)*	Elements Far Field Phase (degree)	Ideal Phase (degree)	S11 at 10GHz as an Individual Element (dB)
1	5.285	5.3	35.03	35	-15.21
2	5.3	5.85	-9.5	-10	-13.98
3	6.7	6.3	-55.66	-55	-11.84
4	7.5	6.512	-100.3	-100	-11.53

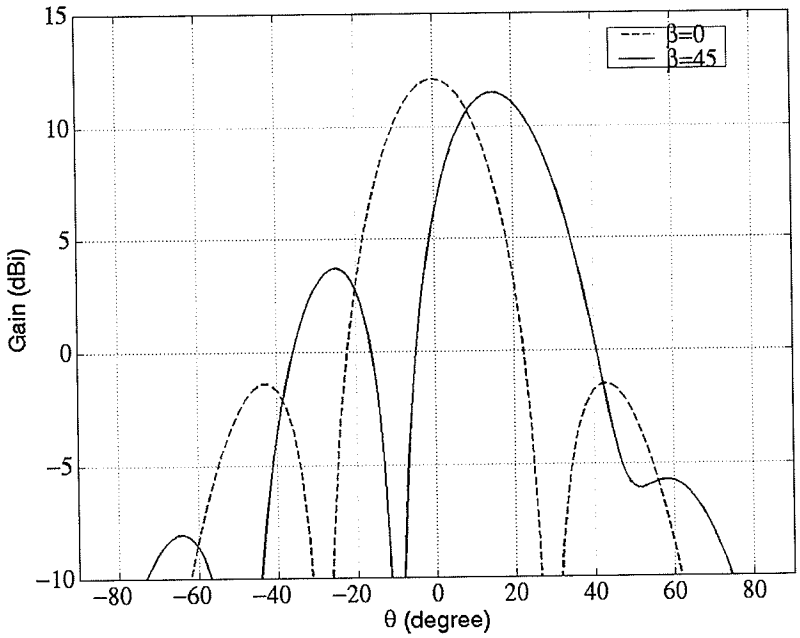

Figure 4.22: Radiation pattern of four elements linear circular stacked microstrip array for β=*0*degree *with* a_{u1}= a_{u2}=a_{u3}= a_{u4}=*6.2mm* and a_{L1}=a_{L2}=a_{L3}= a_{L4}=*5.75mm and* β=*45degrees with* a_{u1}=*5.285mm,* a_{u2}=*5.3mm,* a_{u3}=*6.7mm,* a_{u4}=*7.5mm* and a_{L1}=*5.3mm* a_{L2}=*5.85mm,* a_{L3}=*6.3mm,* a_{L4}=*6.512mm; the other parameters are t=2mm, h=3mm,* ρ=*4mm in Figure 4.21.*

with equal size patches are used, a_{u1}= a_{u2}=a_{u3}= a_{u4}=*6.2mm* and a_{L1}=a_{L2}=a_{L3}= a_{L4}=*5.75mm* with *t=2mm, h=3mm,* ρ=*4mmm,* ε_{r1}=*2.5, and* ε_{r2}=*1.* For β=45 degrees the utilized patch dimensions are: a_{u1}=*5.285mm,* a_{u2}=*5.3mm,* a_{u3}=*6.7mm,* a_{u4}=*7.5mm* and a_{L1}=*5.3mm* a_{L2}=*5.85mm,* a_{L3}=*6.3mm,* a_{L4}=*6.512mm.* It can be seen, that there is a good agreement between the scan angles in this figure, and the theoretical value which is 14.5 degrees.

Figure 4.23 compares numerical results for the array radiation pattern for β=45 degrees implemented by the conventional method and proposed technique. In the conven-

tional method a uniform array with, $a_{u1}= a_{u2}=a_{u3}= a_{u4}=6.2mm$ and $a_{L1}=a_{L2}=a_{L3}= a_{L4}=5.75mm$, $t=2mm$, $h=3mm$, *and* $r=4mm$ are used and the ideal input phase shifts are applied between the elements. In the proposed technique the phase shifts are generated using different radii, (details of the design is presented in Table 4). It shows that, the scan angle in the proposed technique and the ideal conventional method are the same and there is a good agreement between them. However, in comparison with the ideal conventional method, it has a higher side lobe level and cross-polarization. We will be back to this issue in the next section.

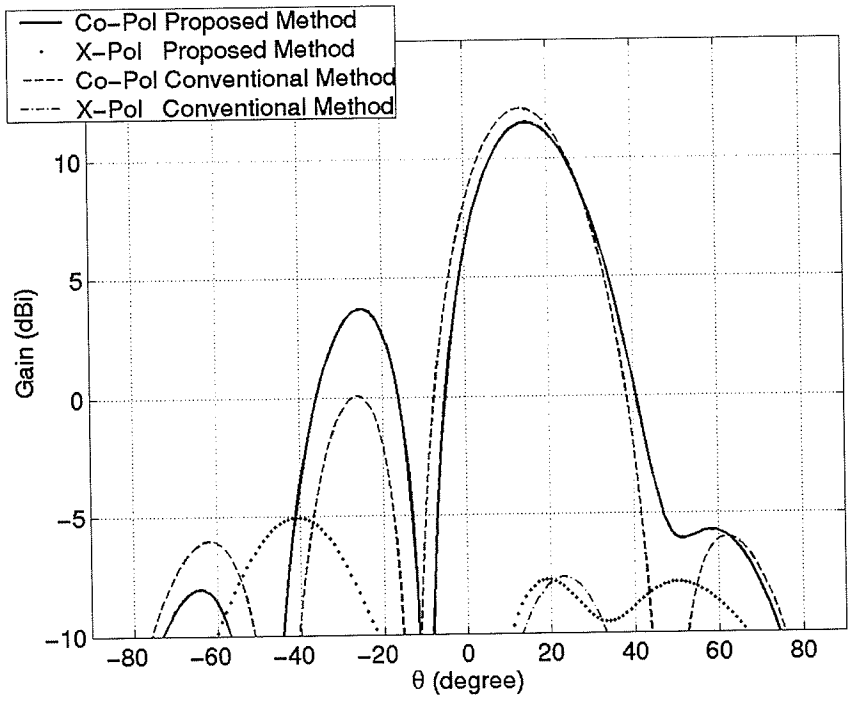

Figure 4.23: Radiation pattern of linear four elements stacked circular microstrip array with $\beta=45$*degrees. The design details for the proposed technique is available in Table4 and the applied dimensions for the conventional case is* $a_{u1}= a_{u2}=a_{u3}= a_{u4}=6.2mm$ and $a_{L1}=a_{L2}=a_{L3}= a_{L4}=5.75mm$, $t=2mm$, $h=3mm$, *and* $\rho=4mm$.

4.6.2. Stacked Circular Phased Array with Feed System

In this section, the performance of the proposed linear stacked circular microstrip array with a realistic symmetric feed system is studied. Wilkinson power dividers are used again. The feed system of section 3.5.2. is employed here for the stacked array configuration, as shown in Figure 4.24. It is positioned under the ground plane.

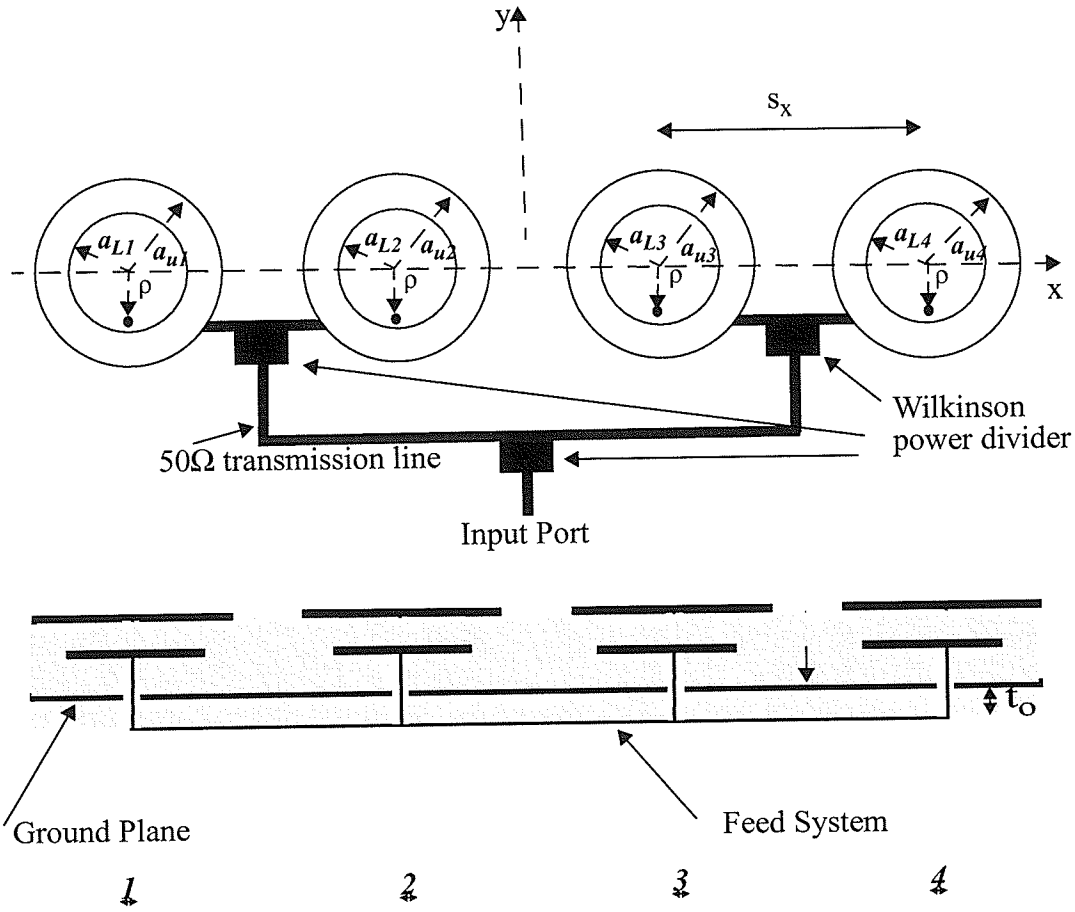

Figure 4.24: Circular stacked microstrip Linear array configuration with feed system.

Numerical results of the array Gain pattern for β=45degrees, for both *x*- and *y*-polarized patches, are shown in Figure 4.25, for a_{u1}=5.285mm, a_{u2}=5.3mm, a_{u3}=6.7mm, a_{u4}=7.5mm and a_{L1}=5.3mm a_{L2}=5.85mm, a_{L3}=6.3mm, a_{L4}=6.512mm; the other dimensions are t_o=0.246, t=2mm, h=3mm, and ρ=4mmm. It shows that the gain is slightly higher for the *y*-polarized case and cross-polarization is lower for the *x*-polarized antenna.

In comparison to Figure 4.23, it can be seen that when the feed system is used, the side lobe level of the antenna decreases to less than -10dB and cross-polarization reduces to around -20 dB. Therefore, with a real feed the antenna does not suffer from the high side lobe level or cross polarization.

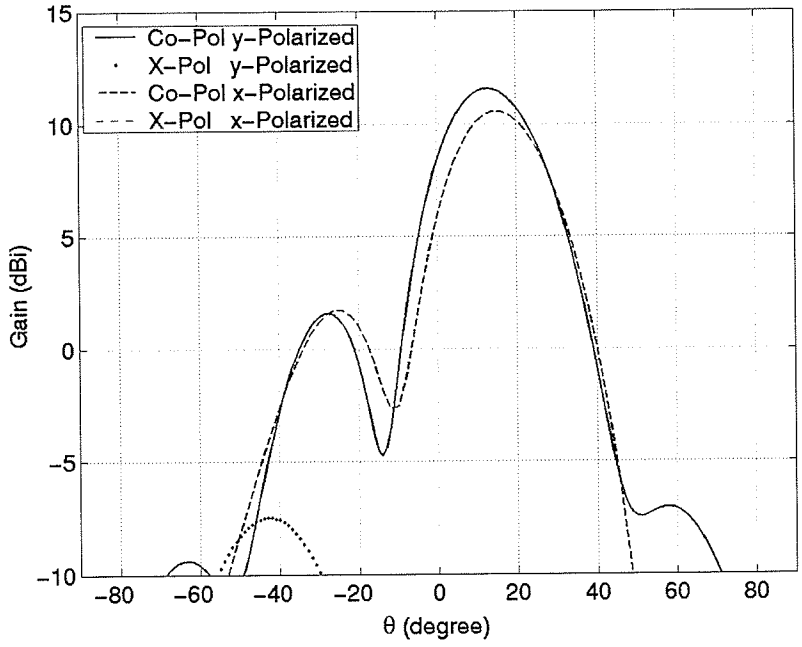

Figure 4.25: Scanned beam for both x- and y-polarized circular stacked microstrip array shown in Figure 4.24 for β*=45degrees,* a_{u1}*=5.285mm,* a_{u2}*=5.3mm,* a_{u3}*=6.7mm,* a_{u4}*=7.5mm* and a_{L1}*=5.3mm* a_{L2}*=5.85mm,* a_{L3}*=6.3mm,* a_{L4}*=6.512mm; the other dimensions are* t_o*=0.246, t=2mm, h=3mm, and* ρ*=4mmm.*

4.6.3. Bandwidth

In section 3.5.3. element impedance bandwidth (EIBW), array impedance bandwidth (AIBW) and signal bandwidth (SBW) for single patch microstrip antenna was explained. The same definitions for stacked microstrip patch can be used too.

In Figure 4.26, the solid curve shows a wide band stacked antenna return loss where a_1=*5.75mm*, a_2=*6.2mm, h=3mm, t=2mm,* ρ=*4mm,* ε_{r1}=*2.5, and* ε_{r2}=*1* (structure of the antenna is the same as Figure 4.1). It shows that the stacked circular antenna element bandwidth is EIBW= 31%. Shifting this curve to the left and right, lower and higher frequencies, phase shift can be obtained. For instance, changing disc radii from a_1=5.3mm and a_2=5.285mm to a_1=6.512mm and a_2=7.5mm, dashed curves, gives about 130 degrees phase shift (Table4 and Figure 4.13). For this phase shift, the antenna is always matched between 9.4 and 10 GHz which is the signal bandwidth of the antenna element, SBW= 6.18%. One notices that by increasing the phase shift range, the available signal band-

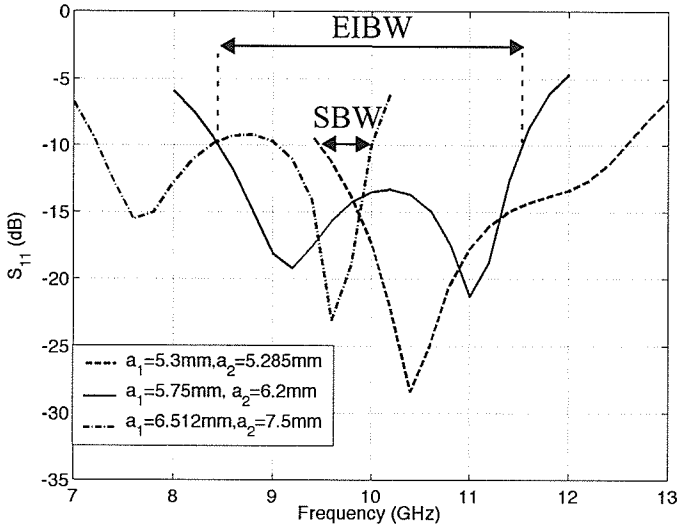

Figure 4.26: Return loss of stacked circular microstrip antenna for three different radii where h=3mm, t=2mm, ρ=*4mm,* ε_{r1}=*2.5, and* ε_{r2}=*1 in Figure 4.1.*

width reduces and for larger bandwidths, less phase shift can be generated.

As it was mentioned before, SBW does not depend on the number of elements in an array. However, by increasing their number, less inter-elements phase shift can be produced and the scan angle reduces while the total phase shift remains constant. This problem can be solved by using extra conventional double digit phase shifter at the input of the antenna to obtain a complete 360 degrees phase shift.

Using 6.18% bandwidth and 135 degrees phase shift, a four elements linear array is designed where t=2mm, h=3mm, ρ=4mm, ε_{r1}=2.5, and ε_{r2}=1. Its configuration is shown in Figure 4.24. Various radii that are used to generate inter-element phase shifts are: a_{u1}=5.285mm, a_{u2}=6.2mm, a_{u3}=6.7mm, a_{u4}=7.5mm and a_{L1}=5.3mm a_{L2}=5.75mm, a_{L3}=6.3mm, a_{L4}=6.512mm. Figure 4.27 shows the return loss for each elements including effect of mutual coupling. The phase curves of elements in terms of frequency without considering the effect of mutual coupling are shown in Figure 4.28. β_1,β_2, and β_3 show the inter element phase shifts of the antennas. Figure 4.29 compares them to those of the transmission line phase shifter which is designed to generate 45 degrees phase shift at 10GHz. $\beta_1$and β_2 are almost in good agreement with the phase shifter and the discrepancy of β_3 is due to the non linearity of phase curves of element 4. More efforts is needed to design an array with more linear phase curves.

Figure 4.30 shows array impedance bandwidth AIBW which is about 21%. As it was mentioned in section 3.5.3., in this range all the elements may not be in good match, but the overall return loss is less than -10dB. Scan angle variation over this band is illus-

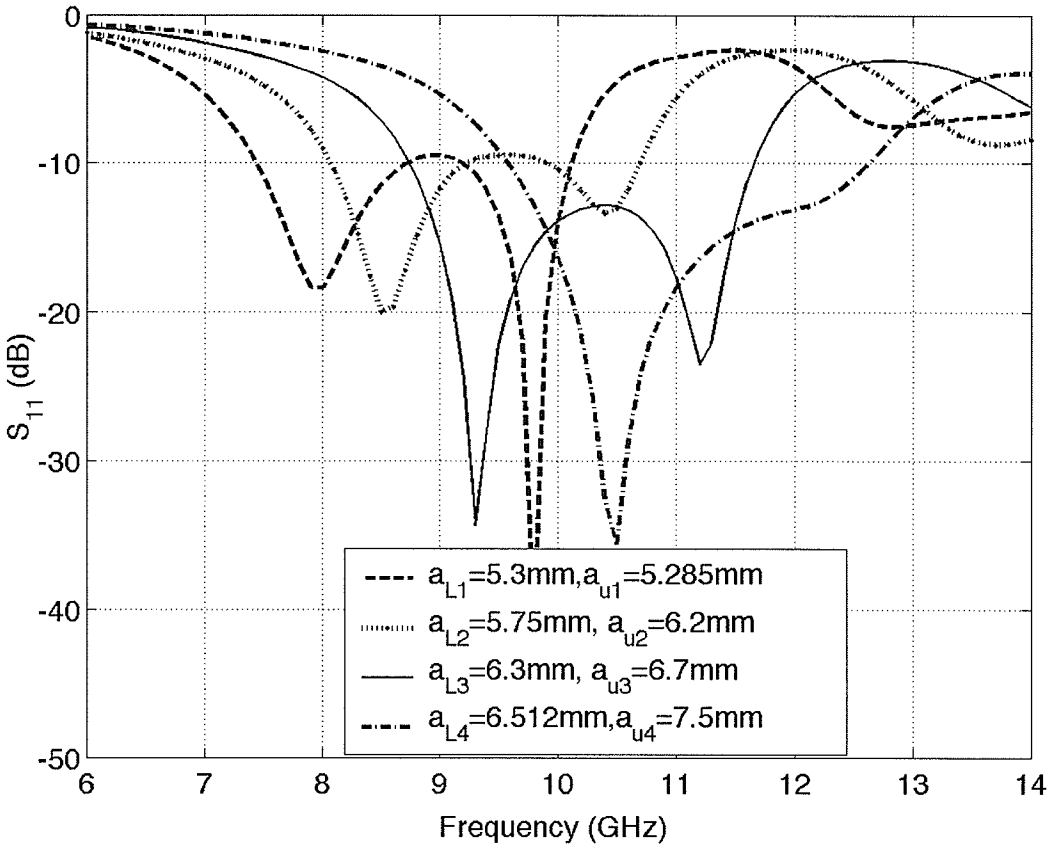

Figure 4.27: Return loss of each element in four elements stacked circular microstrip array in terms of frequency where:t=2mm, h=3mm, ρ=4mm, and ε_r=2.5

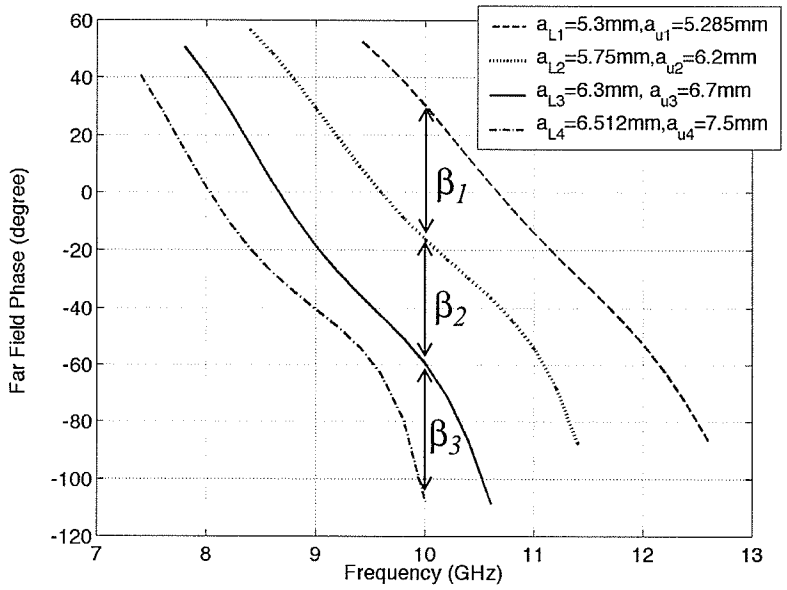

Figure 4.28: Far field phase variation of each elements in four elements stacked circular microstrip array in terms of frequency while S_{11}<-10dB. The other dimensions are:t=2mm, h=3mm, ρ=4mm, and ε_r=2.5.

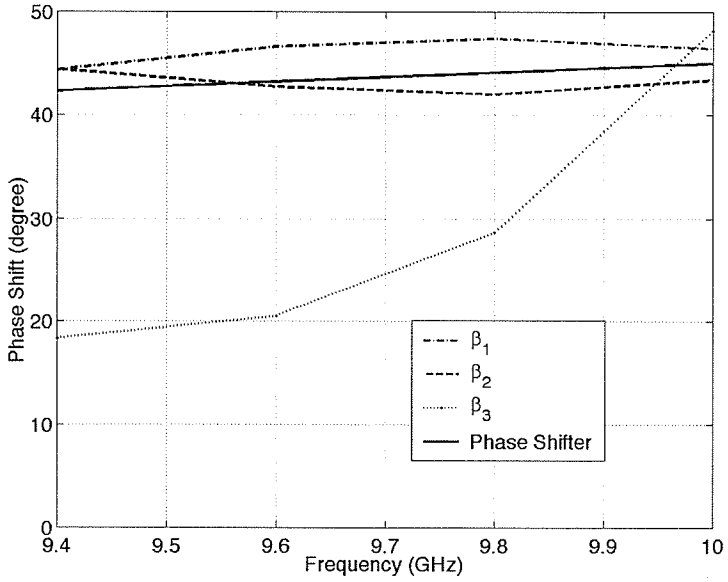

Figure 4.29: Comparison between the inter-element phase shifts generated by proposed method (Figure 4.28) and conventional transmission line phase shifter.

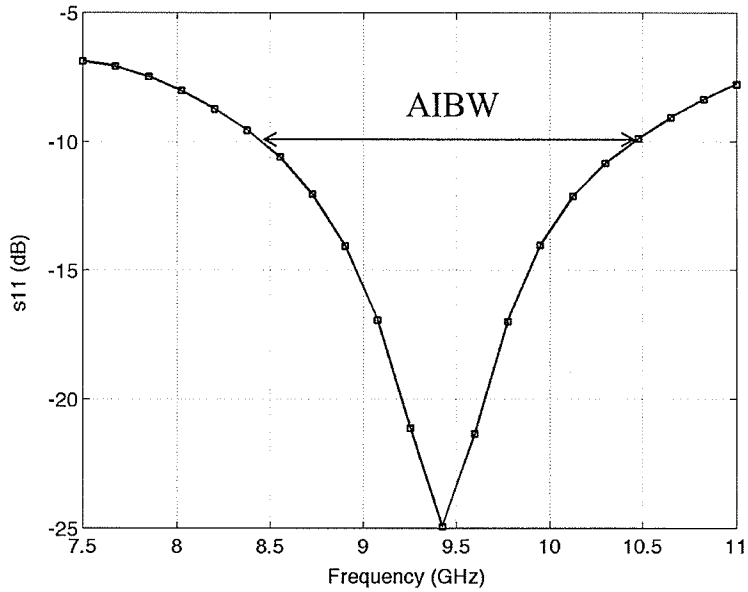

Figure 4.30: Return loss for the proposed array where t=2mm, h=3mm, ρ=4mm, ε_{r1}=2.5, ε_{r2}=1, a_{u1}=5.285mm, a_{u2}=6.2mm, a_{u3}=6.7mm, a_{u4}=7.5mm and a_{L1}=5.3mm a_{L2}=5.75mm, a_{L3}=6.3mm, a_{L4}=6.512mm, for the configuration in Figure 4.24.

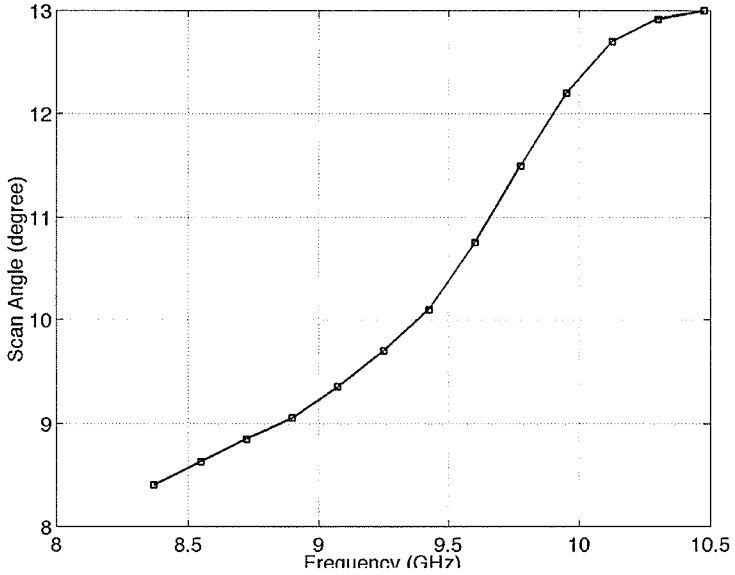

Figure 4.31: Scan angle variation over AIBW shown in Figure 4.30.

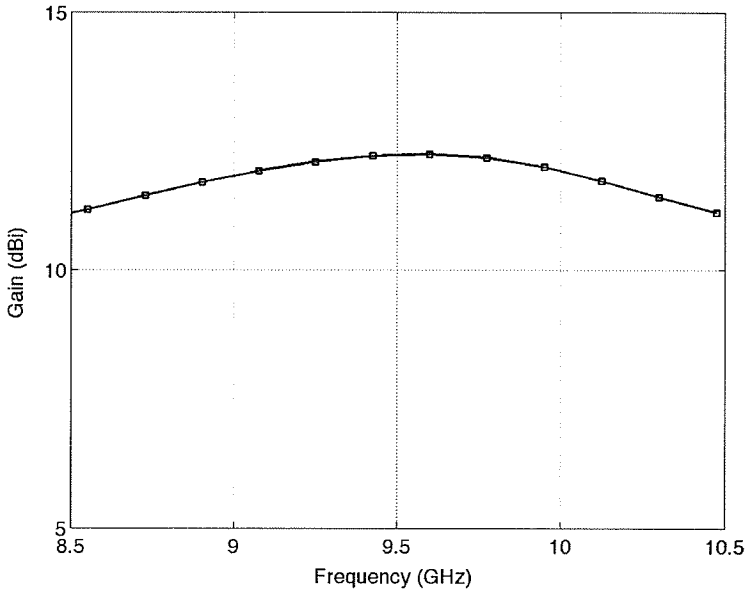

Figure 4.32: Gain variation over AIBW shown in Figure 4.30.

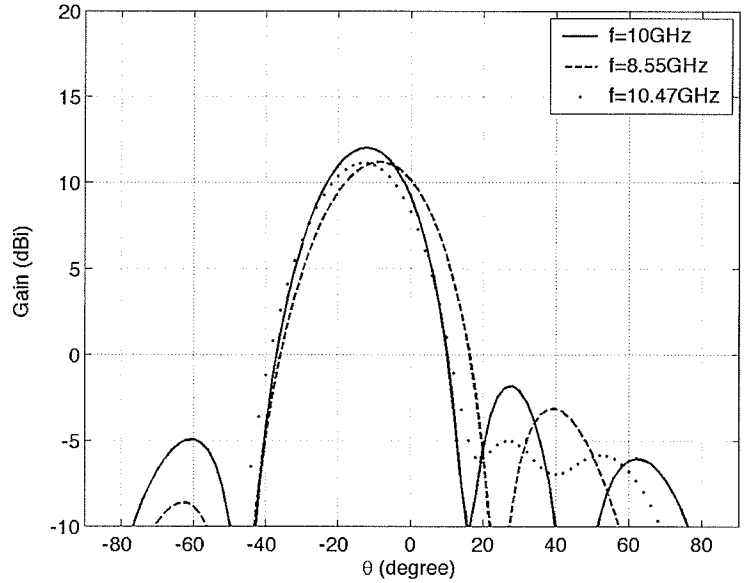

Figure 4.33: Radiation patterns for the proposed array at 10GHz and two ends of AIBW.

trated in Figure 4.31. It shows that the scan angle varies up to 4.5 degrees over the AIBW. Its gain variation is also shown in Figure 4.32 which is between 10.89dBi to 12.25 dBi. The radiation patterns of the antenna at 10 GHz and two end frequencies of AIBW is shown in Figure 4.33.

4.7.Summary

In this chapter, the far field properties of stacked circular microstrip antenna were investigated to be used in phased array antennas.

A circuit model for analytical solution of stacked circular antenna was derived. The results obtained from Matlab programming was in good agreement with the MOM, realized by ENSEMBLE 6. However, its accuracy reduced by increasing the distance between the patches and the ground plane.

The transfer function obtained from the *MOM* showed that the achievable phase shift of this antenna was more than that of a single patch. The antenna was analysed using the transmission line model and the effect of different parameters on the far field phase was investigated. Using both patch radii variation, a phase shift of up to 180 degrees was observed. Then, it was used for design of a four-element linear phased array to scan its beam. For an inter-elements phase shift of 45 degrees, for both x- and y- polarized antennas, a scan angle of 15 degrees was achieved which was in good agreement with the array theory.

For larger scan angles, a single digit phase shifter can be added to the input or two

different transmission lines can be used at the input with 180 degrees phase shift. Therefore, a complete 360 degrees of phase shift can be obtained and the beam can be scanned to larger angles.

Chapter 5

Conclusion

5.1.Summary

A study was carried out on the phase behaviour of single and dual patch microstrip antennas in phased arrays and a novel technique to generate the phase shift by the elements was introduced. A theory based on the cavity model was established and was examined on single and stacked circular microstrip patch antennas. The analytical results, obtained from cavity and transmission line model analysis, were compared to the numerical results based on the Method of Moment and a good agreement was achieved. The array configuration of each case, using the proposed technique, was utilized to scan the beam and was compared to that of the conventional method.

From this research, the following conclusions were drawn:

❋ A microstrip antenna can be considered as a resonating cavity. Each cavity can be modelled by one RLC circuit that resonates at the same frequency as the cavity. It was assumed that the radiation is due to the real part of the circuit, and based on that, the antenna transfer function was derived. Its phase Bode diagram showed that the transfer function of the antenna model has two conjugate poles for each resonance, and introduces 180 degrees phase shift for each conjugate pole. Therefore, by shifting the resonance frequency, a phase shift on the far field can be realized. This is possible by

varying antenna parameters so as the cavity dimensions may be modified, or by adding shorting pin and changing its location.

❋ The above theory was applied to single and dual patch circular microstrip antenna. The single patch with one resonance had one set of conjugate poles, indicating 180 degrees phase shift at its transfer function and that of the stacked antenna had 360 degrees due to its dual resonance frequencies. Different frequency shift techniques were used to realize the maximum phase variation at 10GHz, while maintaining S_{11}<-10dB. The variation of antenna single cavity dimension (i.e. either patch radius, heights, and probe location) leads to achieving about 70 degrees phase shift. However, with stacked antennas, more than one parameter was required to shift the frequency from one patch to the other.Variation of both radii were used to obtain up to 180 degrees phase shifts.

❋ A single open circuit stub was added to the antenna input port, which also increased the bandwidth. Then, not only more phase shift of the transfer function could be used but the stub could also add some phase shift to the antenna. In a single patch the obtained phase shift increased to 150 degrees by two parameter variation (stub length and patch radius) and for stacked patches that enhanced up to 270 degrees by changing three parameters (stub length and both patch radii). However, the antenna suffered from the gain reduction. For instance, for stacked patches it reduced from 8dBi to 6dBi.

❋ One shorting pin was located in the feed probe plane inside the antenna cavity, for

both single and stacked microstrip antennas and its location was varied to shift the frequency. Its performance was not as good as the antenna parameters and only up to 40 degrees phase shift could be achieved.

❋ Linear four element array configurations of single and stacked microstrip antennas were utilized to examine the accuracy of the proposed technique. For both single and dual patches the scanned beam angles showed a very good agreement with the array theory and conventional method. For the single patch a scan angle of 4.5 degrees, and for stacked patches that of 15 degrees were obtained. The technique showed slightly more cross polarization and side lobe levels compared to the ideal conventional method. It was applied using various patch radii for stacked circular microstrip antenna. To increase the scan angle or use more elements, a single digit phase shifter or an extra $\lambda/2$ transmission line may be added to the design.

5.2.Future Research

The proposed concept is new and there are numerous subjects, which need more careful investigations. Some of which are listed below:

❋ Study on the effect of different dielectric constants on the achievable phase shift.

❋ More detailed analysis of dual band stacked microstrip antenna and design of a dualband phased array.

❋ The effect of adding two shorting pins in to the boundary of stacked microstrip antenna and moving them to evaluate their performance to shift the entire frequency bandwidth.

❋ Investigation on rectangular microstrip antennas, since it has one additional degree of freedom which is the width of the patch.

❋ Three patch microstrip antenna to increase the number of resonances and enhance the bandwidth so as to increase the phase shift.

❋ Due to the slightly different input impedance of each element in the proposed technique, the effect of mutual coupling and loading on each elements in the array configuration, requires more detailed analysis.

Reference:

[1] G.ADESCHAMPS, "Microstrip microwave antennas", *Presented at the Third USAF Symposium on Antennas*, 1953.

[2] R.A.SAINATI, "CAD on Microstrip Antennas for Wireless Applications", Artech House, Boston. London, 1996.

[3]A.K.BHATTACHARYYA, "A Numerical Model for Multi layered Microstrip Phased-Array Antennas", *IEEE Transactions on Antenna and Propagation*, Vol.44, No.10, pp.1386-1393, Oct.1996.

[4]G.DUBOST, and G.BEAUQUET, "Linear Transmission Line Model Analysis of a Circular Patch Antenna", *Electronics Letters*, Vol.22, pp.1174-1176, 1986.

[5] "http://www.ansoft.com/products/hf/ensemble", *Ansoft Company.* Four Station Square, Suite 2000, Pittsburgh, PA, 15219-1119, USA

[6] "http://www.mdl.sandia.gov/micromachine/overview.html", *Intelligent Micromachine Initiative, Sandia Nationnal Laboratories*, 7011 East Avenue, Livermore, CA94550.

[7] ROBERT J.MAILLOUX, "Phased Array Antenna Handbook", *Artech House*, 1994.

[8] N.FOURIKIS, "Advanced Array Systems, Applications and RF Technologies", *Academic Press*, Australia, 2000.

[9] R.C.JOHNSON, and H.JASIK, "Antenna Engineering Handbook", *McGraw-Hill*, Sec-

ond Edition, 1984.

[10] F.DE FLAVIIS, N.G. ALEXOPOULOS, and O.M.STAFSUDD, "Planar Microwave Integrated Phase Shifter Design with High Purity Ferroelectric Material", *IEEE Transactions on Microwave Theory and Techniques*, Vol.45, No.6, pp.963-969, June1997.

[11] B.L.SMITH, and M.H.CARPENTIER, "The Microwave Engineering Handbook", *Van Nostrand Reinhold*, Vol. 2, 1993.

[12]""http://www.mwireless.com/products/subassemble.html", Micronetics Wireless INC, 2001.

[13]. I.D. ROBERTSON, "MMIC Design", *The Institution of Electrical Engineers*, London, 1995.

[14] C. BOZLER, DRANGMEISTER, S.DUFFY, M.GOUKER, J.KNECHT, L.KUSHMNER, R.PARR, S.RABE, and L.TRAVIS, "MEMS Microswitch Arrays for Reconfigurable Distributed Microwave Components", *IEEE MTT-s,* Boston, June 11-16, 2000.

[15] R.JAMES, P.S.HALL, and C.WOOD, "Microstrip Antenna Theory and Design", *Peter Peregrinus Ltd*, 1981.

[16] I.J.BAHL, and P.BHARTIA, "Microstrip Antennas", *Artech House*, 1980.

[17] F.ABBOUD, J.P. DAMIANO, and A. PAPIERNIK," Simple model for the input

impedance of coax-fed rectangular microstrip patch antenna for CAD", *IEE Proceedings*, Vol. 135, No.5, Oct.1988.

[18] W.F.RICHARDS, Y.T.LO, D.D.HARRISON, "An Improved Theory for Microstrip Antenna and Applications", *IEEE Transactions on Antenna and Propagation*,Vol.AP.29, No.1, Jan.1981.

[19] C.A.BALANIS, "Antenna Theory, Analysis and Design", *John Wiley and Sons*, 1997.

[20] R.C.DORF, and R.H. BISHOP, "Modern Control Systems", *Addison Wesley Longman,* 1998.

[21] F.J.HALE, "Introduction to Control System Analysis and Design", *Prentis-Hall,* 1988.

[22] K.F.LEE, K.Y.HO, and J.S.DAHELE, "Circular-Disk Microstrip Antenna with an Air Gap", *IEEE Transactions on Antenna and Propagation*, 1984.

[23] K.SOLBACH, "Phased Array Simulation Using Circular Patch Radiators", *IEEE Transactions on Antenna and Propagation*, Vol.AP-34, No.8, pp.1035-1085, 1986

[24] F. ZAVOSH and J.T.ALERLE, "Infinite Phased Arrays of Cavity Backed Patches", *IEEE Transactions on Antenna and Propagation*, AP-42, No.3, pp.390-398, March1994.

[25] M.EDIMO, K.MAHDJOUBI, A.SHARAIHI, and C.TERRET "Simple Circuit Model for Coax-Fed Stacked Rectangular Microstrip Patch Antenna", *IEE Pro-*

ceedings Microwave & Antennas Propagation, Vol.145, No.3 June 1998.

[26]M.R.SPIEGEL, "Mathematical Handbook of Formulas and Tables", Schaum's Outline Series, McGraw-Hill, Inc.,1968

[27] R.GARG, P.BHARTIA, I.BAHL, and A.ITTIPIBOON, "Microstrip Antenna Design Handbook", *Artech House*, Boston.London, 2001.

[28] D.H.SCHAUBERT, F.G.FARRAR, A.SINDORIS, and S.HAYES, "Microstrip Antennas with Frequency Agility and Polarization Diversity", *IEEE Transactions on Antenna and Propagation,* Vol.AP-29, No.1, pp.118-123,Jan.1981.

[29]G.L.LAN, and D.L.SENGUPTA, "Frequency Agile Microstrip Antennas", *IEEE MTT_S Digest*, BB-6, pp.693-695, 1985.

[30]JD.K.CHENG, "Field and Wave Electromagnetics", *Addison-Wesley Publishing Company,* 1989.

[31]P.A.RIZZI, "Microwave Engineering, Passive Circuit", *Prentice-Hall International*, 1988.

[32] Z.F.LIU, P.S.KOOI, L.W. LI, M.S.LEONG, and T.S.YEO "A Method for Designing Broad-Band Microstrip Antennas in Multi Layered Planar Structures", *IEEE Transactions on Antennas and Propagation*, Vol.47, No.9, pp. 1416-1420, 1999.

[33]R.B.WATERHOUSE, "Design of Probe-Fed Stacked Patches", *IEEE Transactions on Antennas and Propagation,* Vol.47, No.12, pp. 1780-1784, 1999.

[34]S.A.LONG, and M.D.WALTON, "A Dual-Frequency Stacked Circular-Disk Antenna", *IEEE Transactions on Antenna and Propagation*, Vol. AP-27, No.2, pp.270-273, 1979

[35]A.K. BHATTACHARYYA, "General Transmission Line Model of Microstrip Patch Antennas and Some Applications", Ph.D Thesis, *Submitted to the Indian Institute of Technology,* Kharagpur-721 302 India, 1985.

[36]R.F.HARRINGTON, "Time Harmonic Electromagnetic Fields", *McGraw-Hill Company,* 1961.

[37]A.K.BHATTACHARYYA, and R.GARG, "Input Impedance of Annular Ring Microstrip Antenna Using Circuit Theory Approach", *IEEE Transactions on Antennas and Propagation,* Vol. AP.33, No.4, pp.369-374, 1985.

[38]A.K.BHATTACHARYYA, and R.GARG, "Generalised Transmission Line Model for Microstrip Patches", *IEE Proceedings*, Vol.132, Pt.H, No.2, pp93-99, 1985.

[39]A.K.BHATTACHARYYA, and R.GARG, "Self and Mutual Admittance Between Two Concentric, Coplanar, Circular Radiating Current Sources", *IEE Proceedings,* Vol.1, Pt.H, No.3, pp.217-220, 1984.

[40]R.B.WATERHOUSE, "Broadband Stacked Shorted Patch", *Electronics Letters,* Vol.35, No.2, January 1999.

APPENDIX I

Effect of Circular Microstrip Antenna Parameters Variation on ωn and ξ

By changing the antenna parameters, ξ doesn't vary much in the antennas pass band. It is shown in Figure I.1, I.2, and I.3. Also, in this range ωn depends approximately linearly on the radius, substrate thickness, and probe location, as shown in Figures I.4, I.5, and I.6. They are calculated using the cavity model, presented in section 3.2. and equations 3-12 and 3-13 for a= 5.112mm, t=1.6mm, and ρ=1.85mm.

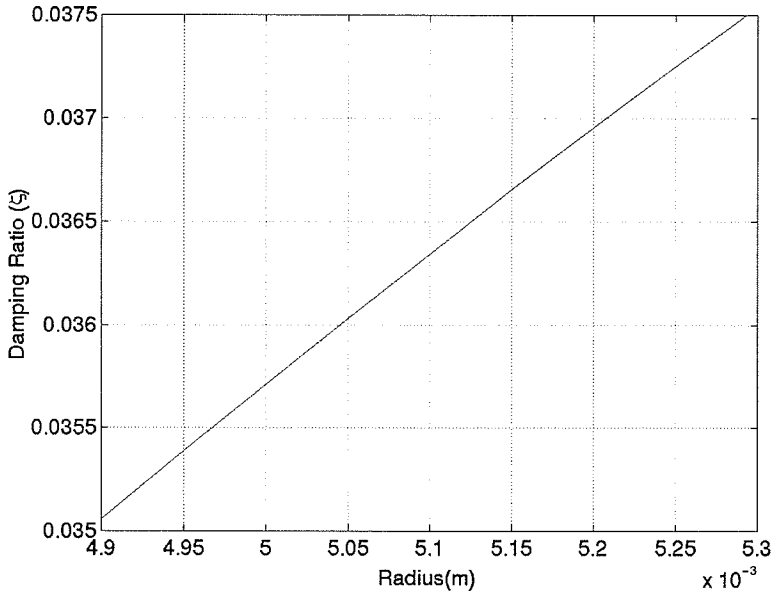

Figure I.1: Effect of the radius variation on damping ratio.

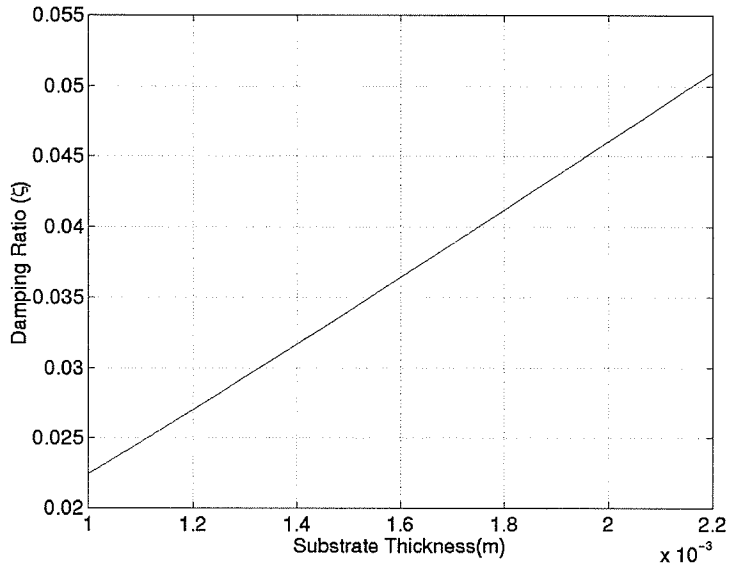

Figure I.2: Effect of the substrate thickness on damping ratio

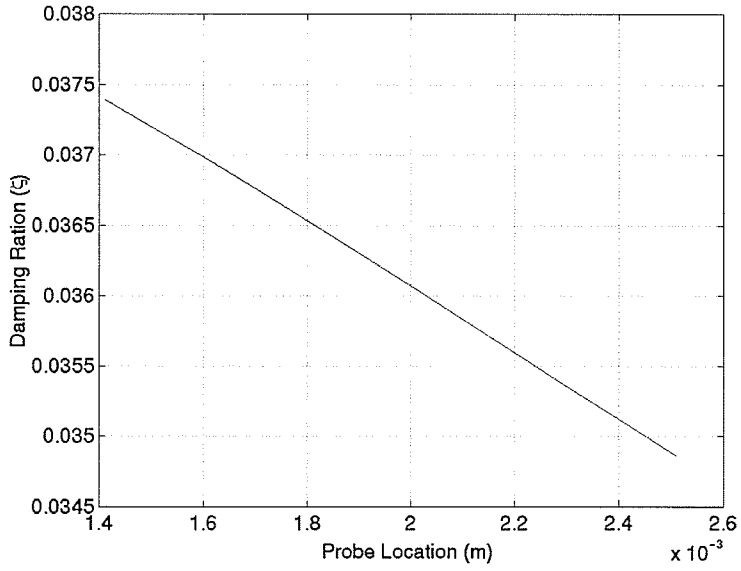

Figure I.3: Effect of the probe location on damping ratio

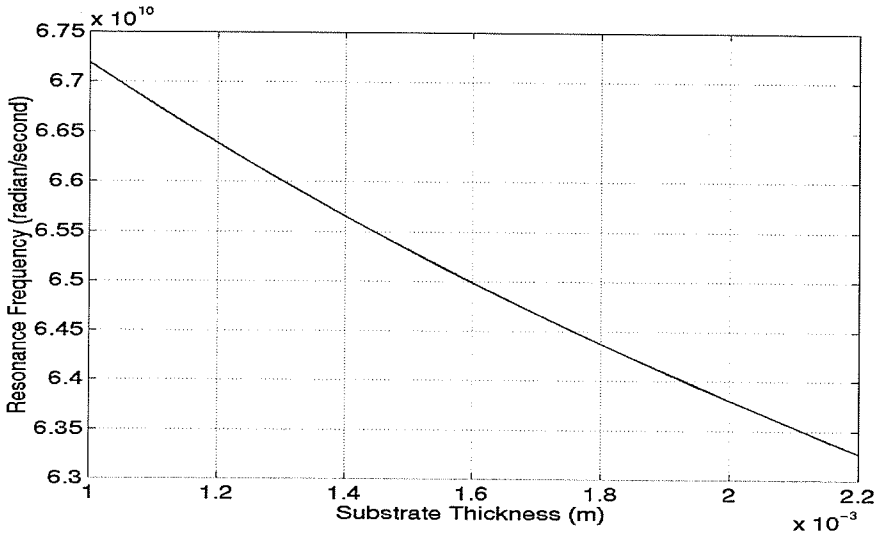

Figure I.4: Effect of circular microstrip antenna radius variation on resonance frequency

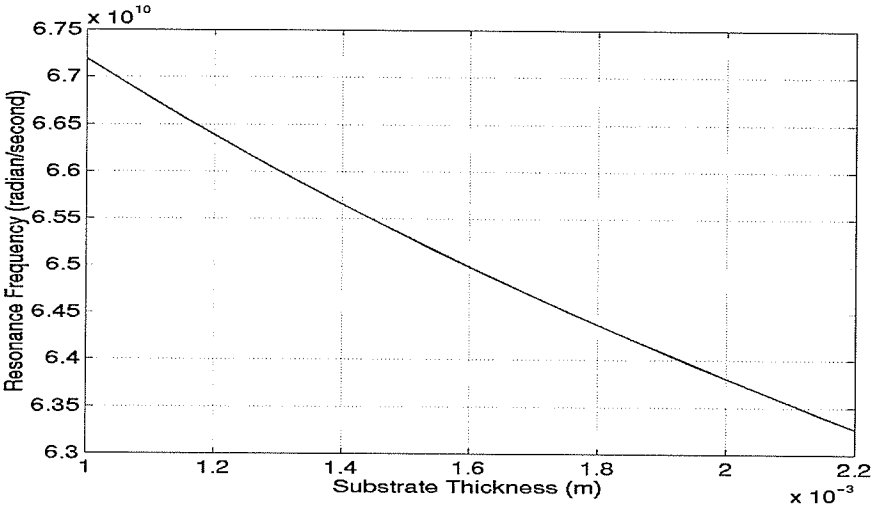

Figure I.5: Effect of circular microstrip antenna substrate thickness variation on resonance frequency.

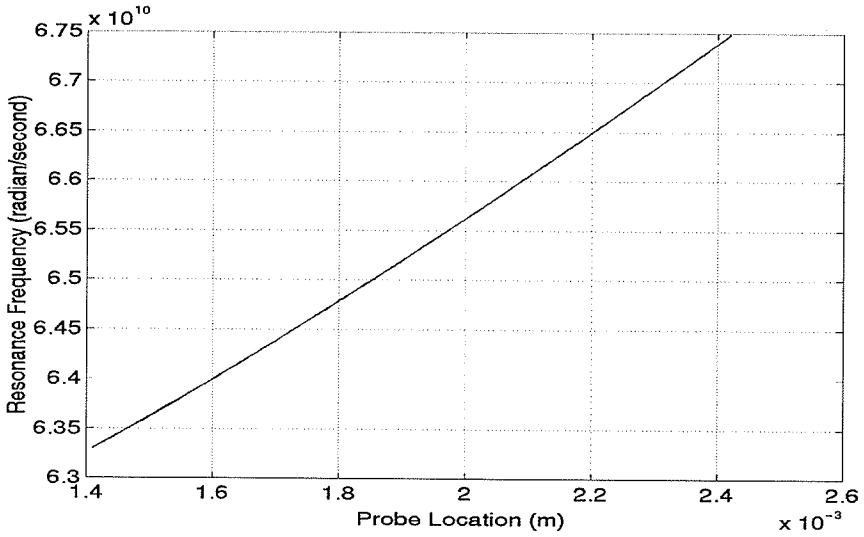

Figure I.6: Effect of circular microstrip antenna probe location variation on resonance frequency

APPENDIX II

Antenna Parameters Variation Effect on the Input Impedance

The following Figures and tables show the effect of radius, substrate thickness, and probe position variation at the input impedance of the antenna. In all cases, the operating frequency is 10 GHz. To achieve these results, first, antenna is matched at 10 GHz and then the parameters are varied. It should be mentioned that in each case, only one parameter is changed. The dimensions at the match frequency are: a= 5.112mm, t=1.6mm, and ρ=1.85mm according to Figure 3.1.

In this appendix, the abbreviations of table 5 are used:

Table .5: Parameter abbreviations

Radius	a
Substrate Thickness	t
Probe Position	ρ
Far Field Phase	FFP
Resonance Frequency	Res. frq
Input Impedance (Real)	INR
Input Impedance (Imaginary)	INX
Input Phase	INP
Explanation	Exp.

Table .6: Effect of circular microstrip antenna radius variation an the input impedance at 10GHZ.

a (mm)	FFP (degree)	S_{11} (dB)	Res.frq (GHz)	INR (Ω)	INX (Ω)	INP (degree)	Exp.
5.285	16.92	-9.99	9.66	27.34	9.7	19.7	
5.27	20.3	-10.7	9.7	28.66	8.82	17.1	
5.25	24.62	-11.77	9.73	30.57	7.6	13.92	
5.2	34.79	-15	9.85	36.19	4.67	7.35	
5.112	48.98	-41	10	49.6	0.82	0.95	Matched point
5.05	56.33	-20	10.1	62.35	1.015	0.93	
5	61.05	-14	10.2	74.3	4.4	3.45	
4.95	64.3	-11	10.33	86.57	12.37	8.13	
4.93	66.28	-10.09	10.34	91.07	16.94	10.53	

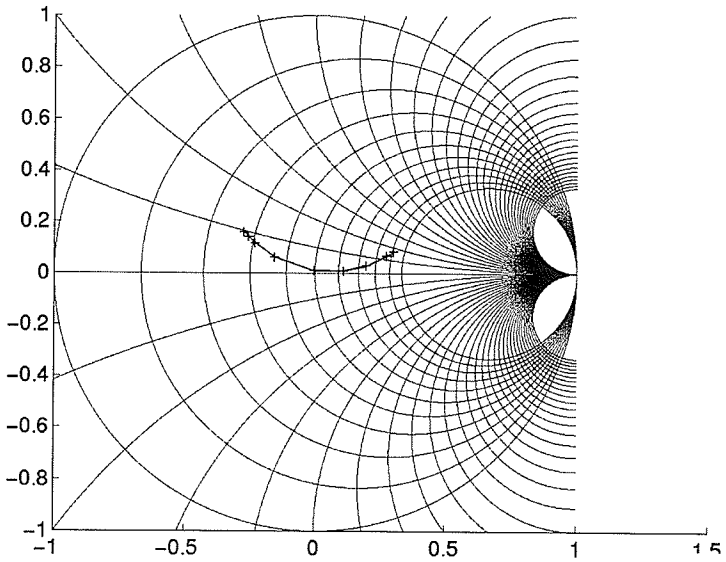

Figure II.1: Effect of the circular microstrip antenna radius variation on the input impedance at 10GHZ

Table .7: Effect of the circular microstrip antenna substrate thickness variation an the input impedance at 10GHZ

t (mm)	FFP (degree)	S_{11} (dB)	Res.frq (GHz)	INR (Ω)	INX (Ω)	INP (degree)	Exp.
2.2	6.11	-10.14	9.7	44.29	30.28	34.36	
2.1	12.5	-11.64	9.8	43.85	24.63	29.32	
2	19.63	-13.52	9.8	44.25	19.46	23.73	
1.9	23.37	-14.76	9.8	41.51	14.65	19.44	
1.8	31.95	-17.85	9.9	43.009	9.7	12.72	
1.6	48.98	-41	10	49.6	0.82	0.95	Matched point
1.4	62.6	-18.49	10.1	62.78	-4.08	-3.72	
1.2	72.3	-11.64	10.2	84.67	6.5	4.4	
1.1	75.99	-9.38	10.3	92.23	24.87	15.09	

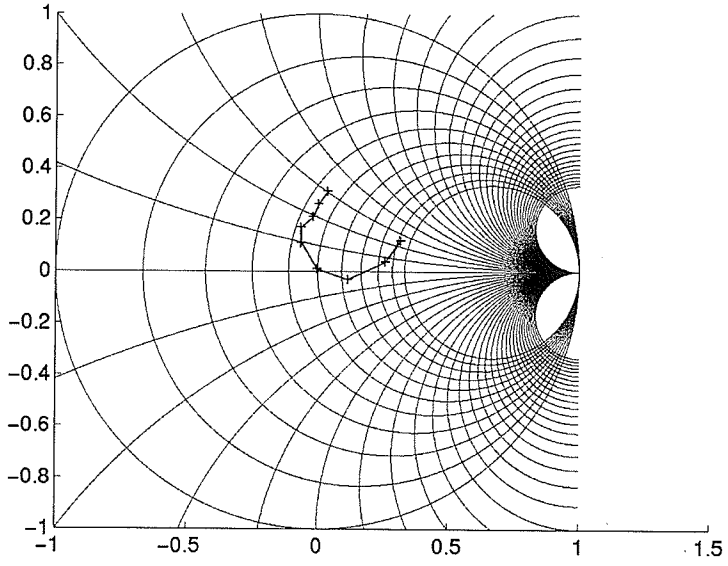

Figure II.2: Effect of circular microstrip antenna substrate thickness variation on the input impedance at 10GHZ

Table .8: Effect of circular microstrip antenna probe location variation on the input impedance at 10GHZ

r (mm)	FFP (degree)	S_{11} (dB)	Res.frq (GHz)	INR (Ω)	INX (Ω)	INP (degree)	Exp.
1.41	19	-10.003	9.7	33.037	21.12	32.59	
1.5	28	-12.5	9.9	37.7	17.2	24.53	
1.6	34.5	-15.4	9.9	40.82	12.56	17.14	
1.8	46	-27.74	9.97	47.9	3.42	4.08	
1.85	48.98	-40.73	10	49.6	0.82	0.92	Matched point
2	57	-20	10.07	57.134	-8.04	-8.012	
2.1	62	-16.1	10.15	61.73	-13.13	-12.007	
2.2	64.4	-13.98	10.2	64.86	-17.86	-15.84	
2.3	67.5	-11.85	10.25	70.65	-23.56	-18.4	
2.4	69.85	-10.55	10.32	74.65	-28.87	-21.14	

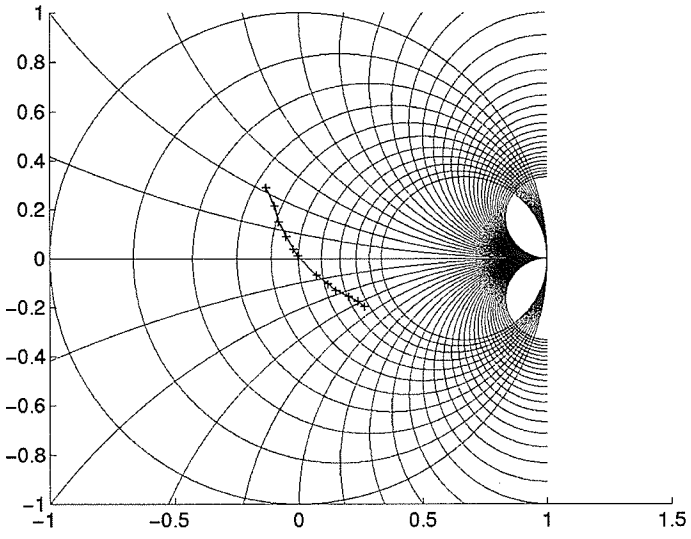

Figure II.2: Effect of circular microstrip antenna probe location variation on the input impedance at 10GHZ